

A COMPARATIVE STUDY OF CARBON NANOTUBES AND GRANULAR ACTIVATED
CARBON: PHYSICOCHEMICAL PROPERTIES AND ADSORPTION CAPACITIES

by

ROJA HARITHA GANGUPOMU

Presented to the Faculty of the Graduate School of
The University of Texas at Arlington in Partial Fulfillment
of the Requirements
for the Degree of

DOCTOR OF PHILOSOPHY

THE UNIVERSITY OF TEXAS AT ARLINGTON

May 2013

Copyright © by Roja Haritha Gangupomu 2013

All Rights Reserved

ACKNOWLEDGEMENTS

I would like to express my sincere appreciation and deepest gratitude to my advisor Dr. Melanie Sattler. Dr. Sattler as my research advisor and committee chair has provided me with continuous support, motivation and professional guidance. I would especially like to thank Dr. David Ramirez for his invaluable inputs, scientific guidance and very well needed support that took me through this research. My appreciation is also extended to my committee members Drs. Hyeok Choi, Frederick MacDonnell, Victoria Chen, and Anand Puppala for devoting their time to serve in my committee.

I would like to take this opportunity to thank Dr. Weatherton for her unending encouragement, invaluable advice and the wonderful moments we shared together. I am really pleased to have worked as her graduate teaching assistant during my doctorate studies and also would thank her for supporting me financially. I would like to express my gratitude to Air and Waste Management Association for their support via scholarship.

I am grateful to Drs. Jiechao Jiang, Muhammed Yousufuddin, and Qinhong Hu for giving me the training and technical support in characterizing my samples. I owe my sincere and earnest thankfulness to Paul Shover, Lewis Crow, Barbara Howser, Sylvia George Williams, and Sara Ridenour at University of Texas at Arlington and Jesus R. Hernandez, Donald Marek and Tamara Guillen at Texas A&M University Kingsville for their timely help. I also wish to acknowledge Annaprabha Athappan, Sagar Chitre, Nereyda Facundo, Danning Wu for their help in the laboratory.

Most of all I want to thank my husband Hari, for his patience, understanding, encouragement, and eternal support to accomplish this dream of my life. I would not been able to see this day in my life without the love and encouragement of my parents and my best friend

Ravi. Finally I want to thank all my friends and family members who have been with me through this journey and have joined me to celebrate this accomplishment of mine.

April 17, 2013

ABSTRACT

A COMPARATIVE STUDY OF CARBON NANOTUBES AND GRANULAR ACTIVATED CARBON: PHYSICOCHEMICAL PROPERTIES AND ADSORPTION CAPACITIES

Roja Haritha Gangupomu, PhD

The University of Texas at Arlington, 2013

Supervising Professor: Melanie L. Sattler

Adsorption technologies with activated carbon have proven their prominence in wide variety of industrial applications for the removal of pollutants from gaseous streams for generations. Nanoadsorbents due to their unique structure and the presence of high-energy binding sites can enhance adsorption of pollutants, particularly for hazardous pollutants difficult to control using conventional sorbents like activated carbon and can help industries in their struggle for greener technologies.

The objective of this study was to characterize raw and purified CNTs and compare their physical and chemical properties to commercially available granular activated carbon (GAC). The CNT purification process was done in two steps: the samples were first heat-treated at 400⁰C in a steam atmosphere, followed by acid treatment. In the acid treatment, the CNTs were chemically treated with different concentrations (3N, 5N, 11N, and 16N) of nitric acid for various time spans (3hr, 6hr, 9hr, 10hr, and 12 hr) in an ultra-sonic bath. This study reports physical and chemical properties of CNTs and GAC including morphology; Brunauer, Emmett and Teller-nitrogen surface area, total pore volume, and pore size distribution; and results of Inductively Couple Plasma-Mass Spectrometry (ICP-MS), Raman Spectroscopy, X-ray photoelectron spectroscopy (XPS) and Thermogravimetric analyses (TGA). Adsorption of

toluene onto CNTs and GAC was conducted using a gas chromatography-flame ionization detector to assess the adsorption capacity and the removal efficiency of the adsorbents. Breakthrough curves and time series plots were developed to obtain the aforementioned parameters.

ICP-MS results showed the presence of metal impurities and Silica in the SW and MW raw samples. Transmission electron microscopy results showed that the nitric acid treatment developed corrugations on the walls of nanotubes and removed impurities. The XPS and Raman results showed that complete removal of amorphous carbon occurred for the SWNTs treated with 3N nitric acid for 3 hours. XPS also showed a few surface functional groups on the purified samples, but these surface functional groups did not ultimately improve the adsorption capacity of the sample for toluene. TGA testing confirmed the results from the above the three experiments, but also showed that the purified MWNTs had a lower stability than the raw sample. The adsorption capacity of GAC and SW 33 were 385 mg/g and 383 mg/g, respectively. The purified SWNTs and MWNTs showed a higher adsorption capacity than the raw SWNTs and MWNTs. The purified samples except for the SW 33 sample had a decrease in the surface area ranging between 890 m²/g and 1100 m²/g, while the pristine sample had a surface area of 1136 m²/g.

This study indicates that purification of carbon nanotubes can make their physical and chemical properties comparable to granular activated carbon. It is important to note that heat and nitric acid treatment that caused different degrees of enhancements in the pore structure, chemical structure and surface chemistry in this study may not produce the same enhancements for carbon nanotubes from different sources.

TABLE OF CONTENTS

ACKNOWLEDGEMENTS	iii
ABSTRACT.....	v
LIST OF ACRONYMS.....	x
LIST OF ILLUSTRATIONS	xi
LIST OF TABLES	xiv
Chapter	Page
1. INTRODUCTIONS	1
1.1 The Need for Control of Hazardous Air Pollutants	1
1.2 Nanotechnologies for Air Pollution Control	4
1.3 Research Objectives	5
1.4 Dissertation Outline.....	6
2. LITERATURE REVIEW	7
2.1 Adsorption	7
2.2 Adsorbents	7
2.3 Carbon Nanotubes	8
2.3.1 Types	9
2.3.2 Synthesis Processes	10
2.3.3 Purification Processes	13
2.3.4 Characterization of Carbon Nanotubes	22
2.3.5 Adsorption on to Carbon Nanotubes	23
2.4 Adsorbate.....	28
2.5 Summary.....	29
3. METHODOLOGY	31

3.1 Sample Description	31
3.1.1 Single-wall Carbon Nanotubes	31
3.1.2 Multi-wall Carbon Nanotubes	32
3.1.3 Granular Activated Carbon	33
3.2 Sample Pre-Treatment	34
3.2.1 Heat Treatment	34
3.2.2 Heat and Acid Treatment	36
3.3 Physical/Chemical Characterization of Samples	38
3.3.1 Inductively Coupled Plasma-Mass Spectrometry	40
3.3.2 Transmission Electron Microscopy	40
3.3.3 Raman Spectroscopy	42
3.3.4 X-ray Photoelectron Spectroscopy	43
3.3.5 Thermogravimetric Analysis	44
3.3.6 Surface Area and Pore Size Analysis	45
3.4 Adsorption Testing	50
3.4.1 Data Collection and Analysis.....	52
4. RESULTS AND DISCUSSION.....	55
4.1 Physical/Chemical Characterization of Samples	55
4.1.1 Inductively Coupled Plasma-Mass Spectrometry	55
4.1.2 Transmission Electron Microscopy	55
4.1.3 Raman Spectroscopy	60
4.1.4 X-ray Photoelectron Spectroscopy	65
4.1.5 Thermogravimetric Analysis	68
4.1.6 Surface Area and Pore Size Analysis	72
4.2 Adsorption Testing	81
4.2.1 Breakthrough and Time Series Curves	81

4.2.2 Explanation of Adsorption Results in Light of Nanotube Physical/Chemical Properties	86
4.2.3 Estimation of Kinetic Parameters	87
5. CONCLUSIONS AND RECOMMENDATIONS	90
5.1 Summary and Conclusions	90
5.2 Global Conclusions	91
5.3 Recommendation for Future Studies	92
APPENDIX	
A. SAMPLE EXPERIMENTAL RESULTS	94
B. SAMPLE OUTPUTS AND PLOTS	103
REFERENCES	109
BIOGRAPHICAL INFORMATION	118

LIST OF ACRONYMS

GAC – Granular Activated Carbon

CNTs – Carbon Nanotubes

HAP – Hazardous Air Pollutants

USEPA – United States Environmental Protection Agency

NAAQS – National Ambient Air Quality Standards

CAAAS – Clean Air Act Amendments

SWNTs – Single-wall Carbon Nanotubes

MWNTs – Multi-wall Carbon Nanotubes

ICP-MS – Inductively Coupled Plasma Mass Spectrometry

TEM – Transmission Electron Microscope

XPS – X-ray Photoelectron Spectroscopy

TGA – Thermogravimetric Analysis

BET – Brunauer-Emmett-Teller

BJH – Barrett, Joyner and Halenda

PFOM – Pseudo-First Order Model

LIST OF ILLUSTRATIONS

Figure	Page
1.1 Atmospheric emissions of HAPs by industry in 2011	3
2.1 Electron micrographs of microtubules of graphitic carbon. A cross-section of each tubule is illustrated. (a) Tube consisting of 5 graphitic sheets, dia. 6.7 nm. (b) 2 sheet tube dia. 5.5 nm (c) 7 sheet tube, dia. 6.5 nm	9
2.2 Structural representations of (a) a MWNT (b) a SWNT	10
2.3 Schematic of various carbon nanotubes production methods (A) Arc-Discharge method (B) Laser Ablation method (C) Chemical Vapor Deposition method.....	12
2.4 TEM images of (a) amorphous carbon and fullerene molecules on the surface of the CNTs, (b) metal nanoparticles covered by amorphous carbon layer, and (c) metal nanoparticles covered by graphitic carbon layer.....	13
2.5 TEM image of an open-ended pair of MWNTs.....	14
2.6 Different adsorption sites on a homogeneous bundle of partially open-ended SWNTs. (1) internal, (2) interstitial channels, (3) external groove site, and (4) external surface	24
2.7 Equilibrium adsorption isotherms A) based on mass, and B) normalized to surface area	27
3.1 SEM Image of single-wall carbon nanotubes.....	32
3.2 SEM Image of multi-wall carbon nanotubes	33
3.3 A picture of GAC	34
3.4 Experimental set-up of the heat treatment	36
3.5 Experimental set up of the nitric acid treatment	37
3.6 Sonicated samples after the acid treatment (a) SWNTs treated in 3N HNO ₃ for 10 hr. (b) MWNTs treated in 11N HNO ₃ for 6 hr.	38
3.7 A schematic outline of a TEM	42

3.8 Absorption and scattering of light in a Raman scattering spectra	43
3.9 A schematic outline of the X-ray Photoelectron Spectroscopy	44
3.10 Experimental set-up of the surface area analyzer	46
3.11 Schematic of a bench scale adsorption system	51
3.12 Experimental set-up of the adsorption testing in the lab.	51
4.1 TEM images of SWNTs pristine sample at (a) high and (b) low resolution	57
4.2 TEM images of MWNTs pristine sample at (a) high and (b) low resolution	57
4.3 TEM image of GAC	57
4.4 TEM images of the purified SWNTs (a) SW 33 (b) SW 36 (c) SW 310 (d) SW 63 (e) SW 66 (f) SW 610	58
4.5 TEM images of the purified MWNT sample (a) MW 116 (b) MW 119 (c) MW 1112 (d) MW 166 (e) MW 169 (a) MW 1612	59
4.6 I_G/I_D value plots for (a) SW raw and treated samples (b) MW raw and treated samples	61
4.7 Raman spectra of the pristine samples of SWNTs, MWNTs, and GAC	62
4.8 Raman spectra of samples (a) SW raw, SW 33, SW 36, SW 310 (b) SW raw, SW 63, SW 66, SW 610	63
4.9 Raman spectra of samples (a) MW raw, MW 116, MW 119, MW 1112 (b) MW raw, MW 166, MW 169, MW 1612	64
4.10 XPS C1s spectra of pristine SWNTs, MWNTs and GAC	66
4.11 XPS C1s spectra after the purification process (a) SWNTs treated in 3N HNO ₃ (b) SWNTs treated in 6N HNO ₃	66
4.12 XPS C1s spectra after the purification process of (a) MWNTs treated in 11N HNO ₃ (b) MWNTs treated in 16N HNO ₃	67
4.13 Thermogravimetric analysis plots of SW raw, MW raw and GAC (a) Weight loss curves of the raw sample (b) First derivative plots of the raw samples.	69
4.14 Thermogravimetric (a) Weight loss curves and	

(b) First derivative plots of SW raw and 3N acid treated samples and (c) Weight loss curves and (d) First derivative plots of SW raw and 6N acid treated samples	70
4.15 Thermogravimetric (a) Weight loss curves and (b) First derivative plots of MW raw and 11N acid treated samples and (c) Weight loss curves and (d) First derivative plots of MW raw and 16N acid treated samples	71
4.16 Pore Size Distribution for SW raw, MW raw and GAC Samples using (a) the DA Method (Micropore Region) and (b) the BJH Method (Mesopore Region)	75
4.17 Pore Size Distribution for SWNTs treated with 3N nitric acid using (a) the DA Method (Micropore Region) and (b) the BJH Method (Mesopore Region)	76
4.18 Pore Size Distribution for SWNTs treated with 6N nitric acid using (a) the DA Method (Micropore Region) and (b) the BJH Method (Mesopore Region)	77
4.19 Pore Size Distribution for MWNTs treated with 11N nitric acid using a) the DA Method (Micropore Region) and b) the BJH Method (Mesopore Region)	78
4.20 Pore Size Distribution for MWNTs treated with 16N nitric acid using (a) the DA Method (Micropore Region) and (b) the BJH Method (Mesopore Region).	79
4.21 Breakthrough curves of SW raw, MW raw and GAC	83
4.22 Time series for the adsorption of toluene onto SW raw, MW raw and GAC	83
4.23 Breakthrough curves for adsorption of toluene onto SW raw, SW 33, SW 36 and SW 63	84
4.24 Time series for the adsorption of toluene onto SW raw, SW 33, SW 36, and SW 63	84
4.25 Breakthrough curves for adsorption of toluene onto MW raw, MW 169 and MW 1612	85
4.26 Time series for the adsorption of toluene onto MW raw, MW 169 and MW 1612	85
4.27 Adsorption capacities that were measured and fitted with the pseudo-first order model for GAC	88
4.28 Adsorption capacities that were measured and fitted with the pseudo-first order model for (a) SW raw (b) SW 33 (c) SW 36 (d) SW 63.	89

LIST OF TABLES

Table	Page
1.1 Toxic releases for facilities in all industries hazardous air pollutants in U.S., 2011	3
2.1 Nanotube pre-treatment gas, temperature, and time combinations from previous studies	16
2.2 Various chemical methods used for pretreatment in previous studies	19
2.3 Summary of the previous studies using both physical and chemical purification techniques	21
2.4 Physical properties of toluene	29
3.1 Properties of Calgon granular activated carbon	34
3.2 Heat treatment temperature and time of the MWNTs and SWNTs	35
3.3 Summary of the weight of the CNTs used, volume and strength of the acid, and the time of treatment of the carbon nanotubes	37
3.4 Characterizing techniques and their features	39
4.1 ICP-MS results for SW and MW raw samples	55
4.2 I _G /I _D ratio of the pristine and purified carbon nanotubes and GAC	62
4.3 Weight% of the samples remaining after TGA	69
4.4 Process conditions and physical properties of the carbon nanotube samples and GAC	74
4.5 Summary of characterization technique results for SWNTs and MWNTs	80
4.6 Maximum removal efficiency and adsorption capacity of the samples	86
4.7 Adsorption capacities experimental and modeled and pseudo-first order model constants for adsorption of toluene onto GAC and SWNTs	88

CHAPTER 1
INTRODUCTION

1.1 The Need for Control of Hazardous Air Pollutants

Air pollution remains an important national issue within the U.S., with 80 million people nationwide still exceeding National Ambient Air Quality Standards (USEPA, 2007). Air pollutant exposure shortens lifespans due to lung cancer and heart disease, and increases cases of asthma attacks, bronchitis, and birth defects (Douglas et al., 1993; Rob et al., 1999; Ritz et al., 2002). Globally, over a billion persons breathe unhealthy air daily (Molly, 1999). The global problem will likely worsen in the near future: over the next 50 years, world population is expected to grow 50%, and global energy and materials use expand 300 % (WRI, 2000).

Regulating air pollution and providing clean air for the public has been a concern for at least a century. In early 1300, release of toxic air pollutants was recognized as a nuisance than a threat to human health. In early 1900s, many ordinances were passed in England and the United States to control pollution for the aesthetic and welfare of public and not for the human health and the environment. These ordinances could be recognized as the initial steps leading to our modern air pollution control acts and laws.

In 1955, the United States federal government took on the daunting task to control the emissions of toxic air pollutants with the passage of the Air Pollution Control Act. The Clean Air Act (CAA) was executed in 1963 and replaced the Air Pollution Control Act. The CAA was focused mainly on developing techniques to minimize air pollution and address issues concerning air pollution related to environmental studies. The creation of the United States Environmental Protection Agency (USEPA) by President Nixon in 1970 led to the establishment of the National Ambient Air Quality Standards (NAAQS) as part of the Clean Air Act Amendments (CAAA). The CAAs were amended again in 1977 and then later in 1990. In

1990 the CAAAs were expanded to control 189 toxic air pollutants under the jurisdiction of the USEPA. These toxic air pollutants, also called the hazardous air pollutants (HAPs), are those pollutants that could cause serious threat to human health or damage to the environment.

USEPA is working with state, local and the tribal governments to reduce emissions of these hazardous air pollutants. When people are exposed to high concentrations or long durations of these air toxics, damage to their neurological, immune, reproductive, and respiratory system can happen at a faster pace. These toxic air pollutants originate from both natural sources like volcanic eruptions and anthropogenic sources like stationary sources (ex: factories, refineries, power plants), mobile sources (ex: cars, trucks, airplanes), and indoor sources (ex: sprays, deodorants, vacuums) (USEPA, 2011). Currently USEPA regulates the emissions of the 179 hazardous air pollutants. The 2011 Toxic Release Inventory reports states that 2.2×10^8 kg of hazardous chemicals were emitted to the atmosphere (USEPA, 2011). Table 1.1 provides the list of the top fifteen HAPs, with their emissions in the year 2011 from all the facilities in the United States. The largest emissions of HAPs occurred in the electric utilities (30.4%), paper (22.6%), chemicals (13.9%), food/beverages/tobacco (5.5%), and plastic and rubber (5.2%) industries in 2011 (Figure 1.1).

Table 1.1: Toxic releases for facilities in all industries hazardous air pollutants in U.S., 2011 (USEPA, 2011)

Rank	Chemical	Total Air Emissions (kg x 10 ⁶)
1	Hydrochloric Acid	74.6
2	Methanol	47.0
3	Hydrogen Fluoride	14.3
4	N-Hexane	14.1
5	Toluene	11.9
6	Styrene	10.4
7	Carbonyl Sulfide	6.2
8	Xylene (mixed isomers)	5.8
9	Certain glycol ethers	5.7
10	Chlorine	4.1
11	Carbon Disulfide	4.0
12	Acetaldehyde	3.7
13	Formaldehyde	2.3
14	Phenol	2.2
15	Benzene	1.8
Total of Top 15 HAPs		208.1 (92.7 %)
Total of All 179 Reported HAPs		248.7

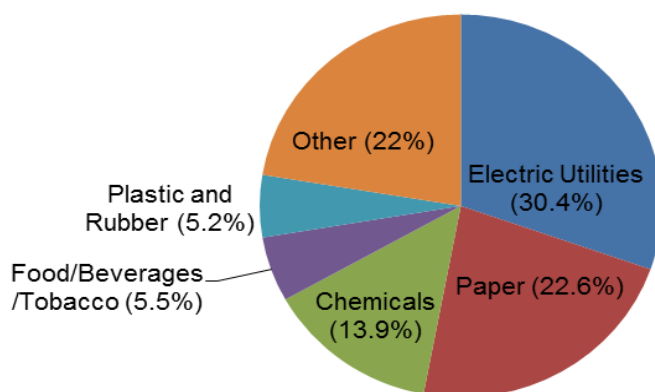


Figure 1.1: Atmospheric emissions of HAPs by industry in 2011 (USEPA, 2011)

There are four main techniques to control the generation and emission of hazardous air pollutants (Wark, Warner and Davis 1998).

1. Adsorption – the pollutant could be adsorbed onto a chosen solid adsorbent,
2. Absorption – the pollutant could be absorbed into a selected liquid solvent,
3. Oxidation – the pollutant may be oxidized into another gaseous form, via high temperature combustion or microbe-mediated oxidation, which could be harmless vapor, and
4. Process Modification – the concentration of the pollutant can be altered to decrease the initial production of the pollutant from the original process of generation.

1.2 Nanotechnologies for Air Pollution Control

According to the Environmental Protection Agency (EPA) Nanotechnology White Paper, nanotechnology can potentially improve the environment directly, by preventing and removing pollutants, as well as indirectly, through design of cleaner industrial processes and products (USEPA 2007). The National Nanotechnology Initiative (NNI) identified “Nanoscale Processes for Environmental Improvement” one of its original “grand challenges” (NSTCCT 2003). In particular, nano scale sorbents, catalysts, and photocatalysts hold promise for improving air pollution control systems Masciangioli and Zhang 2003). Investigating the potential of advanced nanotechnology to improve air pollution remediation was deemed important by the NNI “Nanotechnology and the Environment” workshop report (2003), NNI Strategic Plan (2004), and Air & Waste Management Association 2005 Critical Review “Nanoparticles and the Environment” (NSTCCT 2003; NSTC 2004; Biswas et al. 2005).

Nano-scale sorbents, catalysts, and membranes hold promise for improving traditional air pollution control systems. Because of their high-energy binding sites, nano scale sorbents have the potential to improve adsorption of pollutants, particularly for hazardous air pollutants (HAPs) that are difficult to control using the traditional sorbents. In particular, carbon nanotubes

are crystalline pores of cylindrical shape with walls consisting mainly of graphite sheets. Carbon nanotubes (CNTs) can be manufactured as single-walled carbon nanotubes (SWNTs) and multi-walled carbon nanotubes (MWNTs). SWNTs consist of single layer of graphene sheet with mostly micropores and MWNTs consist of at least two layers of graphene sheets arranged coaxially and are mostly mesoporous in nature. Due to this unique structure, CNTs have high-energy adsorption sites which can increase adsorption compared to other kinds of carbon-based adsorbents.

1.3 Research Objectives

The goal of this research was to evaluate the use of CNTs for adsorption of HAPs and compare the adsorption capacities of the CNTs with granular activated carbon. CNTs were physically and chemically characterized using state-of-the-art instruments including surface area analyzer, high resolution transmission electron microscope (HRTEM), x-ray photoelectron spectroscopy (XPS), raman spectroscopy, and gas chromatography flame ionization detector (GC-FID). Kinetic curves were developed to study the kinetic parameters for the adsorption of toluene onto the CNTs and granular activated carbon.

Specific research objectives include:

1. To assess carbon nanotubes physicochemical properties with and without pre-treatment: morphology, average pore width, thermal stability, specific surface area, average pore width, total, micro, and meso pore volume.
2. To determine the adsorption capacities of the chemically treated carbon nanotubes versus granular activated carbon.
3. To obtain the adsorption kinetic rate constants of toluene on to carbon nanotubes and the granular activated carbon.

This work is important as it demonstrated a new way to reduce the emission of pollutants that are difficult to remove with conventional methods and will also serve as a

foundation for future studies in nano adsorption, which could test other air pollutants, other CNT treatments and CNT adsorption performances.

1.4 Dissertation Outline

This dissertation is divided into 5 chapters as summarized below:

- Chapter 1 provides an introduction and presents the problem statement and objectives of the research.
- Chapter 2 presents a literature review of the various physical and chemical pretreatments of carbon nanotubes, adsorption studies using various solvents.
- Chapter 3 describes the experimental procedures followed for the acid treatment of the CNTs, the physical and chemical characterization of the CNTs and the granular activated carbon and the adsorption testing of the three adsorbents using toluene as the adsorbate.
- Chapter 4 presents the experimental results, determines the equilibrium capacities and kinetic rate constants, and identifies models that provide a good fit to the experimental data, results are also discussed.
- Chapter 5 summarizes the main conclusions from the current research and provides recommendations for future work.

CHAPTER 2
LITERATURE REVIEW

2.1 Adsorption

Adsorption is a control technology used worldwide to control hazardous air pollutants from gas streams. Activated carbon is the most common adsorbent used in the adsorption processes to control the gaseous pollutants. The term activated is given to an adsorbent material which has some fairly selective properties. Properties like surface area, particle diameter, total pore volume, pore size distribution and surface functional groups are used to determine the effectiveness of an adsorbent material (Gregg and Sing, 1982). These desirable properties of certain adsorbent materials give them the ability to remove gaseous or liquids from a pollutant stream. Adsorption advantages include high removal efficiencies and simple, reliable operation.

2.2 Adsorbents

Adsorbents that are typically used for removal of hazardous air pollutants from gas streams include activated carbon, silica gel, alumina and zeolites. Activated carbon is by far the most commonly used adsorbent, and has effectively replaced all other materials in both air and water quality control. Activated carbons are amorphous carbon-based materials with a microcrystalline structure, having high surface area and adsorption capacities (Bansal et al., 1988, 2005). Coconut shells, bones, coal, petroleum, coke, lignite, and lignin (Cooper and Alley, 1994), wood chips (Khezami et al., 2005; Ramirez et al., 2008) and waste tires (Lehmann et al., 1998) are some of the raw materials used to make activated carbon. These raw materials are first dehydrated and then carbonized. The activation of the carbon is done when the dehydrated material is heated in a controlled environment in the presence of an oxidizing gas. Bituminous coal is the most industrial grade carbon used for the air and water applications (Cooper and

Alley, 1994). Activated carbon can be classified as powdered activated carbon (PAC), forms of activated carbon fibers (Bansal et al., 1988, 2005), activated carbon monoliths (Luo et al., 2002, 2006), activated carbon fiber cloths (Sullivan et al., 2004; Ramirez et al., 2004) and granular activated carbon (GAC).

GAC is the traditional morphology of activated carbon used for the removal of organic vapors from gas streams. Granular carbon has a nominal diameter of 4 – 7 mm. GAC has smaller external surface area per unit volume compared to PAC because GAC granules are larger than PAC. GAC granules sizes vary according to their application. GAC size is of concern for pressure drop in the adsorption bed.

2.3 Carbon Nanotubes

In recent years, it was discovered that pyrolysis of carbon in the gas phase can produce a sooty mass which has forms of carbon in the nanometer size range. These are the graphene layered structures in a spherical shape famously known as fullerenes (Marsh et al., 2006). Iijima (1991) reported a new type of hollow fibrous graphitic structure which was fine and long, as shown in Figure 2.1. These were initially called helical microtubules and now famously known as carbon nanotubes. Since this work of Iijima, due to its unique properties the research on carbon nanotubes is progressing rapidly.

Carbon nanotubes are graphene sheets rolled as seamless cylinders in a regular hexagonal arrangement, with closed ends. Carbon nanotubes have diameters in nanometer size, but have lengths up to 1 μm (Saito et al., 2003). The closed ends along with a high aspect ratio give the carbon nanotubes exceptionally high mechanical (stability, strength, stiffness, and elastic deformability), transport (coherent electron transport), and surface properties (Ajayan, 2000). They are also known for having higher strength than any other material available and being the best super-conducting material, as well as having some exceptional field emission properties (Ajayan, 2000).

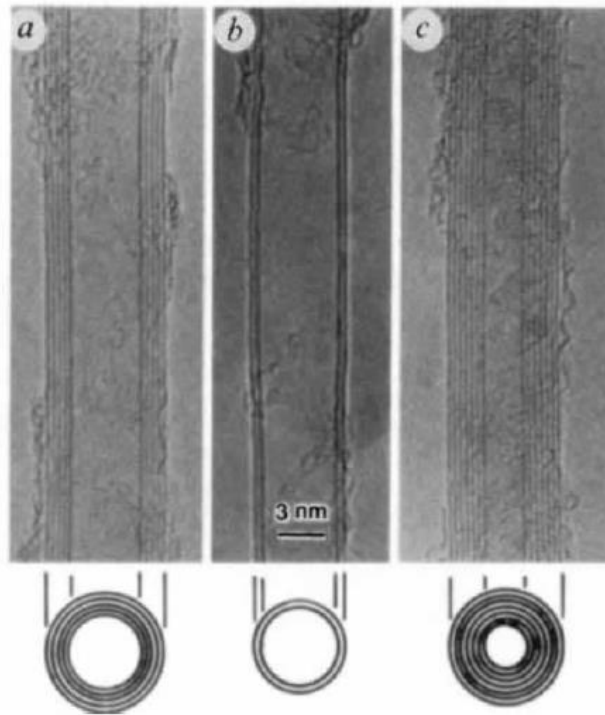


Figure 2.1: Electron micrographs of microtubules of graphitic carbon. A cross-section of each tubule is illustrated. (a) Tube consisting of 5 graphitic sheets, dia. 6.7 nm. (b) 2 sheet tube dia. 5.5 nm. (c) 7 sheet tube, dia. 6.5 nm. (Reprinted with permission from Iijima, 1991)

2.3.1 Types

Carbon nanotubes can be manufactured as single-walled carbon nanotubes (SWNTs) and multi-walled carbon nanotubes (MWNTs). Single-walled carbon nanotubes are graphene sheets in cylindrical shape aligned in one dimension. SWNTs have diameters ranging between 0.7 and 10 nm, though most of them have diameters less than 2 nm (Saito et al., 2003). The diameter of the carbon nanotubes is of trivial importance when considering their high aspect ratio (length/diameter), which can be as large as $10^4 - 10^5$ (Saito et al., 2003). The multi-walled carbon nanotubes have thicker walls, consisting of several tens of graphitic shells with adjacent shell separation of ~ 0.34 nm, and high aspect ratio (Popov, 2004). The outer diameters of MWNTs range between 2 and 25 nm and the inner hollow range from ~ 1 to 8 nm. (Ajayan,

2000). When produced, CNTs are completely closed and cannot accept substances inside until opened. Figure 2.2 gives a structural representation of a SWNT and a MWNT.

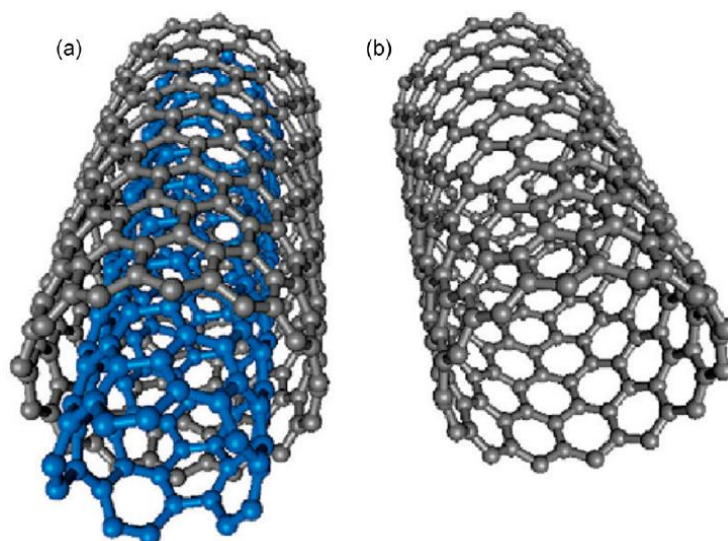


Figure 2.2: Structural representations of (a) a MWNT (b) a SWNT (Reprinted with permission from Zhao et al., 2009)

2.3.2 Synthesis Processes

Both the SWNTs and the MWNTs can be manufactured by the same techniques. Arc discharge, laser ablation, and chemical vapor deposition (CVD) are the three commonly used methods to produce carbon nanotubes.

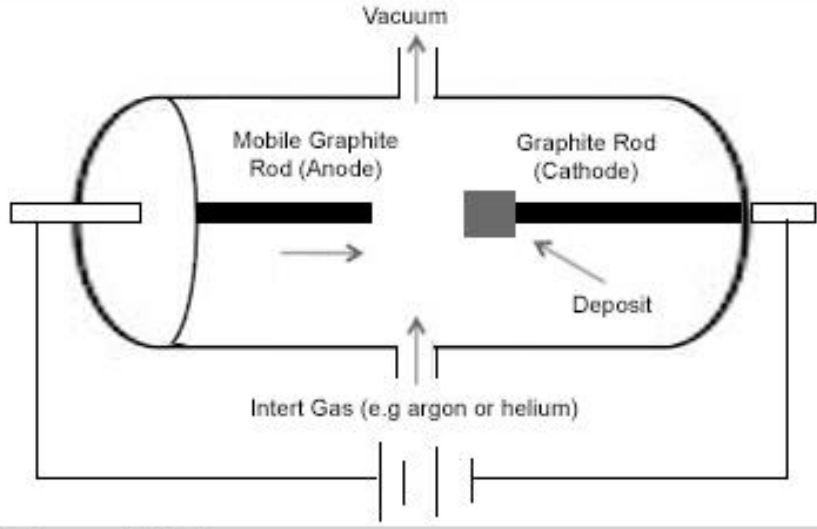
In the arc discharge technique (Figure 2.3A), the high temperature of the carbon arc provides direct current between the electrodes to vaporize the carbon atoms of one electrode for simultaneous deposition on the other. (Saito et al., 2003; Sandeep, 2005). Carbon nanotubes self-assemble from the carbon vapor. The arc discharge method can be performed both with and without a catalyst. MWNTs are obtained in the carbon vapor if performed without a catalyst; if the graphite electrode is impregnated with Iron (Fe), Cobalt (Co), or Nickel (Ni), SWNTs are the end product (Bethune et al., 1993). The Fe or Co catalyst used in this process

also produces nanometer-size carbide particles along with SWNTs, thus requiring a purification process after the production of the carbon nanotubes.

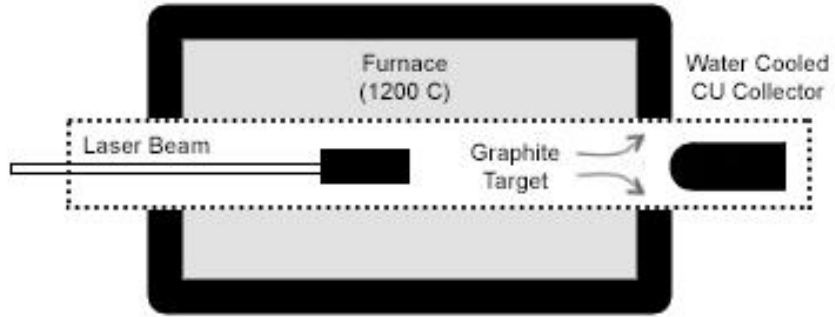
Laser Ablation is a technique where carbon nanotubes with narrow diameter can be produced in bundles with a high structural quality. It was the first technique used to produce fullerenes in clusters. In Figure 2.3B we can observe the graphite is laser irradiated in a furnace at 1200⁰C in the presence of Ni and Co, while an inert gas like Argon (Guo et al., 1995) is used to sweep the grown carbon nanotubes into the colder zone just outside the furnace (Saito et al., 2003). By varying the growth temperature, the physical properties of the carbon nanotubes can be varied.

Chemical vapor deposition (CVD) (Figure 2.3C) is energy efficient compared to other two methods, has a low price/unit ratio, and inherent scalability in the production of both MW and SW nanotubes (Aqel et al., 2012; Sandeep, 2005). Fe, Co, and Ni powder are some of the common metal catalysts used for the CVD method of production of carbon nanotubes. This process involves catalytic cracking in which feedstock like methane (Bittner et al., 2003), ethylene (Hafner et al., 1998) and hydrogen gases are reacted in presence of the metal catalysts at temperatures ranging between 850⁰C and 1100⁰C. This process is promising in producing carbon nanotubes continuously; hence, if optimum conditions could be found, then it can be used to produce carbon nanotubes in bulk quantities.

(A) Arc - Discharge



(B) Laser Ablation



(C) Chemical Vapor Deposition

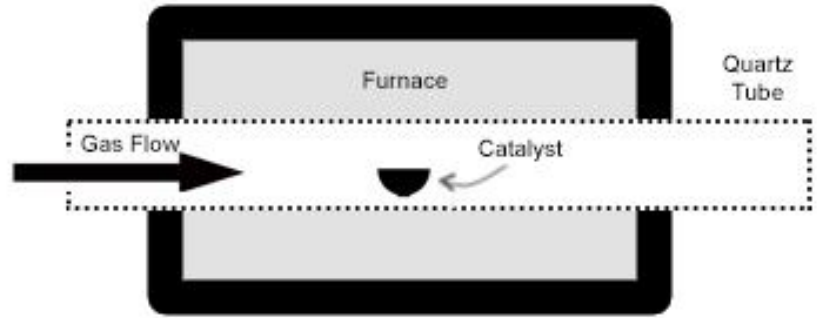


Figure 2.3: Schematic of various carbon nanotubes production methods (A) Arc-Discharge method (B) Laser Ablation method (C) Chemical Vapor Deposition method

2.3.3 Purification Processes

As listed above, we have seen that there are several methods for the production of carbon nanotubes. The main concern of production is the unavoidable by-products of the manufacturing process. As-produced carbon nanotubes generally contain tubular structures of nanomaterial and also impurities like amorphous carbon, metal particles, carbon nanoparticles or soot, and other forms of carbon (Hou et al., 2002; Chen et al., 2002; Haddon, 2002; Ren et al., 2011; Hernadi et al., 1996; Saito et al., 2003), as shown in Figure 2.4. The type and amount of the impurities solely depend on the method of production. The impurities interfere with the desired properties of the carbon nanotubes and also hinder proper characterization of the carbon nanotubes. In order to better understand the vast diversity of the carbon nanotubes, a homogeneous sample will make the job much easier. Purification techniques can be classified into three categories: physical, chemical, and a combination of both.

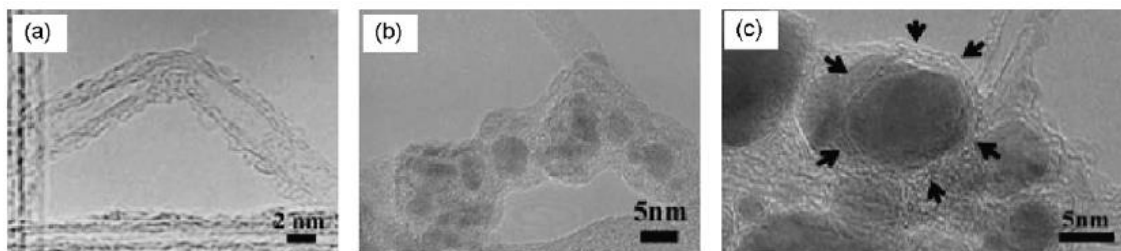


Figure 2.4: TEM images of (a) amorphous carbon and fullerene molecules on the surface of the CNTs, (b) metal nanoparticles covered by amorphous carbon layer, and (c) metal nanoparticles covered by graphitic carbon layer (Reprinted with permission from Fang et al., 2004)

An important implication to purifying the carbon nanotubes is the opening of the carbon nanotubes. Carbon nanotubes present in as-grown materials are close-ended structures, meaning the internal hollow space of a nanotube remains unavailable until they are subjected to additional treatment to remove the caps from their ends (Figure 2.5).

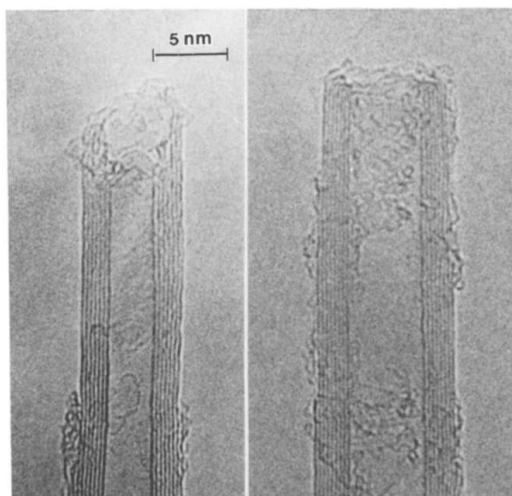


Figure 2.5: TEM image of an open-ended pair of MWNTs (Reprinted with permission from Iijima 1993)

2.3.3.1 Nanotube Pre-Treatment – Physical Method

CNTs must be heat-treated to open “windows” to the inside space, to allow air toxics to penetrate (Bekyarova et al., 2003). Heat treatment (HT) is a common physical method involving heating the as-produced carbon nanotubes in the presence of an oxidizing gas such as air, carbon dioxide, or ozone. HT is known to remove impurities like amorphous carbon and graphitic materials, but also lose some carbon nanotubes in the process (Ebbessen et al., 1992; Yudasaka et al., 2003). Carbon nanotubes can be purified by oxidizing in air at 350⁰C – 470⁰C (Moon et al., 2001; Shi et al., 1999). Tsang et al. (1993) treated CNTs with CO₂ at 850⁰C for 5 h and observed a slight increase in the surface area and a slight erosion of the caps, but when Ajayan and his team treated carbon nanotubes at the same temperature in air for 30 min, they observed that all the carbon nanotubes disappeared (Ajayan et al., 1993). Oxidizing gas, the HT temperature and time, and the metal content in the sample play a vital role in defining the efficiency of the process (Pan and Xing, 2008). Window number and size is impacted by the pre-treatment temperature and time. Pre-treatment temperature and time affect window size, with either higher temperatures or longer times opening larger windows. Larger windows would be needed for larger molecules; however, for smaller molecules, larger windows would cause

unnecessary surface area loss. A couple of studies were done using ammonia as an oxidizing gas, at temperatures of 400, 500, and 1000⁰C; the results showed that HT at 1000⁰C produced a higher surface area sample with a larger hydrogen adsorption capacity, but showed 25% more weight loss, higher micropore volume, and lot more etching than the raw and other 2 heat treated samples (Lin et al., 2009; Lv et al., 2011). Treating CNTs in inert atmospheres (in Ar, N₂, H₂ and vacuum) up to 1600⁰C removes the impurities in the sample, but above 2000⁰C, CNTs begin to coalesce with neighbors and form CNTs in the form of bundles which have double/triple diameters of the original. At 2400⁰C, SWNTs convert to MWNTs (Bougrin et al., 2001; Yudasaka et al., 2003). Table 2.1 summarizes the various pre-treatment gases, temperatures, and times from the studies listed above.

Pre-treatment gas is important because it will impact the number of oxygen-containing surface groups (e.g., hydroxyl, carbonyl, and carboxyl). No study in Table 2.1 involved pretreatment of CNTs with steam; this study will provide information about optimal temperature and time ranges for treating CNTs in steam, followed by chemical treatment.

Table 2.1: Nanotube pre-treatment gas, temperature, and time combinations from previous studies

Type of sample	Pre Treatment Gas	Temperature (°C)	Time	Surface Area (m ² /g)	Conclusions	Source
CNT	CO ₂	850	5 hr.	31		Tsang et al., 1993
CNT	Air	850	15 min.	NA	Entire sample disappeared	Ajayan et al., 1993
CNT	O ₃ /O ₂ (10% O ₃)	200	90 min.	NA	In gas phase – high levels of impurities	Hernadi et al., 2001
		60 - 70	24 hr.		In acidic phase – obtained a high purity sample	
MWNT	Ammonia	450 and 1000	2 hr.	156 and 196	MW treated at 1000 ^o C higher surface area and higher H ₂ storage capacity	Lin et al., 2009
MWNT	Ammonia	500 and 1000	2 hr.	74 and 88	At higher temperature there was 25% more weight loss and a decrease in wall thickness	Lv et al., 2011
SWNT	Argon	1400 - 2400	30 min.	N/A	Removes impurities (1600 ^o C)	Bougrine et al., 2001
SWNT	Vacuum	2000 - 2400	5 hr./2 hr.	N/A	Forms bundles with double/triple diameter of the original and at 2400 ^o C, SWNTs convert in to MWNTs	Yudasaka et al., 2003
MWNT	Vacuum	2000	5 hr.	N/A		Wang et al., 2003

2.3.3.2 Nanotube Pre-Treatment – Chemical Method

The chemical method, or in other words liquid phase treatment, is the oxidation of the nanomaterial in concentration acids like nitric acid (HNO_3), hydrochloric acid (HCl), sulfuric acid (H_2SO_4) or in non-acidic environment like in ammonium hydroxide/hydrogen peroxide ($\text{NH}_4\text{OH}/\text{H}_2\text{O}_2$), potassium permanganate/hydrogen peroxide ($\text{K}_2\text{MnO}_4/\text{H}_2\text{O}_2$). Chemical methods have proven to be more effective than the heat treatment method as the chemicals dissolve graphitic and metal particles, but they still result in destruction of the raw sample and also lose a lot of raw sample. For example, SWNTs produced by arc-discharge method are known to have metal catalysts as impurities and would require purification. They can be purified using nitric acid (Hu et al., 2003; Vaccarin et al., 1999). Use of HNO_3 is the most common acid treatment for purification, as it is known to be more effective than the other acid treatments in removing metal impurities (Jorio et al., 2008). The acid treatment has given higher yields, but resulted in shorter carbon nanotubes and also was seen to introduce defects into the purified samples (Pumera et al., 2009; Datsyuk et al., 2008). So we can say that treatment efficiency depends on key variables like acid type and strength, temperature and duration of the treatment. Rosca et al. (2005) treated MWNTs from 6 to 48 hr. and found that there is an optimum treatment time: after 12 hr. of refluxing, the rate of generation of amorphous carbon has exceeded the rate of consumption. Nitric acid treatment showed better adsorption capacity when compared with treatment with other acids like H_2SO_4 and HCl (Lu et al., 2008); also when HCl was used, the purified sample still consisted of Fe particles (Hou et al., 2002). CNTs when used to adsorb nonpolar benzene derivatives in aqueous phase showed lower adsorption after treatment than the pristine samples (Chin et al., 2010), but when used to adsorb Pb(II) in aqueous phase, showed a higher adsorption capacity than the as-produced CNTs (Wang et al., 2007). The unique structural characteristics of carbon nanotubes show that the addition of functional groups on to the carbon nanotubes is not always the best choice to produce better

adsorption capacity (Salam, 2012). Table 2.2 summarizes the results from various chemical treatment methods.

Table 2.2: Various chemical methods used for pretreatment in previous studies

Type	Weight of the sample	Strength and time	Result	Source
SWNT	1g /150 mL	3 M-12, 24,48 hr 7 M – 6,12 hr 16 M – 6, 12 hr	3 M – 12 hr and 7 M – 6 hr gave the best results. They had the highest % of yield and least % of carbon loss.	Hu et al., 2003
SWNT	2 g/200 mL	2.5 M @ 100°C for 24 hr	90% pure sample was obtained.	Hou et al., 2002
MWNT	2 g/200 mL	8 M refluxed for 4 hr at 140°C	Adsorption of PCP to pristine onto treated MWNTs was lower than the pristine samples. This was because of the oxygen functional groups present due to treatment.	Salam, 2012
MWNT	0.3 g/25 ml	65 wt% was refluxed for 48 hr	Oxidation of MWNTs in HNO ₃ acid under extreme conditions increases the defect population and shortens the length of the CNTs as verified using Raman and XPS.	Datsyuk et al., 2008
MWNT	NA	6 M for 36 hr @ 80°C	Nitric acid treatment showed very low effect on the surface area. Morphological defects increase the surface area.	Pumera et al., 2009
MWNT	NA	Refluxed for 2 hr at 140°C – 1,2,6,10 hr	6 and 10 hr showed better adsorption capacity compared to 1 and 2. 6 and 10 hr were very close.	Wang et al., 2007
MWNT	0.2 – 1 g 100 – 200 mL	60, 70 wt% - 9,12,24,36,48 hr	9 – 12 hr oxidation showed the best results, as they had the same amount of amorphous carbon as the pristine sample.	Rosca et al., 2005
CNT	NA	68% refluxed for 2 hr at 100°C	CNTs were treated with H ₂ SO ₄ , HCl and HNO ₃ . The samples treated with HNO ₃ adsorbed more BTEX in aqueous soln. than the other acid-treated sample.	Lu et al., 2008
SWNT	0.02 g/110 ml	3M HNO ₃ refluxed at 120°C for 3 hr	Surface area of the SWNTs increased, but showed decrease in the adsorption of C ₆ H ₆ and its derivatives.	Chin et al., 2010

2.3.3.3 Nanotube Pre-Treatment – Physical and Chemical Method

The third kind of method is a combination of the heat treatment and the acid/non-acidic treatment. The heat treatment is known to remove most of the amorphous carbon in the sample by oxidizing the sample in air to 400⁰C (Nagasawa et al., 2000); if the acid treatment is next employed, a 98% purity sample can be obtained (Dillon et al., 1999) The combination technique is known to be non-destructive and scalable. Colomer et al. (1999) in his study compared air oxidation and potassium permanganate in acidic solution to remove amorphous carbon and observed similar results. The conclusion is if very harsh acid treatments are used, SWNTs transform into MWNTs or onion-like structures, hence destroying the as-produced sample completely (An et al., 2004). Acid reflux time, as discussed earlier, is an important factor in the determination of the metal nanoparticles in the sample. Martinez et al. (2003) reported that nitric acid treatment removed 95% of the metal impurities, as well produced intercalation of the HNO₃ molecules into the CNT bundles. The heat treatment after the acid treatment helped in complete de-intercalation, hence forming thick and highly ordered bundles. To achieve 100% purified samples, if we employ two acid treatment techniques, studies have shown that it can completely destroy the sample (Gotovac et al., 2007). The challenging part of the purification of the CNTs is that the same treatment can give exactly opposite results for the same sample produced by two different techniques (Colomer et al., 1998). Table 2.3 summarizes all the studies discussed above.

So, in this study, to overcome the challenges of purification, we the have chosen to do various heat treatment methods, to choose the optimum heat treatment condition, and then proceed with trying different concentration and time combinations of nitric acid treatment.

Table 2.3: Summary of the previous studies using both physical and chemical purification techniques

Type	Strength and time	Result	Source
SWNT	3 M - 24,45,69 hr	After acid treatment, air oxidation was done at 300°C and after that annealing in Ar at 950°C for 10 hr. 3.3 wt % of metal loss occurred at 24 hr and further 2.1 wt % at 45 hr and no further loss. At 45 hr, 95% of metal and 50% of the sample was lost.	Colomer et al., 1998
SWNT	3 M – 16 h @ 120°C 3 M – 4,48 hr	TGA images show 50 wt% pure sample. The samples were oxidized in air after acid treatment.	Dillion et al., 1999
CNT	Treated with HF acid	Optimum reaction temperature is 500°C for amorphous carbon removal.	Colomer et al., 1999
SWNT	70% - for 20 min and refluxed for 4 hr at 120°C	HT at 350°C for 10 min. showed no effect. 400°C for 10 min. showed sharp tips. At 500°C most of it was gasified and only catalytic metal particles and graphite pieces were remaining.	Nagasawa et al., 2000
MWNT	Heated at 470°C for 50 min. 6 M HCl for 24 hr and refluxed in 30% HNO ₃ @ 100°C for 10 min. to 20 hr	30 min to 1 hr revealed no effect. Monthieux observed 2-3 M HNO ₃ refluxed for 45 hr converts all SWNT into amorphous carbon. 70% for 24 hr at 25°C makes them partially exfoliated and highly disordered.	An et al., 2004
SWNT	Dry N ₂ /O ₂ – 563 K for 4 hr 35% HCl and 2 M HNO ₃ – 10 min. 3 M HNO ₃ – 24 hr	Sample treated with HCl alone showed better adsorption than the other two samples. The 3M HNO ₃ treated sample showed better adsorption than the 2M HNO ₃ .	Gotovac et al., 2007
SWNT	3 M – 24,45,69 hr Air – 300°C for 1hr Annealed @ 950°C for 10 hr	95% pure samples and 50% removal of carbonaceous material.	Martinez et al., 2003

2.3.4 Characterization of Carbon Nanotubes

As we seen above there are many methods to produce CNTs, but each method produces CNTs with different diameters, lengths, purity, chirality, impurities, pore volume, surface area, and defects. These CNTs could have open or closed ends; after purification, we have yet another new kind of morphology of the raw sample. So characterization of carbon nanotubes is essential for the nano-world to determine the usage of the material for further applications.

There are various techniques to determine the structural and morphological characteristics of CNTs, but only a few of these can investigate properties at an individual nanotube level. Inductively Coupled Plasma-Mass Spectrometry (ICP-MS) is a common analytical technique used to identify the elements (metal impurities) in the carbon nanotubes (Strong et al., 2003 and Ge et al., 2008). A Scanning/Transmission electron microscope (SEM/TEM) and a scanning tunneling microscope (STM) are several of the techniques which can determine the physical properties directly. A SEM/TEM can be used to measure the size, shape, interlayer space and structure of a nanotube. Li et al. (2004) used a HRTEM and found that the average inter wall spacing for SWNTS is ≈ 0.83 nm. HRTEM could also be used to determine the pore size distribution. X-ray photoelectron spectroscopy (XPS) is another technique that can provide information about the chemical structure of the nano-material. It is widely used to compare the structure of the CNTs before after purification and/or interaction with organic/inorganic gases (Droppa et al., 2002). In a research study done to compare the pre-treatment of MWNTs, a high resolution XPS showed that the nitric acid treatment produced COOR and C-OR functional groups, while oxygen plasma produced C=O groups (Xia et al., 2007). Unlike XPS, X - ray diffraction (XRD) is used to obtain information about structural strain, impurities and interlayer spacing. Diameter and chirality distributions could also be determined using an XRD machine. Like XRD, neutron diffraction technique is used to determine chiralities and can be used as a check for the XRD.

There are other spectroscopic techniques like absorption spectroscopy and Raman spectroscopy which are used more globally. Absorption spectroscopies are used for the determination of the purity of the sample. Infra-red spectroscopy specifically reveals the nature of functional groups attached to the CNTs and also their modifications due to any kind of treatment (Hussain et al., 2011). Raman spectroscopy is one of the most powerful and easiest tools for characterization and also is a nondestructive technique. Raman is used to determine the structure of the CNTs and can also explain the defects caused by acid treatment and the surface functional groups attached at these defective sites (Hussain et al., 2011). To determine the purity and degree of change of CNTs with any chemical or physical treatment, a thermal gravimetric analyzer (TGA) or derivative thermal gravimetric (DTG) device are best suited tools. TGA is one technique that has been used to define the thermal stability of MWNTs after oxidation; it has shown that annealed diamond is less stable than oxidized MWNTs (Bom et al., 2002). Determining the surface area of the CNTs is important for comparative studies with commercially available adsorbents. The N_2 -BET (Brunauer Emmett and Teller) surface area is one of the important properties of the CNTs for adsorption studies and also for comparative studies with commercially available adsorbents like activated carbons (Diaz et al., 2007).

2.3.5 Adsorption on to Carbon Nanotubes

Understanding the chemistry behind the adsorption of various organics and toxic pollutants on to carbon nanotubes has been the main focus of recent studies. It is known that physical adsorption is the main type of adsorption of pollutants on to carbon nanotubes. Due to their tubular structure, carbon nanotubes have a large hollow space, which creates inner sites for adsorption. Nano-adsorbents possess high-energy adsorption sites in their interiors (internal pores); due to the curved walls, molecules adsorbed there experience van der Waal's interactions from a greater number of nearest neighbor C atoms (Byl et al., 2003). The interiors are open for adsorption only if the caps are uncapped and the ends are opened (Ren et al., 2000). The exterior surface is open to adsorption unconditionally. Figure 2.6 shows the four

possible adsorption sites in CNT bundles: (1) internal sites: the interior of individual carbon nanotubes; (2) interstitial channels: channels between carbon nanotubes in bundles; (3) grooves: the grooves present on the circumference of the nanotube bundle and the exterior surface of the outermost carbon nanotubes, and (4) outside surface: the curved surface of individual carbon nanotubes on the outside of the nanotube bundles (Ren et al., 2011). For CNTs, the highest energy binding sites are in the grooves and the interstitial sites (Babaa et al., 2004).

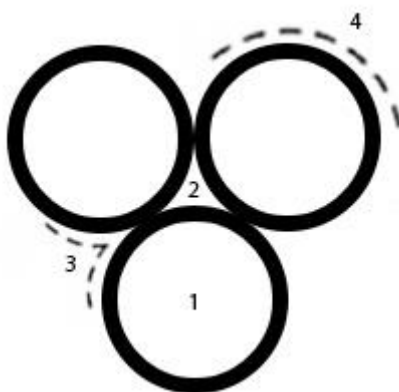


Figure 2.6: Different adsorption sites on a homogeneous bundle of partially open-ended SWNTs. (1) internal, (2) interstitial channels, (3) external groove site, and (4) external surface

2.3.5.1 Adsorption of Organic Vapors onto Carbon Nanotubes

High-energy adsorption sites mean that adsorption capacity for certain pollutants can be increased:

- CNTs have found to have high loading efficiency for anticancer agents like epirubicin hydrochloride (EPI), due to π - π interactions of the carboxylic groups on the MWNTs with EPI, which could form supermolecular complexes and facilitate the adsorbing capacity (Chen et al., 2011).
- CNT have been found to adsorb substantially more NO_x than any other sorbent at room temperature (Long et al., 2001)

- Sorption energy of dioxin onto CNT is 3 times that onto AC and the amount of dioxin adsorbed is 1034 higher, due to strong π - π interactions between the two benzene rings of dioxin and the CNT surface. (Long et al., 2001; WRI 2000)

Other studies have found higher adsorption capacities of CNT compared with AC for pollutants in the liquid phase (Su and Lu, 2007; Lu et al., 2006; Lu et al., 2005). Although several studies have found low adsorption capacities for CNT, these studies did not open the CNT ends to allow pollutants to access interior space for adsorption (Bittner et al., 2003; Diaz et al., 2007).

Aromatic compounds in particular are good CNT adsorption candidates, due to strong π - π coupling of their benzene ring structure with bulk π systems on the CNT surface; the dioxin study cited above is an example of this (Long et al., 2001; Pan and Xing, 2008). Each carbon atom in the cylindrical wall of a CNT has an π electron orbit perpendicular to the CNT surface (Zhou et al., 2001). π - π bonds between aromatic compounds and CNT have been confirmed by experimental data (Lin and Xing, 2008; Chen et al., 2008; Chen et al., 2008). The strength of the bond depends greatly on the functional groups attached to the aromatic benzene ring (Chen et al., 2008).

Adsorption of toluene (Agnihotri et al., 2005; Chin et al., 2010; Su et al., 2010; Chen et al., 2007; Woods et al., 2007; Agnihotri et al., 2005) onto CNT has been conducted; these studies, however, included no comparisons with PAC, as proposed in this study. Only one previous study explored adsorption of water vapor onto SWNTs; however, this study did not conduct any pretreatments nor did a comparative study with other forms of MWNTs or PAC, as proposed in this study.

The adsorption advantage of CNT over traditional AC arises from high-energy binding sites and weak interaction with water, not from greater overall surface area (Pan and Xing, 2008). Nanotube surface areas are typically in the range of 290 ± 170 m²/g (mean \pm standard error) (Cho et al., 2008). By comparison, AC surface areas range from 800-1200 m²/g (Cooper

and Alley, 2002). Organic chemical adsorption onto CNT, however, is comparable to or even higher than that onto ACs (Pan et al., 2008). CNTs have also been shown to have shorter equilibrium times than traditional AC (Lu et al., 2006; Lu et al., 2005; Peng et al., 2003).

CNTs grow in a triangular lattice with narrow intertubular gaps, which limits adsorption on the tubes' exterior and the interstitial sites. Opened CNT would thus be able to adsorb pollutants in their interior and on their exterior (Ren et al., 2011). The ratio of the opened to the closed nanotubes can greatly influence the overall adsorption capacity (Pan and Xing, 2008).

Ji et al. (2000) studied the adsorption properties of tetracycline in aqueous solutions onto MWNTs, SWNTs, AC, and graphite. The results showed the adsorption affinity of tetracycline increased in the order of AC << MWNT < SWNT/graphite. The strong adsorption capacity shown by tetracycline towards SWNTs and graphite could be explained by the strong adsorptive forces like π - π electron-donor-acceptor interactions, Van der Waal's forces, and cation- π bonding.

Ramirez et al. (2004) and Luo et al. (2006) have investigated the effect of physical properties of organic contaminants on their adsorption onto activated carbons with varied morphology. An increased adsorption capacity for activated carbon fiber cloth (ACFC) was observed as the molecular weight and boiling point of a series of ketone compounds increased. Similar enhanced adsorption was observed with a decrease in the ketones' saturation vapor pressure. Nanoporosity of carbon-based adsorbents with different morphologies also impacted the adsorption of organic vapors (Luo et al., 2006). Ramirez determined over 100% larger mass-based adsorption capacity of methyl ethyl ketone when using the more nanoporous ACFC as compared to the less nanoporous coal- (CDAC) and tire- (TDAC) derived activated carbons and carbon nanotubes (CNTs, Figure 2.7A).

However, adsorption capacities for ACFC, CDAC, TDAC and CNT are similar when the adsorption capacity is normalized to the specific surface area of the adsorbent (Figure 2.7B). At relative pressures >0.7 (relative pressure = P/P_0 , P is the chemical's vapor pressure, and P_0 is

the chemical's saturation vapor pressure, Figure 2.7B), CNT nanomaterials exhibited larger adsorption capacities compared to other morphologies of larger particles of activated carbon. CNT had only 45% open-ended carbon nanotubes. This suggests that CNT have the potential for larger adsorption capacities than activated carbon if the number of open-ended CNT is increased. This also suggests enhanced adsorption of ketone compounds as material size falls in the nanoscale range at large and most likely at low relative pressures based on Figure 2.7B. More studies are needed to assess and explain the adsorption mechanisms of air pollutants onto engineered nanomaterials, particularly at pollutant relative pressures >0.7 and <0.004 in gaseous streams.

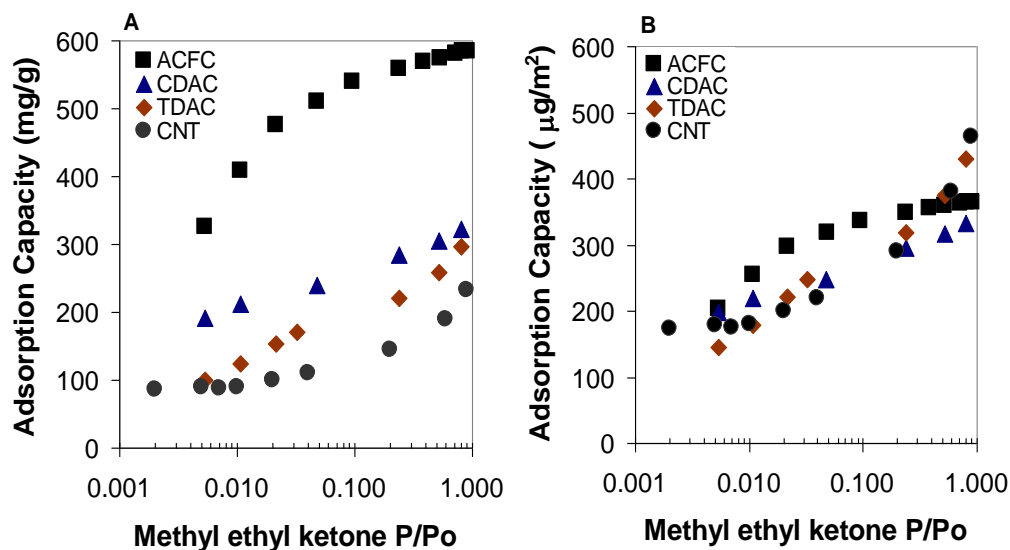


Figure 2.7: Equilibrium adsorption isotherms (A) based on mass, and (B) normalized to surface area (Ramirez et al., 2004)

Chin et al. (2010) studied the adsorption of benzene, toluene and chlorobenzene on SWNTs with and without nitric acid treatment. It was observed that the adsorption of the compounds on treated SWNTs decreased after the treatment due to the addition of oxygen-containing functional groups. The change in the surface chemistry due to the attached functional groups can account for the decrease in the adsorption.

Three synthetic organic compounds (SOCs), phenanthrene, biphenyl, and 2-phenylphenol, were used to study the effects of aggregation and surface chemistry of three different single wall carbon nanotubes (SWNT, SWNT-COOH, SWNT-OH). The specific surface area normalized adsorption values at saturated concentrations showed a reduction in adsorption of SOC on carbon nanotubes (Zhang et al., 2009). The decrease in adsorption could be correlated to the increase in the surface functional groups and surface polarity of the CNTs.

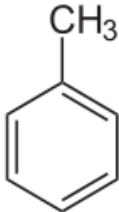
The two studies above address a new issue with adsorption onto carbon nanotubes: any change in the chemistry of the pristine CNTs done for opening pores, increasing the purity and/or adding surface functional groups is not necessarily the best approach for increasing the adsorption of organic vapors on carbon nanotubes.

2.4 Adsorbate

This research developed kinetic curves for the adsorption of toluene on to SWNTs, MWNTs and GAC at room temperature (70-75°F). Equilibrium adsorption capacities and curves of rate of change of concentration are important in adsorption system design. This equilibrium adsorption capacity, multiplied by a factor to account for non-ideal conditions, is used to size the adsorption bed.

Volatile organic compounds (VOCs) contribute to ozone smog formation through reactions with NO_x; form fine particles via reactions with gases such as NH₃, SO₂, and NO_x; and are in many cases listed explicitly as Clean Air Act hazardous air pollutants (HAPs). Toluene, the VOC of interest in this study, is also listed as HAP; it ranks sixth in terms of point source releases and third in terms of fugitive air emissions nationally (USEPA 2011). USEPA's 2011 Toxic Release Inventory reports states that 11.9×10^8 kg of toluene was emitted to the atmosphere. The largest air emissions of toluene occurred were from the printing and publishing (27%), paper (18%), chemicals (16%), petroleum (10%) and plastic and rubber (8%) industries in 2011. Physical properties of toluene are listed in Table 2.4.

Table 2.4: Physical properties of toluene

Characteristic	Toluene	Source
Class	Aromatic	
Molecular Formula	C ₇ H ₈	David 2003
Chemical structure		
Molecular weight (g/mole)	92.13	David 2003
Molecular diameter (Å)	6.95	Reid et al. 1984
Boiling Point (°C)	110.6	David 2003
Dipole Moment (D)	0.375	David 2003
Density at 200C (g/cm ³)	0.866	David 2003
Saturation vapor pressure @ 200C (kPa)	22.0	USEPA 2010
Anthropogenic air emissions (X10 ⁶ kg)	5.3	USEPA 2010

2.5 Summary

Characterization of carbon nanotubes plays a key role in understanding the applications of the nanotubes. Previously many studies have been done which looked at various heat treatments or acid treatments on carbon nanotubes and characterized them to detect and understand the structural transformations in the samples. There were also some studies which looked at the effect of pretreatments on the adsorption capacities and adsorption behavior of the samples. These studies used organic, inorganic compounds, and ions. They were fewer studies which looked at a combination of heat and acid treatments, and most of them worked with one combination of each of the pretreatments. This study looks at various heat and acid treatments to arrive at an optimum treatment condition. Also, this study uses 5 different characterization techniques and also examined the adsorption behavior of the samples. As per

my knowledge, most of the previous studies worked on either the single-walled carbon nanotubes or multi-walled carbon nanotubes; this study included both.

CHAPTER 3

METHODOLOGY

3.1 Sample Description

Three different samples were selected for this study. Two of the samples are the two forms of carbon nanotubes: single-wall carbon nanotubes and multi-wall carbon nanotubes. The third sample is a type of granular activated carbon (GAC). BPL 4X6 is the chosen granular activated carbon for this study. BPL 4x6 is used as the base sample for the comparative study in this work.

3.1.1 Single-wall Carbon Nanotubes (SWNTs)

SWNTs were purchased from Nanostructured & Amorphous Materials (NanoAmor). Houston, TX. These SWNTs are commercially available as purified SWNTs (1-2 nm tube diameter, 5-30 μm tube length) that are manufactured by chemical vapor deposition (CVD). According to the manufacturer, the average outside diameter is 1.1 nm. The produced and purified samples come with a concentration of 90% single-walled carbon nanotubes and the rest non-nanotube material. After production, the carbon nanotubes were processed and purified by the manufacturer. For purification, samples are heated in air at 300⁰C and then followed by acid washing with either HCl or HNO₃, and then the final step is cleaning with a solvent (acetone, ether, and etc.) and hot air drying. A pore special surface area analysis instrument was used by the manufacturer to measure the specific surface area to be 330 m²/g. The elemental analysis done using CHNO/S analyzer (Perkin Elmer 2400 Series II) at the Nanostructured Center of Materials lab at UTA showed that the pristine SWNTs have 90% carbon in them. Figure 3.1 is the scanning electron microscopy image of the SWNTs provided by NanoAmor.

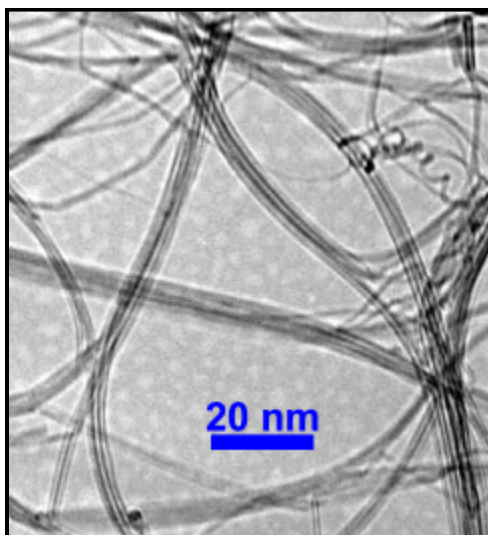


Figure 3.1: SEM image of single-wall carbon nanotubes (Reprinted with permission from NanoAmor, Inc.).

3.1.2 Multi-wall Carbon Nanotubes (MWNTs)

MWNTs were purchased from MER Corporation, Tucson, AZ. MWNTs were manufactured by catalytic chemical vapor deposition (CCVD) using iron as a catalyst. According to the manufacturer, their average outside diameter lies between 110 and 170 nm and inside diameter is between 3-8 nm; their lengths can extend up to 4 to 6 μm . The sample contained more than 90 mass% MWNTs. Like the SWNTs, the MWNTs were also subjected to further processing and purification after production. They were heat-treated at high temperatures to remove the residual iron and anneal the tubes. According to the manufacturer, the final product yielded 97% purity, with 1-2 wt% of graphitic carbon and amorphous carbon and traces of iron. The annealing helped in forming the very ordered graphitic tube structure of MWNTs, as shown in Figure 3.2. The pristine MWNTs are known to have very low surface area, around $13 \text{ m}^2/\text{g}$. The elemental analysis done by CHNO/S analyzer (Perkin Elmer 2400 Series II) at the Nanostructure center for materials at UTA showed that the pristine MWNTs consist of 100% carbon.

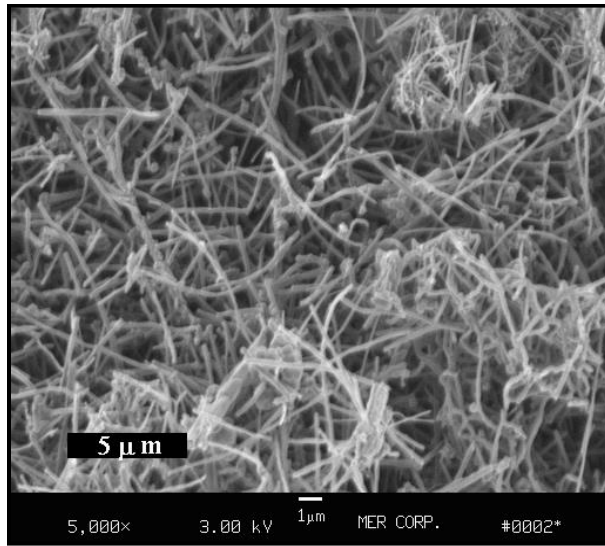


Figure 3.2: SEM image of multi-wall carbon nanotubes (Reprinted with permission from MER Corporation).

3.1.3 Granular Activated Carbon (GAC)

GAC (Figure 3.3) was purchased from Calgon Carbon Corporation, Pittsburgh, PA. It is a bituminous coal based product, activated by steam at high temperatures. It is a type of granular activated carbon used primarily for gas phase applications. It has a strongly adsorbing pore structure which helps in the adsorption of a broad range of contaminants and different levels of concentrations. GAC is preferred when there is a problem with taste and odor control and also for decolorization and separation of components in a flow system (Bansal, 1988; Marsh et al., 2006). Out of its various applications, one of the main is VOC control. Table 3.1 lists the physical properties of GAC, according to the manufacturer.



Figure 3.3: A picture of GAC

Table 3.1: Properties of calgon granular activated carbon (Calgon Carbon Corporation)

Iodine Number	1000 mg/g (min)
Butane Activity, by weight	23.3% (min)
Moisture, as packed by weight	2% (max)
Hardness Number	95 (min)
Apparent Density	0.43 g/cc
Mean Particle Diameter	3.7 mm (min)

3.2 Sample Pretreatment

In the first step of the pretreatment, the SWNTs and MWNTs were heat treated at different temperatures and tested for the optimum heat treatment condition. Then in the second step, a new set of samples was heat treated at the chosen optimum temperature, followed by the chemical treatment. After the chemical treatment, the sample was dried in an oven.

3.2.1 Heat Treatment (HT)

The heat treatment was done on pristine carbon nanotubes. Weight amounts (0.5-1.2 g) of purchased nanotube material was placed in a glazed ceramic boat and was heated in a mini-brute tube furnace (Lindberg, Type TF55035A) in the presence of steam at a heating rate of 20⁰C/min. The steam generation was done by boiling water in a conical flask using a temperature controlled hot plate. A conical flask filled with water was used as a bubbler at the other end of the furnace to make sure a continuous flow of steam was generated. The required

temperature and hold time was entered on to the digital panel of the tube furnace. After the designated time was completed, the steam flow was shut off and the CNTs were cooled in the furnace down to 25⁰C. Once the samples were removed from the furnace, they were placed in a desiccator for complete cooling. Table 3.2 lists the various temperatures and times used for treating the MWNTs and SWNTs. These temperature ranges were chosen based on previous studies (Tsang et al., 1993; Kiang et al., 1999; Hernadi et al., 2001; Bougrine et al., 2001; Yudasaka et al., 2003; Wang et al., 2003). Due to the availability and the expense of the sample only couple of temperatures were tested on the SWNTs as compared to the MWNTs. This heat treatment was used to open more carbon nanotubes and to eliminate any remaining amorphous carbon in the CNTs. Initially only two temperatures (300⁰C and 700⁰C) were chosen for testing of the SWNTs, to see if heat treatment was effective. As surface area results showed that there was no difference observed between those two samples, no further temperatures were tested. Another constraint was that the SWNTs are expensive and we wanted to limit the use of the sample.

Table 3.2: Heat treatment temperature and time of the MWNTs and SWNTs

Sample	Temperature (⁰C)	Time (min)
MWNT	300	60
MWNT	400	60
MWNT	500	60
MWNT	600	60
MWNT	700	60
MWNT	800	60
SWNT	300	60
SWNT	700	60



Figure 3.4: Experimental set-up of the heat treatment

3.2.2 Heat and Acid Treatment (H&AT)

Heat treatment in the presence of steam at 400°C was chosen as the optimum heat treatment condition. A similar procedure of heat treatment was followed as the aforementioned. After completion of the HT, the samples were subjected to acid treatment. SWNTs (1.0 g) were added to 100 ml of nitric acid of two different normalities (3N & 6N), as listed in Table 3.2. Three sets of SWNT-3N and SWNT-6N were sonicated in an ultrasonic bath (Bransonic, 2510R-DTH) for 3, 6, and 10 hr., respectively, as shown in Figure 3.5. Similarly MWNTs (2.0 g) were added to 200 ml of nitric acid of two different normalities (11N & 16N). Three sets of the above mentioned 2 combinations were made and sonicated in an ultrasonic bath (Bransonic, 2510R-DTH) for 6, 9, and 12 hr. These different pretreatment conditions were chosen for SWNTs and MWNTs, depending on work done previously by other researchers. As shown in Figure 3.6, the sonicated HNO_3 suspensions were visually homogeneous. After the sonication, the resulting suspension was centrifuged (Hermle labnet, Z323) and the supernatant was decanted off. After each step of decantation, the CNTs were rinsed with de-ionized water multiple times until the pH of the supernatant solution reached around 7. The pH was tested using litmus paper. After the solution reached a pH of 7, the settled sample was kept in an oven at 80°C for 10 hr. and

after that transferred into a ceramic boat and kept in the oven again at 110⁰C for another 5 hr. to remove any remaining moisture in the treated sample.

Table 3.3: Summary of the weight of the CNTs used, volume and strength of the acid, and the time of treatment of the carbon nanotubes

Type of Sample	Weight of CNTs and Volume of the acid	Strength of the acid (N)	Time of the treatment (hr.)	Sample Notations
SWNTs	1 g in 100 mL	3	3, 6 and 10	SW 33, SW 36, SW 310
		6		SW 63, SW 66, SW 610
MWNTs	2 g in 200 mL	11	6, 9 and 12	MW 116, MW 119, MW 1112
		16		MW 166, MW 169, MW 1612



Figure 3.5: Experimental set up of the nitric acid treatment

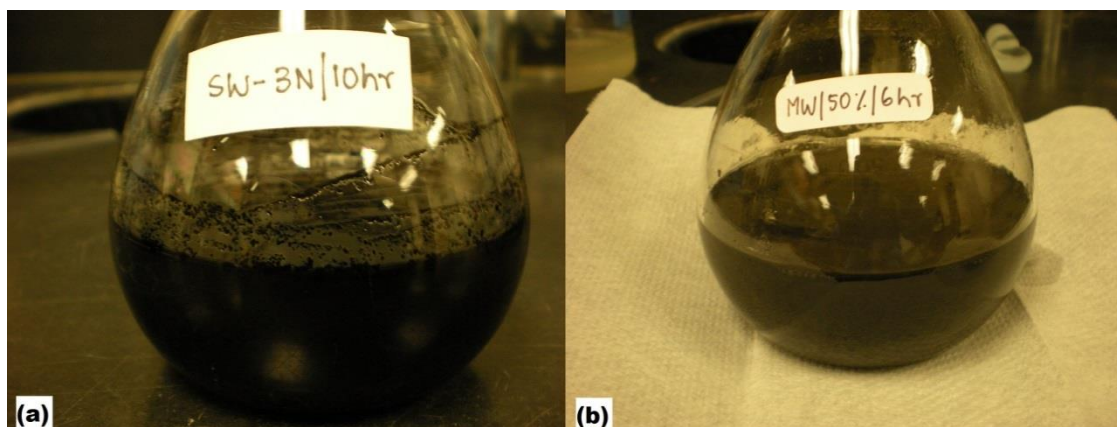


Figure 3.6: Sonicated samples after the acid treatment (a) SWNTs treated in 3N HNO₃ for 10 hr. (b) MWNTs treated in 11N HNO₃ for 6 hr.

3.3 Physical/Chemical Characterization of Samples

Characterization of the nanotube structures was performed by inductively coupled plasma-mass spectrometry (ICPMS), high-resolution transmission electron microscopy (HRTEM), Raman spectroscopy, X-ray photoelectron spectroscopy (XPS), thermogravimetric analysis (TGA), and surface area and pore size analysis. The pristine SWNTs, pristine MWNTs and the heat and acid treated samples were characterized using these techniques. Table 3.4 summarizes the characterization techniques used in this study. As limited time/funds were available for adsorption testing, better understanding of the samples due to the characterization results helped in choosing the preferred samples for conducting adsorption testing.

Table 3.4: Characterizing techniques and their features

Characterization Techniques	Features of Characterizing Techniques
Inductively Coupled Plasma – Mass Spectrometry (ICPMS)	Identifies metal impurities in the samples
Transmission Electron Microscopy (TEM)	Can be used to visually characterize the sample structure and changes induced in the samples with treatment
Raman Spectroscopy	Identifies impurities like amorphous carbon and also the formation of graphitic structures or defects on the treated materials
X-ray Photoelectron Spectroscopy (XPS)	Helps in understanding the surface chemistry by identifying the surface functional groups formed on the carbon nanotubes
Thermogravimetric Analysis (TGA)	Provides a good understanding about the thermal stability of the samples
Surface Area and Pore Size Analysis	Gives information about the surface area and porosity of the sample and also provides information about their pore size distribution

3.3.1 Inductively Coupled Plasma-Mass Spectrometry

Inductively Coupled Plasma-Mass Spectrometry (ICP-MS) is one of the analytical methods with high sensitivity levels developed in 1980's used to determine the minor and major trace elements in materials. It could be used to identify a variety of elements like alkali, alkaline earth elements, transition and other metals, metalloids, rare earth elements, most of the halogens and some of the non-metals. It has become a common laboratory tool for the detection of metal impurities in carbon nanotubes (Source: ICP-MS manual).

In this study a PerkinElmer SCIEX ICP Mass Spectrometer Elan® DRC II available at the UTA's GeoScience Department was used to analyze the raw samples. Both the standards and the samples were analyzed using the ICP-MS. A series of working multiple-element standards, at the concentration of 0, 0.1, 0.5, 2, 10, 40, and 200 µg/L, were prepared from the stock solutions of SPEX CertiPrep (Metuchen, NJ). For standard and sample preparation, the dilute was 1% high-purity HNO₃ (ARISTAR® Ultra, BDH Chemicals, West Chester, PA), using ultrapure water from a water purification system (Element A10 and Elix 10, Millipore, Billerica, MA). The MWNT and SWNT raw samples were analyzed using the ICP-MS. The ICP-MS was operated at a forward power of 1,300 W with argon flow rates of 16, 1.2, and 0.8 L/min, respectively for plasma, auxiliary gas, and carrier gas flows. Meinhard Type A concentric quartz nebulizer, quartz cyclonic spray chamber, 2-mm quartz injector, and platinum sampling and skimmer cones were used for sample introduction and analyses. A solution containing 5 ppb of internal standard elements ⁶Li, ⁴⁵Sc, ¹¹⁵In, and ²⁰⁹Bi was introduced on-line to spike the standard and sample, which was analyzed for 5 replicates with a dwell time of either 10 ms (for minor and trace elements) or 1 ms (for major element) and 20 sweepings per reading.

3.3.2 Transmission Electron Microscopy

Transmission electron microscopy (TEM) was the first kind of electron microscopy to be developed. It works exactly like a light microscope, but uses electrons instead of light. The main advantage of using an electron microscope over a light is that the limitation on the wavelength

due to the light source is completely over-ruled by the use of electrons as a “light” source. The possibility of a 1000 times better and a 0.2 nm resolution makes a TEM a highly valuable tool for characterization in the medical, biological and materials research fields. (Source: Mongillo, 2007).

TEM is used to characterize the structure and type of the carbon nanotubes (Aqel et al., 2012) and also to study the interlayer spacing in the MWNTs (Kiang et al., 1998). TEM (Figure 3.7) uses a high energy electron beam, which travels through the vacuum in the column of the microscope. Electromagnetic lenses are used to focus the electrons into a thin beam and pass the beam through the sample holder which has the specimen of interest. Depending on the sample density and porosity, the electrons are scattered. Another set of electromagnetic lenses are used at the bottom of the microscope to focus the scattered electrons and to project the image of the specimen onto a fluorescent screen. The captured image is actually a shadow image representing the sample in varied darkness, depending on its density. The operator can study it directly or can photograph the image and save it for future use.

In this study an H-9500 high-resolution transmission electron microscope (HRTEM) that is available at the UTA Characterization Center for Materials and Biology was used to analyze the nanotube samples. This electron microscope uses a 300kV electron source and has a resolution of 1.8 Å. The size of the condenser aperture is 50 µm and the objective aperture size is 150 µm. The samples were prepared by dissolving the carbon nanotubes in acetone followed by sonication for 15 min. A Cu-Cu grid was used as a sample holder and was dipped in the sonicated dispersion. Once the specimen is prepared, it is introduced in to its slot in the HRTEM machine and is ready for analysis.

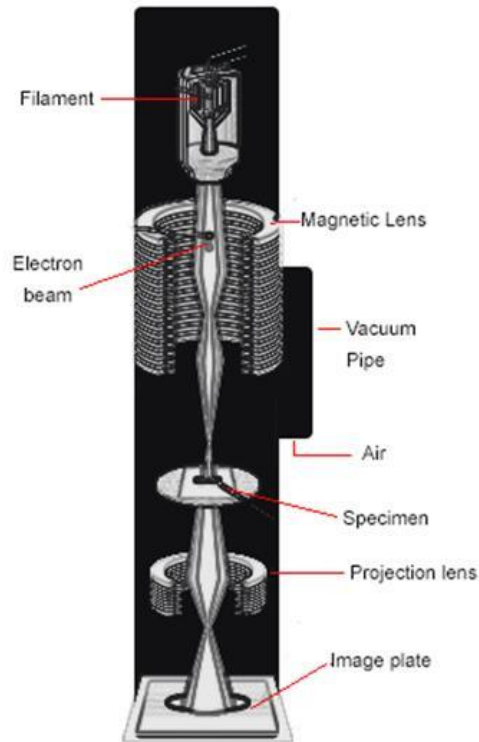


Figure 3.7: A schematic outline of a TEM

3.3.3 Raman Spectroscopy

Raman scattering works on the principle of inelastic scattering of light. When a beam of light hits a sample, an electron is excited. The electron in its excitation state absorbs photons and as it is relaxing it emits the photons back. Some photons are inelastically scattered at a wavelength (Raman scattering) different from the Rayleigh scattering wavelength. Raman spectra for the scattered photons have smaller energy than those of the phonon of the incident photon. The phonon frequencies of the material are obtained by developing a plot of the intensity of the scattered light versus the amount of energy loss of the scattered light (Source: Dresselhaus et al., 2004).

Raman spectroscopy is a powerful tool used to characterize carbon nanotubes. It can be used to explore the electronic structure and other physical properties like purity, crystallinity,

diameter, and structural changes due to any treatment of the carbon nanotubes (Rinzler et al., 1998; Kim et al., 2006). In a Raman experiment as shown in Figure 3.8, a sample is illuminated using a monochromatic light. The incidental photons are scattered at the user-defined wavelength and the energy of the scattered photons is used to create (Stokes) or destroy (anti-stokes) vibrations in the sample. The scattered light is collected on a charged-couple device (CCD) detector which shows the Raman scattering spectra (Source: Website of Cornell Center of Materials Research).

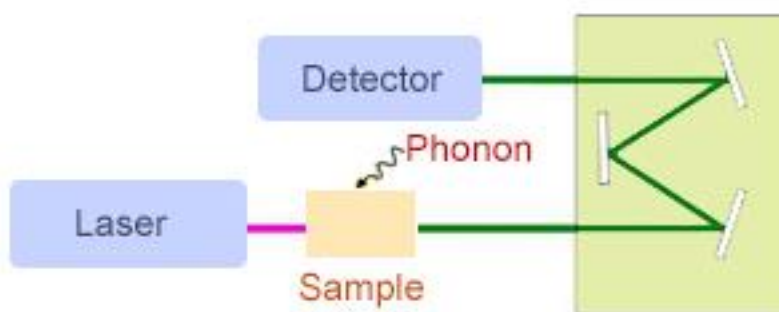


Figure 3.8: Absorption and scattering of light in a Raman scattering spectra

In this research, the CNTs and the GAC were characterized using a Horiba Jobin Yuon LabRam Aramis Raman Spectrometer ($\lambda = 633 \text{ nm}$) at the Center for Nanostructured Materials at UTA. There is no sample preparation for analysis with Raman spectroscopy. A few specks of the sample to be analyzed are placed on a glass slide and then placed under the incident monochromatic beam for analysis.

3.3.4 X-ray Photoelectron Spectroscopy (XPS)

X-ray photoelectron spectroscopy is based on the concept of the photoelectric effect. The sample is irradiated with low energy x-rays; the surface atom absorbs the energy of the x-ray photon. If high enough photon energy is absorbed, then the electron is emitted from the surface with a kinetic energy that can be related to the binding energy of that electron. Hence,

the binding energy of the electron of a certain atom can be used to distinguish the peaks in the spectrum (Source: Website of West Virginia University).

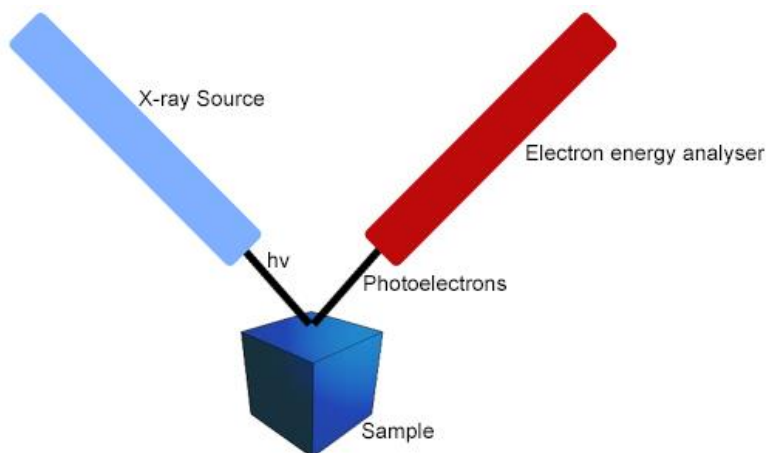


Figure 3.9: A schematic outline of the X-ray Photoelectron Spectroscopy

XPS is a technique mainly used to characterize the surface chemistry with the capacity of determining the impurities in the sample. In this study, a Kratos Axis Ultra X-ray Photoelectron Spectrometer at the Center for Nanostructured Materials at UTA was used for characterizing the CNTs and the GAC. Survey scans were run between 15 eV and 1200 eV at 1 second dwell time and 160 eV pass energy. High resolution scans were run at various energies depending on the element and were run at 0.1 second dwell times and 10eV pass energy. A neutralizer may have been used occasionally for charge balance.

3.3.5 Thermogravimetric Analysis (TGA)

Thermogravimetric analysis is a study done to discern the thermal stability of a material caused due to change in temperature. In this process the change in weight of the sample is monitored with the change of temperature in a controlled manner. TGA measures the increase or decrease in weight due to decomposition, oxidation or dehydration with the heating or cooling of the sample in a thermogravimetric analyzer (Source: Website of Perkin Elmer).

The thermal stability testing helps in understanding the changes that occurred during processing of a material in certain controlled conditions. For instance, it works easily to analyze the relative changes in carbon nanotubes after heat or acid treatment. It also helps in accounting for the degree of purity in the sample. In TGA, a sample pan along with a reference pan is used in a precision balance. In a typical run, sample (1 to 4 mg) was placed in the sample pan that was assembled in a vertical electric furnace. Research grade air and nitrogen gases at a flow of 100 ml/min were used as the combustion gases during the air and nitrogen testing runs respectively. 10⁰C/min was used as the heating rate and the testing was done up to 1000⁰ C for both the gases. A plot of weight loss% versus temperature is plotted to analyze the stability of the sample.

In this study, the materials of interest were analyzed using a SDT Q600 V20.9 Build 20 thermogravimetric analyzer available in the UTA's Chemistry Department. There was no sample preparation required for this analysis.

3.3.6 Surface Area and Pore Size Analysis

Nitrogen (N₂) adsorption testing and analysis is known to be a sensitive technique to better understand the pore size distribution, pore structure and surface area of various porous materials. In this study, adsorption surface area, porosity, total pore volume, and micro and mesopore volume and area of CNTs and GAC were measured by nitrogen adsorption isotherm data at 77K by the BET method (Gregg and Sing, 1995; Webb and Orr, 1997) following ASTM D 4820-95 procedure using a high-speed surface area and pore size analyzer (Quantachrome, NOVE 2200e). N₂ is known to be a common gas for such analysis. Figure 3.10 shows the high-speed surface area and pore size analyzer used in this study, which is at the Department of Environmental Engineering, Texas A&M University-Kingsville.



Figure 3.10: Experimental set-up of the surface area analyzer

3.3.6.1 Nitrogen Adsorption Testing

All the samples with and without pretreatment were analyzed for their N_2 adsorption properties. They are two main steps in the N_2 adsorption testing: (1) degassing (2) analyzing. In the degassing step, the samples were vacuum degassed at 200°C for 2 hours to make sure the sample was free from any adsorbed vapors, gases or even any moisture. This temperature depends on the sample and its thermal stability. It is known that at higher temperatures the sample could have changes in its structure and cause some additional changes in the sample which are not wanted. After degassing, the samples are analyzed by cooling the samples to 77 K by ultra-high purity N_2 (99.99% UHP N_2 , Matheson Tri-Gas, Inc.).

3.3.6.2 BET Surface Area

The Brunauer-Emmett-Teller (BET) method was used to calculate the surface area of the sample from the adsorption testing experiments. It uses a multi-point BET equation shown

below in equation 3.1 to deduce the surface area of the sample (Source: Nova Operational Manual).

$$\frac{1}{W((P_0/P)-1)} = \frac{1}{W_m C} + \frac{C-1}{W_m C} \left(\frac{P}{P_0}\right) \quad (3.1)$$

Where:

W = weight of the nitrogen gas adsorbed

P/P₀ = relative pressure

W_m = weight of monolayer of adsorbate

C = is the BET constant which indicates the strength of the adsorbent/adsorbate interactions

A plot of 1/[W(P₀/P)-1] vs (P/P₀) is generated, which is a straight line. The adsorption isotherm data best fits the points in the confined area which has a P/P₀ range of 0.05 to 0.35. The slope (s) and the intercept (i) of the linear plot are used to calculate the weight of the monolayer (W_m) (Source: Nova Operational Manual).

$$W_m = \frac{1}{s+1} \quad (3.2)$$

Using the weight of the monolayer of the adsorbate (W_m) value as calculated by equation 3.2, the surface area of the sample is calculated as shown in equation 3.3.

$$S_t = \frac{W_m N A_{cs}}{M} \quad (3.3)$$

Where:

S_t = total surface area

N = Avogadro's number (6.023 x 10²³ molecules/mol)

A_{cs} = cross-sectional area of nitrogen (16.2 Å²)

M = molecular weight of nitrogen

After the calculation of the total surface area, the specific surface area is calculated using equation 3.4 (Source: Nova Operational Manual).

$$S = \frac{S_t}{w} \quad (3.4)$$

Where:

S_s = specific surface area

w = weight of the sample

3.3.6.3 Total Pore Volume and Average Pore Radius

Total pore volume is obtained from the amount of vapor adsorbed at $P/P_0 \approx 1.0$. Nitrogen is the adsorbate used for filling the pores of the sample material. It is assumed that at $P/P_0 \approx 1.0$, the pores are completely filled with nitrogen. This assumption helps in determining the total pore volume of the sample. The pore volume along with the pore geometry of the sample helps in determining the average pore width. If the pore is assumed to be cylindrical then the average pore radius can be calculated using equation 3.5 (Source: Nova Operational Manual).

$$d_p = \frac{4}{S} \left(\frac{P_a V_{ads} V_m}{R T_a} \right) \quad (3.5)$$

Where:

d_p = average pore radius

P_a = ambient pressure (atm)

V_{ads} = volume of gas adsorbed at $P/P_0 \approx 1.0$ (cm^3/g)

V_m = bulk molar volume of N_2 ($34.7 \text{ cm}^3/\text{mol}$)

S = BET surface area

R = universal gas constant

T_a = ambient temperature (K)

3.3.5.4 Pore Size Distribution

The pore size distribution is the pore volume distribution with respect to their pore width. The Barrett, Joyner and Halenda (BJH) method was used to compute the mesopore size distribution for the carbon nanotubes and the GAC. The mesopore size adsorbents are solids with particles having pores ranging between 20 Å - 500 Å (Heinsohn and Kabel, 1999). Adsorption onto mesoporous solids is defined by a dual step process: formation of an adsorbed layer on the pore walls and capillary condensation. The pore size distribution in the BJH method is known to be better described by the desorption step than the adsorption step of the isotherm. The desorption part of the isotherm is known to have a true thermodynamic stability, as it adsorbs the same amount of the adsorbate at a lower relative pressure compared to the adsorption isotherm (Barrett et al., 1951). The equations used to develop the BJH pore size distribution are shown below in equations 3.6, 3.7, and 3.8.

$$V_{pn} = \left(\frac{r_{pn}}{r_{kn} + \frac{\Delta t_n}{2}} \right)^2 (\Delta V_n - \Delta t_n \sum_{j=1}^{n-1} A c_j) \quad (3.6)$$

$$r_k = \frac{4.15}{\log(P_0/P)} \quad (3.7)$$

$$c = \frac{\bar{r}_p - \bar{t}_r}{\bar{r}_p} \quad (3.8)$$

Where:

V_{pn} = volume of the largest pore

r_{pn} = actual pore radius

r_{kn} = radius of the condensate capillary

Δt_n = change in thickness of the physically adsorbed layer

Δv_n = amount of gas adsorbed after lowering in P/P_0

A_p = area of the pore exposed after the lowering in P/P_0

t_r = thickness of the adsorbed layer

r_p = kelvin radius of the capillaries emptied of their condensate averaged for radii corresponding to the lower and upper limits of P/P0

3.4 Adsorption Testing

A bench-scale adsorption system was designed for conducting the adsorption testing. The bench-scale setup consists of gas generation system, an adsorption bed and a gas detection system, as shown in Figure 3.11. The gas generation system consists of compressed ultra-high purity nitrogen (UHP-N₂, Matheson Tri-gas) as the carrier gas, a syringe pump (Model NE-300, New Era Pump Systems Inc.) that injects toluene in to the carrier gas stream, a flow meter (FL-2060, Omega) to measure and control the volumetric flow rate of the gas stream, and a mixing chamber which allows for homogeneous mixing of toluene and the carrier gas. The adsorption bed contains the adsorbent (raw or pretreated SWNTs/MWNTs or GAC). The gas detection system includes a gas chromatography-flame ionization detector (chromaFID C31022, American Ecotech) to assess the pollutant concentration. The inlet concentration of toluene during the purge and the exit concentration of toluene during the adsorption step were measured by the gas chromatography-flame ionization detector (GC-FID).

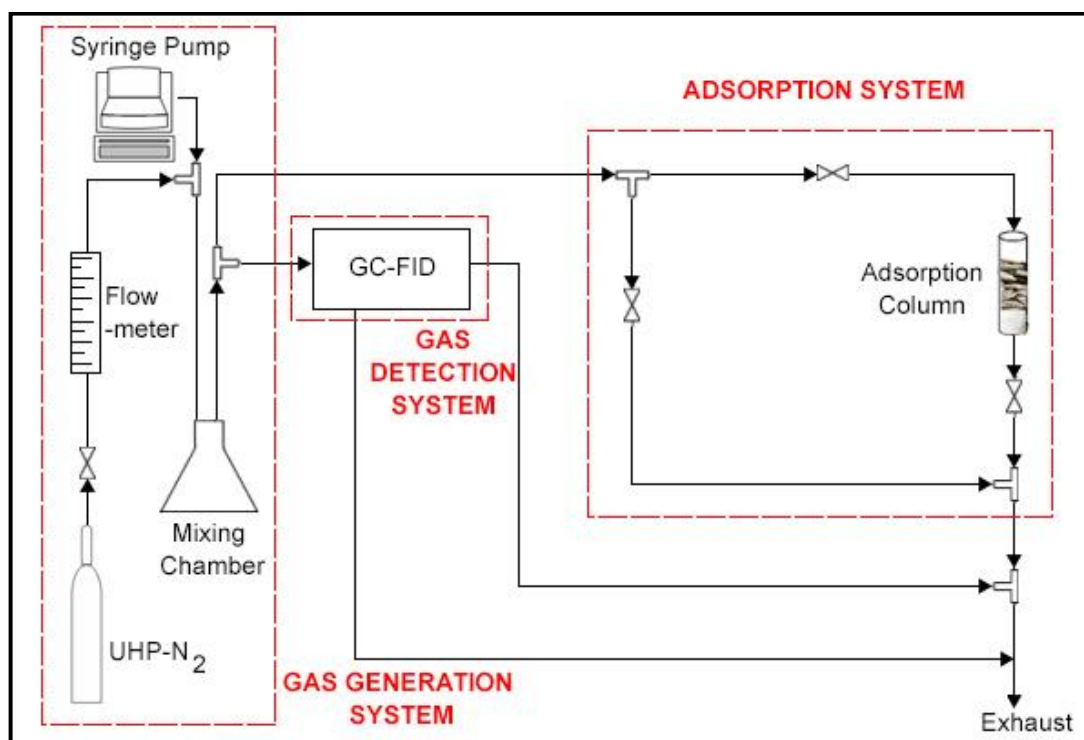


Figure 3.11: Schematic of a bench scale adsorption system

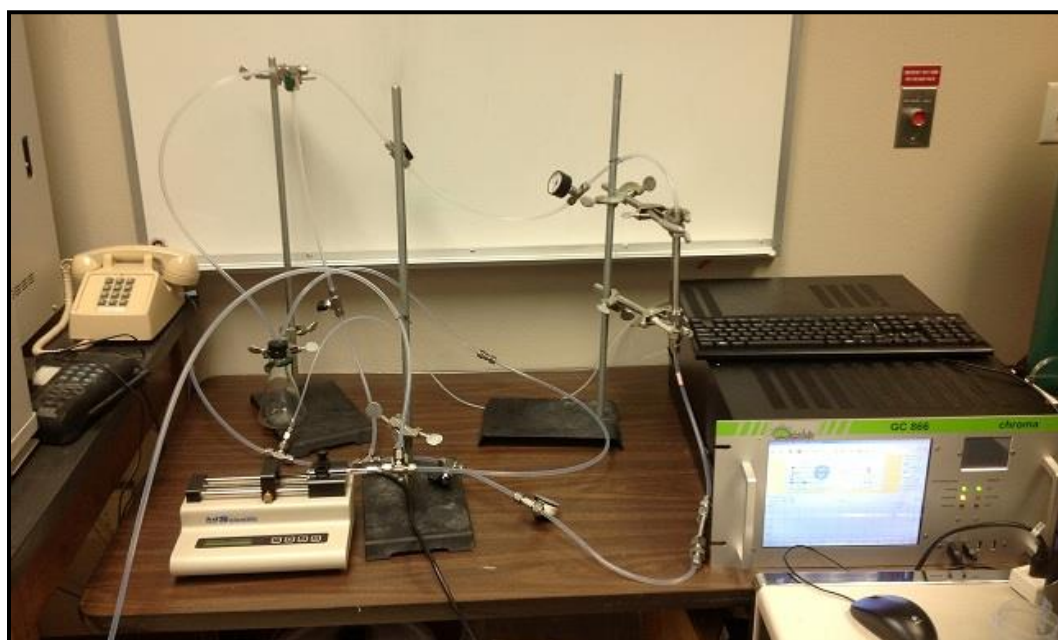


Figure 3.12: Experimental set-up of the adsorption testing in the lab

The general configuration of the apparatus to test the CNTs and GAC in fixed-bed toluene adsorption experiments is depicted in Figure 3.12. In the gas generation system, ultra-high purity nitrogen (Matheson, 99.999% pure) was used as the carrier gas with a flow rate of 0.2 Lpm, and flows through a pressure regulator and a volumetric flow meter (FL-2060, Omega). Liquid toluene was injected into a UHP-N₂ stream using a hypodermic needle, a syringe (25 ml, Hamilton) and a syringe pump (Model NE-300, New Era Pump Systems Inc.). The flow rate of liquid toluene was set at 0.01 ml/hr to achieve the required final inlet concentration (225 to 260 ppm) of toluene in to the adsorption column. Before the adsorption process was started, purging was done for at least 60 min to verify a steady and uniform inlet concentration of toluene upstream. After the 60 minutes, the valves to the adsorption column were opened and the valves through the purge were closed. Toluene was passed through a mixing chamber before the gas stream entered into the bed to achieve a homogeneous mixing of nitrogen and toluene. The mixed gas was sent into the adsorption bed, which was made of stainless steel (grade 304). Glass wool was used as the packing material at the bottom of the adsorption bed to prevent channeling. The concentration of the vapor at the outlet of the vessel was continuously monitored with the GC-FID. Adsorption was conducted until the saturation of the adsorbent was observed.

3.4.1 Data Collection and Analysis

Breakthrough, time series and kinetic curves were plotted with the obtained inlet and outlet concentrations of toluene during the adsorption testing. It is a common practice to fit a model to the data obtained from these curves and determine model parameters to design a commercial adsorbent column in future. Adsorption capacity (q) and equilibrium rate constant (k) are two such parameters which help in designing and characterizing the performance of a system. The breakthrough curves are C/C_0 vs. t/t_{50} plots, whereas kinetic curves are C/C_0 vs. time plots. C is the outlet concentration at any given time t ; C_0 is the inlet concentration of the adsorbate at $t=0$; t is the adsorption time; and t_{50} is the time when the outlet concentration is

50% of the inlet concentration. Breakthrough curves can also be used to calculate the total mass of toluene adsorbed at equilibrium (Sullivan et al., 2004).

Mass of adsorbed toluene and equilibrium adsorption capacity can be calculated using equations 3.9 and 3.10, respectively.

$$m_{total} = \sum_{t=0}^{t=t} Q\rho \times \left(\frac{C-C_0}{C} \right) \times t \quad (3.9)$$

$$q_e = \frac{m_{total}}{m_{adsorbent}} \quad (3.10)$$

Where:

m_{total} = total mass of toluene adsorbed

Q = toluene injection rate (0.2 ml/hr)

ρ = density of toluene (92.14 g/mol)

C_{in} = inlet concentration of toluene

C_t = outlet concentration of toluene at time t

t = time at which the concentration is C_t

$m_{adsorbent}$ = mass of adsorbent used in the adsorption column

In order to understand the mechanism of sorption and the limiting rate controlling steps involved in the sorption studies, a few existing kinetic models have been used to fit the experimental data. The pseudo-first order model (PFOM) first represented by Lagergren has been a widely-used kinetic model. It was used in the study by Lagergren for the sorption of oxalic acid and malonic acid on to charcoal (Lagergren, 1898). Trivedi et al. (1973) in his study for the sorption of cellulose acetate from chloroform on to calcium silicate first applied the PFOM. Several studies have used the PFOM since its first development.

The pseudo-first order model can be represented as shown below in equation 3.11 and the linear form of the equation can be represented by equation 3.12.

$$\frac{dq_t}{dt} = k_1 (q_e - q_t) \quad (3.11)$$

$$\ln(q_e - q_t) = \ln q_e - k_1 t \quad (3.12)$$

$$q_t = q_e * \exp(-k_1 t) \quad (3.13)$$

Where:

q_e = amount of toluene adsorbed at equilibrium (mg/g)

q_t = amount of toluene adsorbed at any time t (mg/g)

k_1 = equilibrium rate constant for pseudo-first order (min^{-1})

t = adsorption time (min)

Previous works have shown that the pseudo first-order equation does not give a good fit for the whole range of the experimental data of the sorption process (Ho and Mckay, 1998). So to get a good fit and to model the kinetics, a trial and error method is required to determine the equilibrium adsorption capacity, q_e . The non-linear regression form of the pseudo-first order equation shown in equation 3.13 is used for calculating the parameters (q_e and k_1).

CHAPTER 4

RESULTS AND DISCUSSION

4.1 Sample Physical/Chemical Characteristics

4.1.1 Inductively Coupled Plasma-Mass Spectrometry

ICP-MS results showed the presence of metal impurities like Fe, Na, and trace amounts of Mg, Zn, Ni, Co, and Al in raw SWNT samples. The MW raw samples also shows presence of metal impurities like Na, Zn, Al, Fe and minor amounts of Ni, Co and Mg. Si has also been noticed as one of the main sources of impurity in both the SW and MW raw samples. In this work there were 3 batches of SWNT and 2 batches of MWNT ordered. The characterization was done for one batch of each. It was assumed that the other batches would contain similar amounts of metals. The initial amount of sample used was unknown, hence the amount of metal impurities were not normalized. Table 4.1 lists the metals and non-metals present in the raw SW and MW samples.

Table 4.1: ICP-MS results for SW and MW raw samples

ppb (parts per billion)	Fe	Na	Si	Mg	Zn	Ni	Co	Al
SW raw	1358	836	139	69.1	55	30	5	1.6
MW raw	81	646	296	29.4	122	2	1	115

4.1.2 Transmission Electron Microscopy

TEM images showed that the pristine samples of SWNTs and MWNTs had a mixture of metal catalysts, amorphous carbon and carbon nanotubes. Figure 4.1 shows the TEM images of SWNT aggregates without any pretreatment; (a) shows the SWNTs at high resolution, while (b) shows the same with a low resolution. Disordered carbon and spherical nanoparticles of Fe or Fe-C coated with graphene layers and with a diameter of several nanometers were observed in the aggregates. SWNTs have regular black circular spots (indicated by green arrows) in

Figure 4.1b, showing the presence of carbon-coated metal catalysts like Fe, and less dark irregular spots (indicated by blue arrows), showing presence of amorphous carbon. Figure 4.2 shows the TEM images of the MWNTs, (a) high resolution, and (b) low resolution. MWNT images show the nanotube diameter distribution and demonstrate that, in contrast to SWNTs, these MWNTs do not associate in bundles. Figure 4.3 is the TEM image of the GAC. Unlike the carbon nanotubes we can observe the GAC has relatively large particles with fractal-like shape. It can also be noticed that GAC does not have different types of adsorption sites like the carbon nanotubes, which is one main difference between the activated carbon and carbon nanotubes.

The structural transformation in the SWNTs induced by the purification process can be observed by the TEM images shown in Figure 4.4. We can observe in Figure 4.4a and 4.4b the corrugation of the tube walls, indicating defects caused by acid treatment, while in Figure 4.4c and 4.4d, we can locate bundles of SWNTs. Unlike the others, Figures 4.4e and 4.4f show more crystalline graphene structure, but generation of amorphous carbon (indicated by blue arrows) due to the harsh nitric acid treatment can also be observed.

Similar to the SWNTs, slight changes in the structure of the MWNTs could be observed with purification in Figure 4.5. From visual inspection, it appears that increase in the acid treatment time thinned and shortened the MWNTs. This could be confirmed using measurements from the images. Comparing 4.5c and 4.5f, we can observe that more damage is done to the MWNTs treated with 16N nitric acid than the 11N nitric acid. It is known that shorter and thinner CNTs have lower quality, with less desirable mechanical and transport properties (Wang et al., 2003). All the above conclusions were made after viewing at least 10 – 15 TEM images of each treatment condition for the SWNTs and MWNTs. To draw quantitative conclusions from these images, software like Threshold Image could be used.

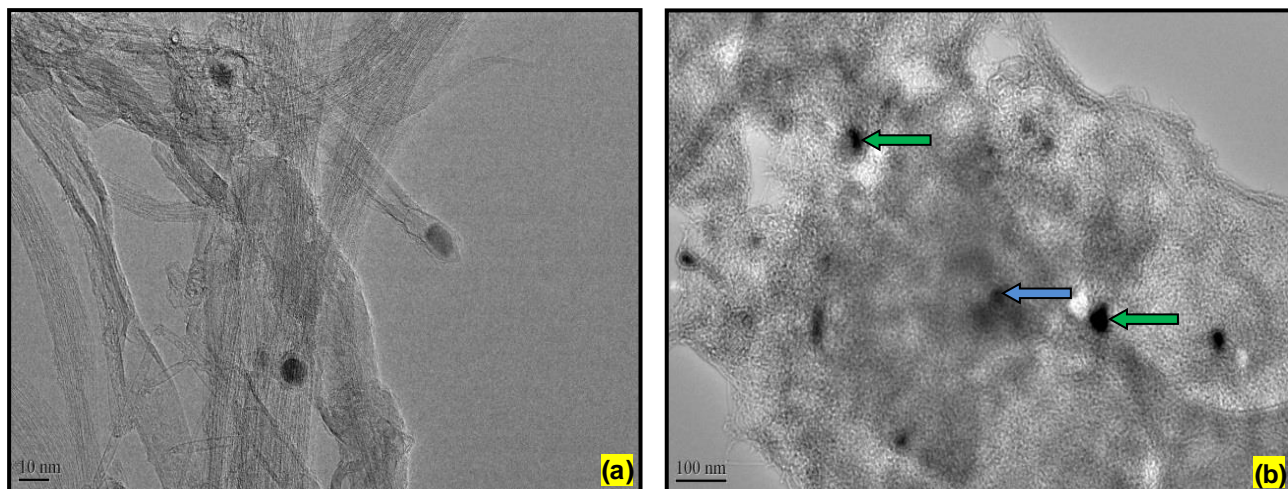


Figure 4.1: TEM images of SWNTs pristine sample at (a) high and (b) low resolution

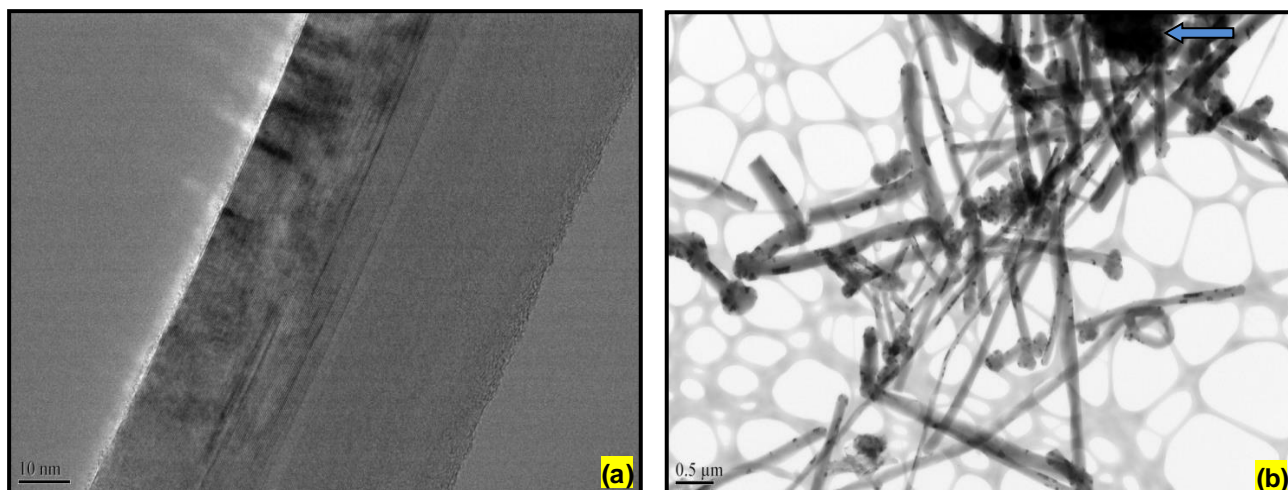


Figure 4.2: TEM images of MWNTs pristine sample at (a) high and (b) low resolution

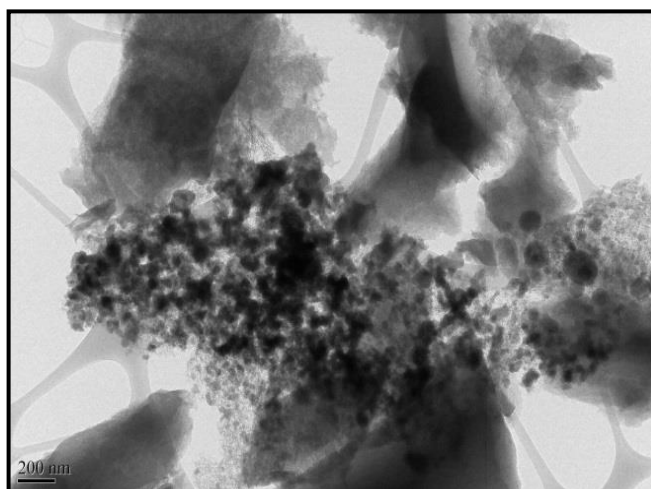


Figure 4.3: TEM image of GAC

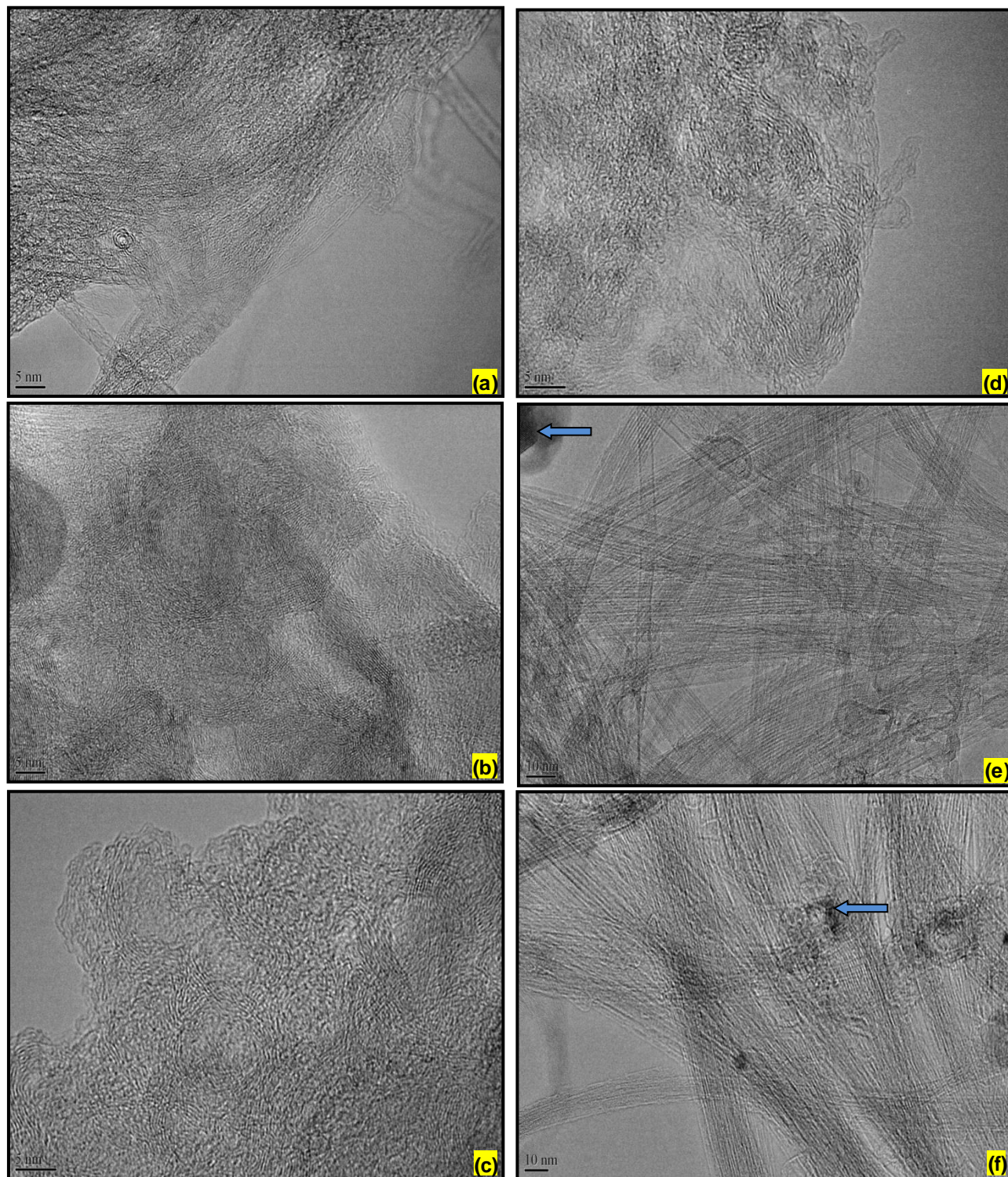


Figure 4.4: TEM images of the purified SWNTs (a) SW 33 (b) SW 36 (c) SW 310 (d) SW 63 (e) SW 66 (f) SW 610

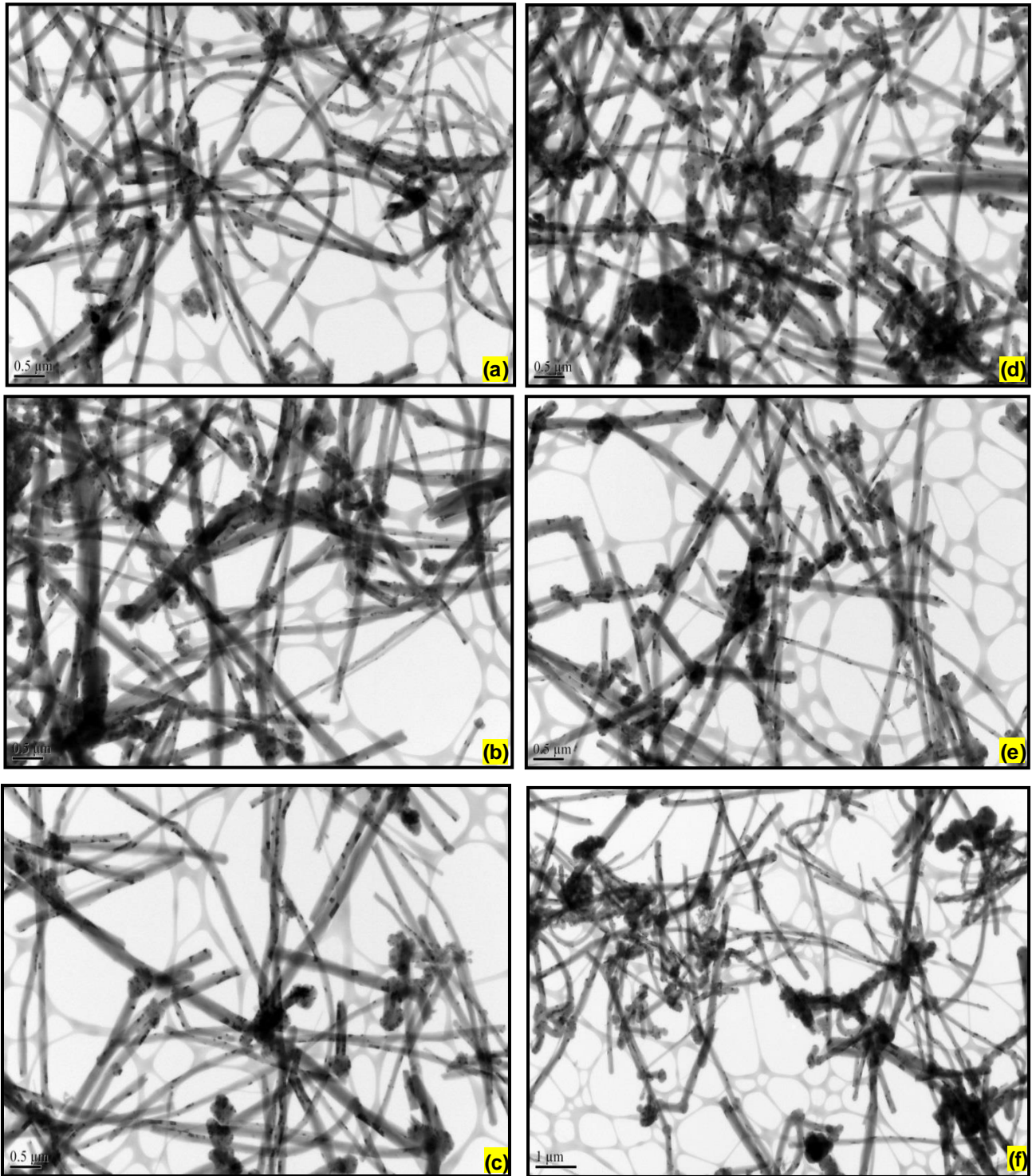


Figure 4.5: TEM images of the purified MWNT sample (a) MW 116 (b) MW 119 (c) MW 1112 (d) MW 166 (e) MW 169 (f) MW 1612

4.1.3 Raman Spectroscopy

The Raman spectra of the pristine SWNTs, MWNTs and GAC are shown in Figure 4.7. Raman spectra for the carbon nanotubes consist of two different kinds of bands, a D-band around 1350 cm^{-1} and a G-band at $1500\text{-}1600\text{ cm}^{-1}$. The D-band signifies the presence of amorphous or non-nanotube graphitic carbons, while the G-band depicts the in-plane stretching of the carbon-carbon bonds in the graphene structure. The D-band is around 1320 cm^{-1} for the carbon nanotubes and at 1366 cm^{-1} for GAC, showing the presence of amorphous phase in the nanomaterial and GAC.

Figure 4.6a and 4.6b show the trend of the I_G/I_D in the SWNTs and MWNTs, and Table 4.2 summarizes the I_G/I_D (Intensity of G band/Intensity of D band) ratio values calculated from the spectroscopy results obtained during the measurements. A high I_G/I_D ratio indicates less amorphous carbon, and thus fewer defects in the sample. The SWNTs treated with 3N HNO_3 show an increasing ratio with time, whereas the SWNTs treated with 6N did not follow a trend (the highest ratio was for 3 hours of treatment). For the MWNTs, the 11N raw sample showed the highest ratio, while the 16N showed a decrease in ratios with increasing treatment time.

The D-band in Figure 4.8a flattened as the treatment time increased from 3 hours to 10 hours when the SWNTs were treated with 3N nitric acid, showing complete removal of amorphous carbon. The results as shown in Figure 4.8b are exactly opposite when the SWNTs were treated with 6N nitric acid, which supports the results from the TEM images showing the regeneration of the amorphous carbon, or in other words increases of the content of disordered carbon. The ratio of the intensity of G to D band increases with refluxing time for 3N treated samples of the SWNTs, indicating structural deformation in the tubes of the nanomaterial. The G band in the MWNTs is known to be not as evident as it is for the SWNTs (Moon et al., 2001). The D-band at 1280 cm^{-1} (Figure 4.9) in the MWNTs is moderately intense and broader than in the SWNTs, which is a characteristic of MWNTs. Due to this nature of the D-band in MWNTs, it

is hard to analyze presence of amorphous material, but MW 169 shows no peak around 1280 cm^{-1} , indicating complete removal of impurities.

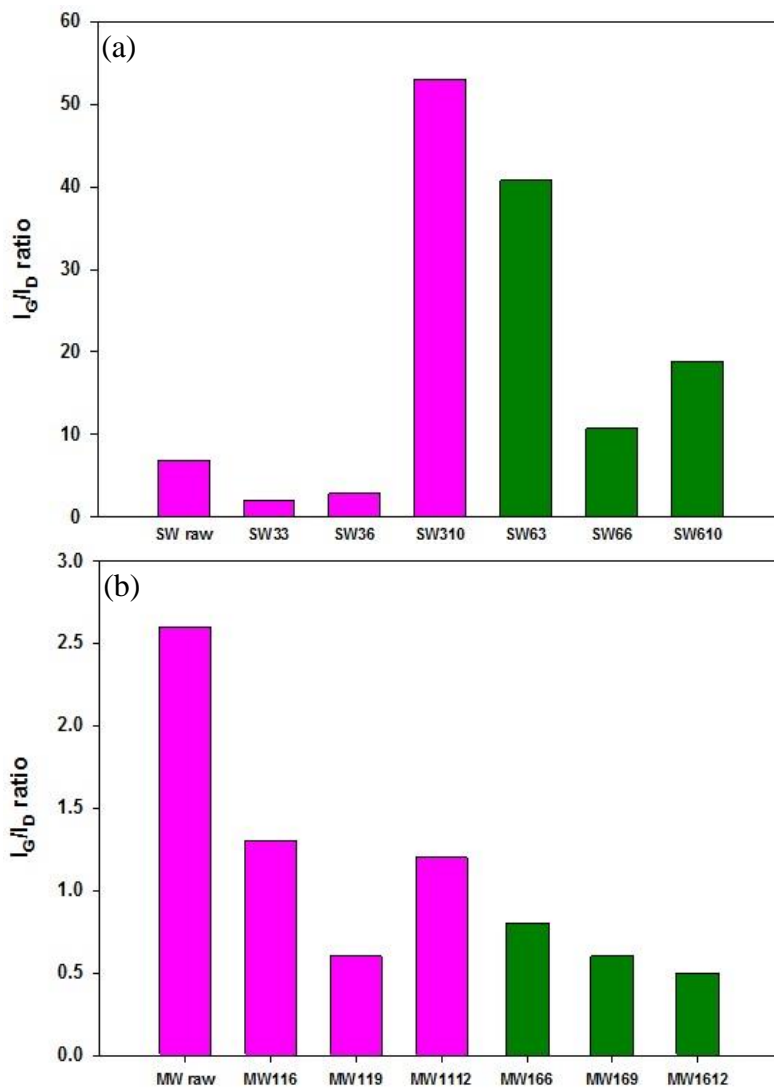


Figure 4.6: I_G/I_D values plots for (a) SW raw and treated samples (b) MW raw and treated samples

Table 4.2: I_G/I_D ratio of the pristine and purified carbon nanotubes and GAC

Sample Name	I_G/I_D	Sample Name	I_G/I_D
GAC	26.5	MW raw	2.6
SW raw	6.9	MW 116	1.3
SW 33	2.0	MW 119	0.6
SW 36	2.9	MW 1112	1.2
SW 310	53.0	MW 166	0.8
SW 63	40.8	MW 169	0.6
SW 66	10.7	MW 1612	0.5
SW 610	18.8		

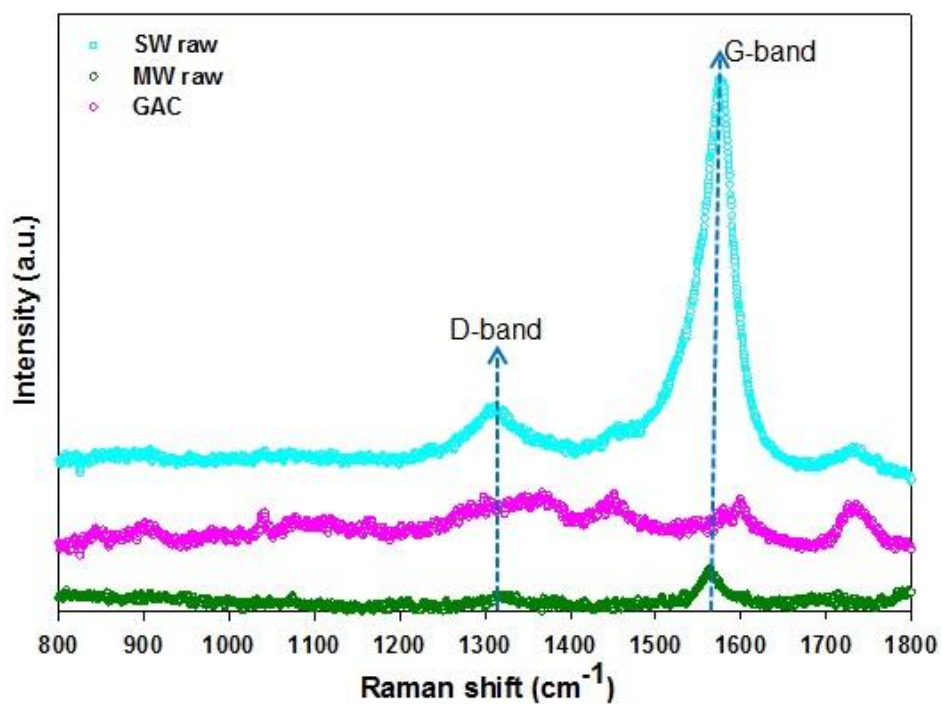


Figure 4.7: Raman spectra of the pristine samples of SWNTs, MWNTs and GAC

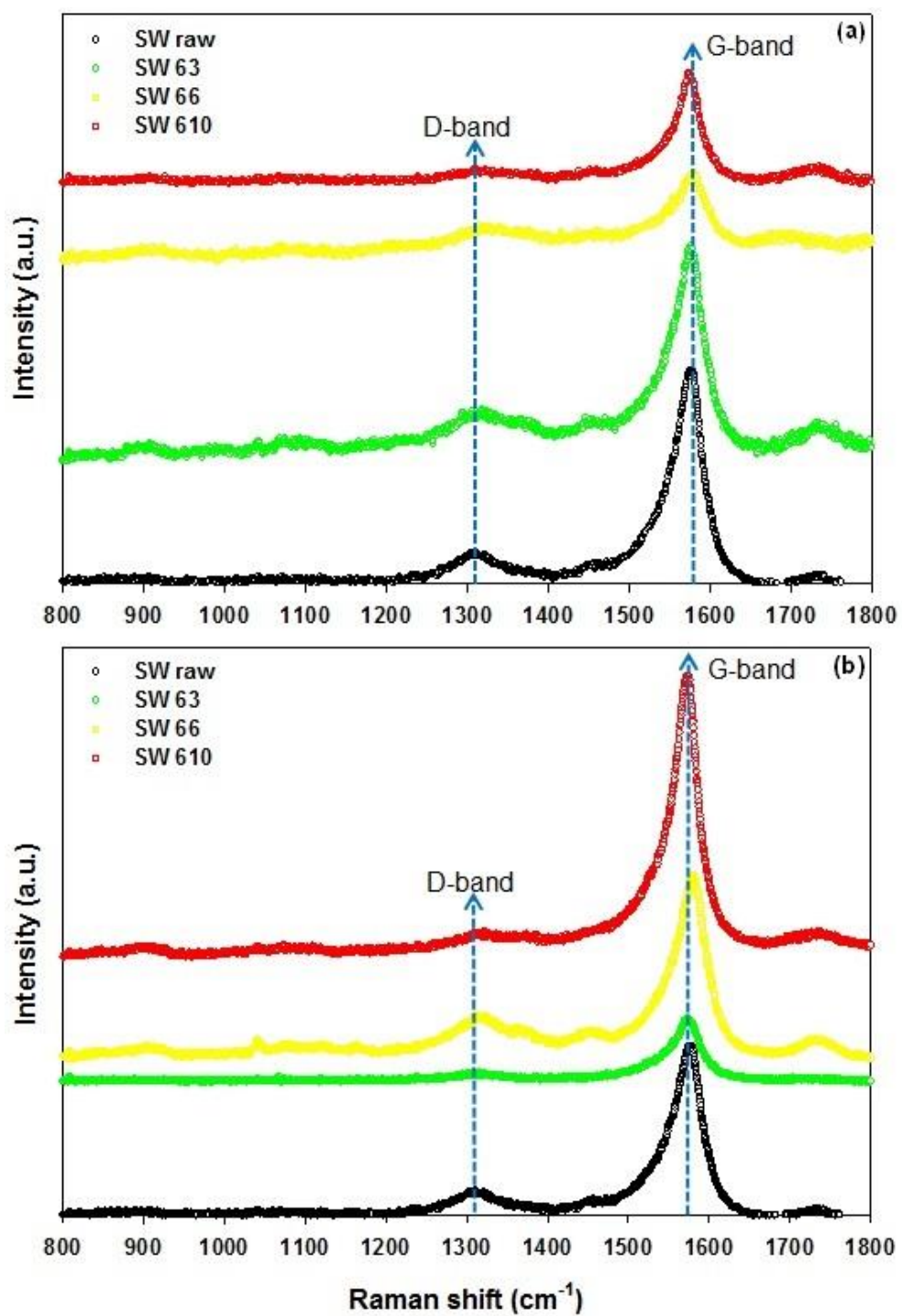


Figure 4.8: Raman spectra of samples (a) SW raw, SW 33, SW 36, SW 310 (b) SW raw, SW 63, SW 66, SW 610

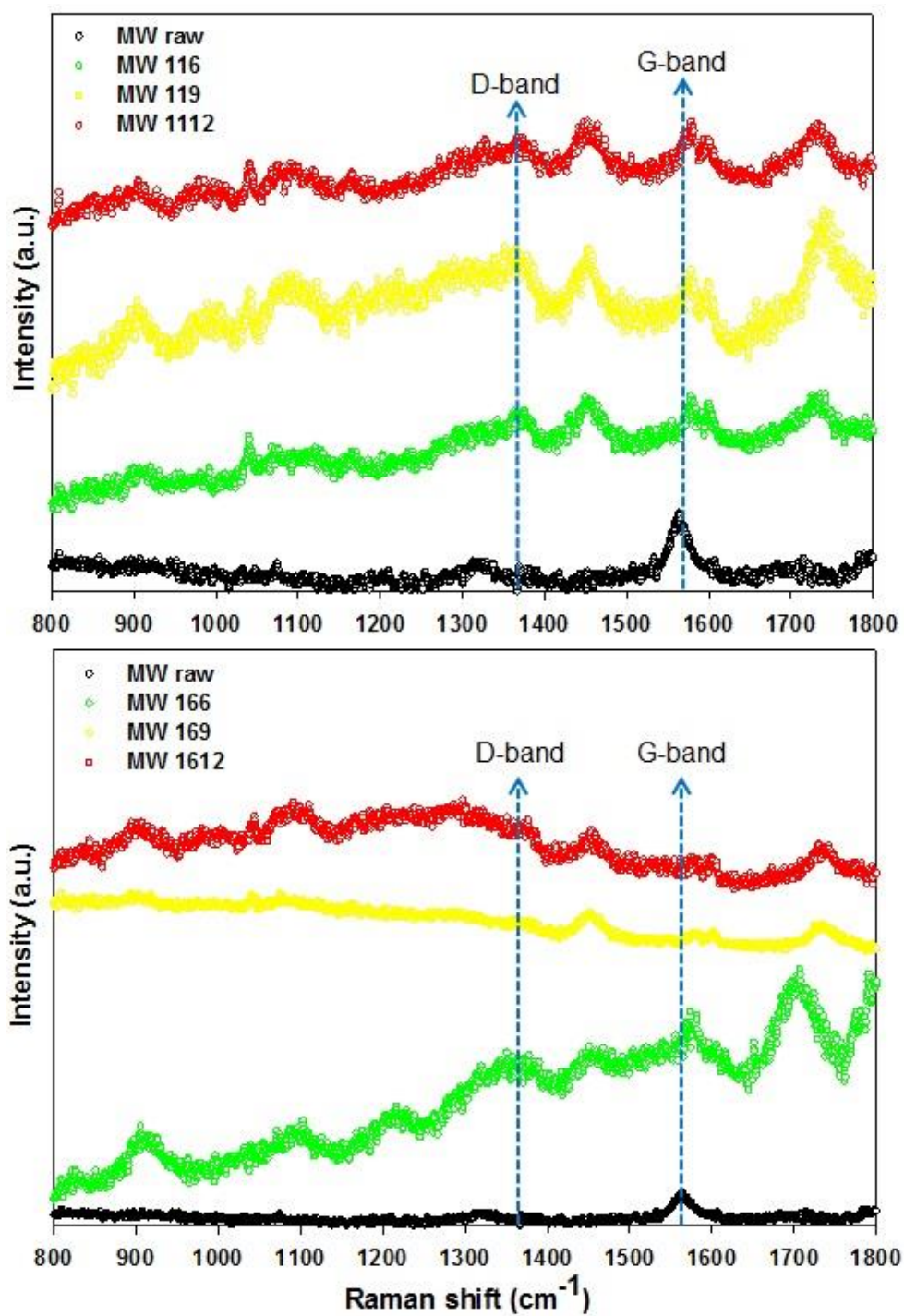


Figure 4.9: Raman spectra of samples (a) MW raw, MW 116, MW 119, MW 1112 (b) MW raw, MW 166, MW 169, MW 1612

4.1.4 X-ray Photoelectron Spectroscopy (XPS)

The X-ray photoelectron spectroscopy records the XPS spectra of carbon C1s core levels, bringing insight into the type and nature of the surface functional groups. We can mainly observe two kinds of peaks in the XPS spectra: one is a long peak, which is the photoemission peak, and another which is lower in intensity and broader, which is caused by the inelastic scattering. Figure 4.10 shows the XPS spectra of carbon C1s core levels of raw SWNTs, raw MWNTs and GAC. In this we can observe a peak at around 284 eV, which corresponds to sp^2 hybridization of graphene sheets in carbon nanotubes; and this is also the main peak in activated carbon. For all the plots, an inset of the figure amplifies the intensity scale, which helps in better identifying the peaks.

Figure 4.11 shows XPS spectra for the SWNT following treatment. In the inset of Figure 4.11a, we can observe a peak for the alcohol/ether group (C-O) around 286.2 eV for both SWNTs treated with 3N HNO_3 for 3 and 6 hours, but this peak is not available for the 10 hour treated sample. Raw SWNTs have a carbonyl group (287.5 eV); the presence of a carbonyl group could be attributed to the pretreatment done by the manufacturer. Figure 4.11b shows the carbonyl group attached to SWNTs treated with 6N HNO_3 for 6 and 10 hours, but not on the one treated for 3 hours. The peak around 286 eV can also be attributed to sp^3 hybridized carbon; this carbon can also be attributed to the presence of amorphous phase or damaged carbon. Due to this overlap, attributing this peak is difficult.

As for surface functional groups, the treated MWNTs did not show any substantial difference compared to the pristine sample, except for the one sample treated with 16N HNO_3 for 9 hours shows a peak at 287.3 eV (carbonyl group), as shown in Figure 4.12.

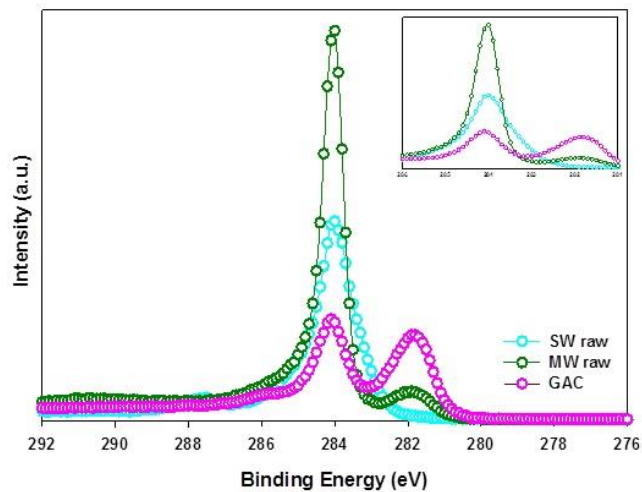
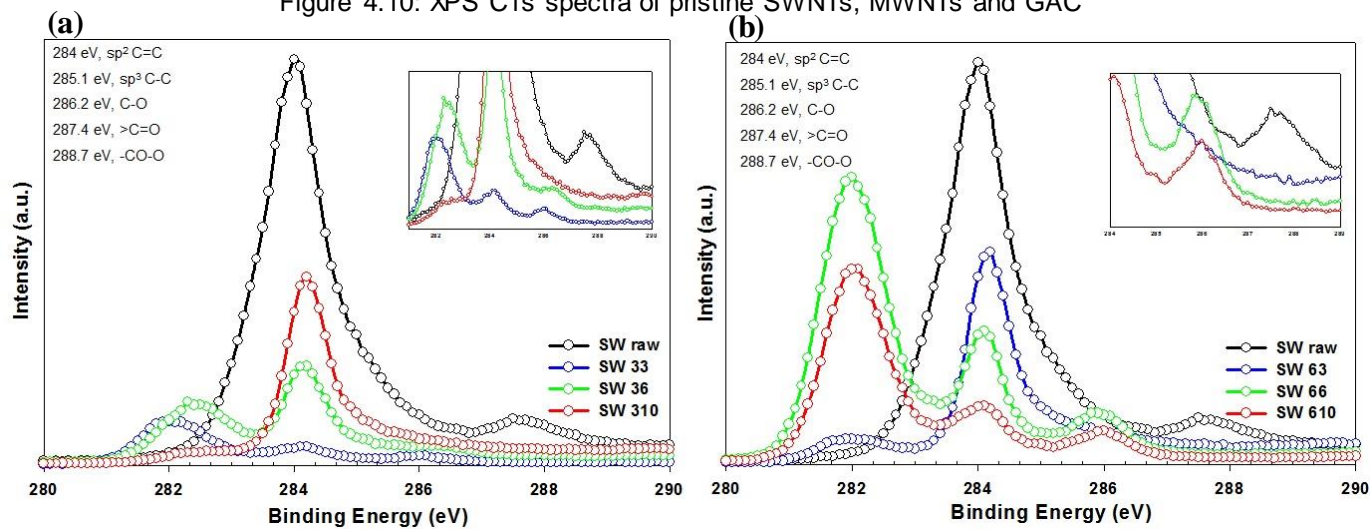


Figure 4.10: XPS C1s spectra of pristine SWNTs, MWNTs and GAC

Figure 4.11: XPS C1s spectra after the purification process (a) SWNTs treated in 3N HNO₃ (b) SWNTs treated in 6N HNO₃

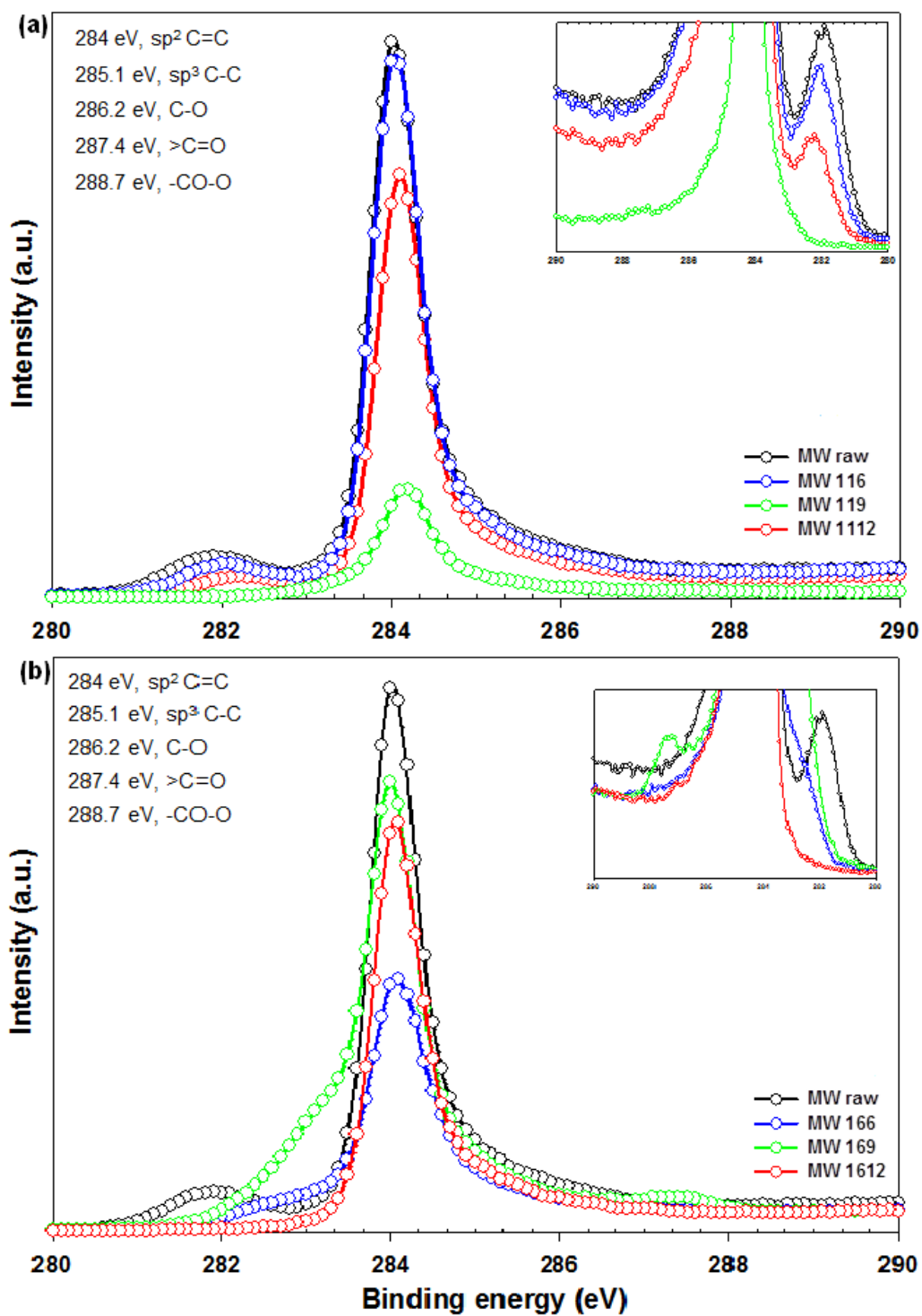


Figure 4.12: XPS C1s spectra after the purification process of (a) MWNTs treated in 16N HNO₃
 (b) MWNTs treated in 16N HNO₃

4.1.5 Thermogravimetric Analysis (TGA)

To assess the extent of purification of the samples, thermogravimetric analysis was done on the pristine and purified samples. Plots of weight loss % against temperature were used to identify the main weight loss regions during the whole combustion process. The weight loss derivative ($-dw/dt$) curve depicts the onset of thermal events with the change of temperature. Weight loss % curves shown below have three main regions of combustion. The first region is due to the removal of any adsorbed moisture and also removal of surface functional groups formed due to acid treatment (Datsyuk et al., 2008). The second region is a steep fall in the curve is due to the combustion of the carbon nanotubes. The final region is attributed to combustion of any other material present in the sample.

Figure 4.13 shows that the MWNTs burned off at a higher temperature (760°C) than GAC (620°C) and the SWNTs (480°C). According to Figure 4.14, the SWNTs showed greater thermal stability after purification, burning off at a higher temperature; however, there was not a huge difference among the various treatments. All of the peaks for SWNTs after treatment with nitric acid have moved to a higher temperature compared to the raw sample, indicating the partial removal of the metal impurities. SWNTs treated with 3N nitric acid for 3 hours had the least amount of sample (0.6 wt%) remaining at the end of combustion, showing that this sample is the most purified sample.

According to Figure 4.15, the MWNTs showed less thermal stability after purification, burning off at a lower temperature; however, there was not a huge difference among the various treatments. In all of the treated MWNT samples, the weight of sample remaining after 1000°C was lower than the weight remaining for the un-treated sample, showing a higher carbon content in the treated samples. Table 4.3 shows the weight % of the samples remaining after the TGA experiment. For MWNTs, for most of the samples there was no sample remaining after the TGA testing.

Table 4.3 Weight% of the samples remaining after TGA

Sample Name	Wt. %	Sample Name	Wt. %	Sample Name	Wt. %	Sample Name	Wt. %	Sample Name	Wt. %
GAC	4.6	SW 33	0.65	SW 63	4.8	MW 116	8.7	MW 166	0
SW raw	16.8	SW 36	3.7	SW 66	2.3	MW 119	0	MW 169	0
MW raw	6.7	SW 310	6.8	SW 610	1.2	MW 1112	0	MW 1612	8.4

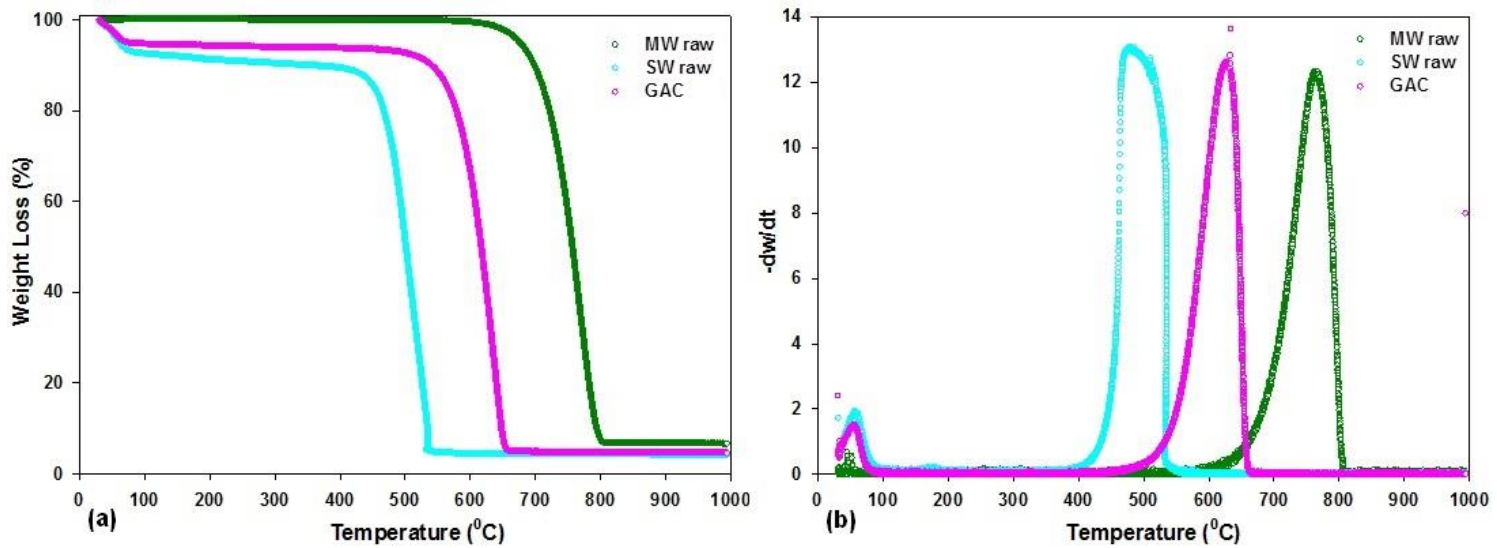


Figure 4.13: Thermogravimetric analysis plots of SW raw, MW raw and GAC (a) Weight loss curves of the raw sample (b) First derivative plots of the raw samples

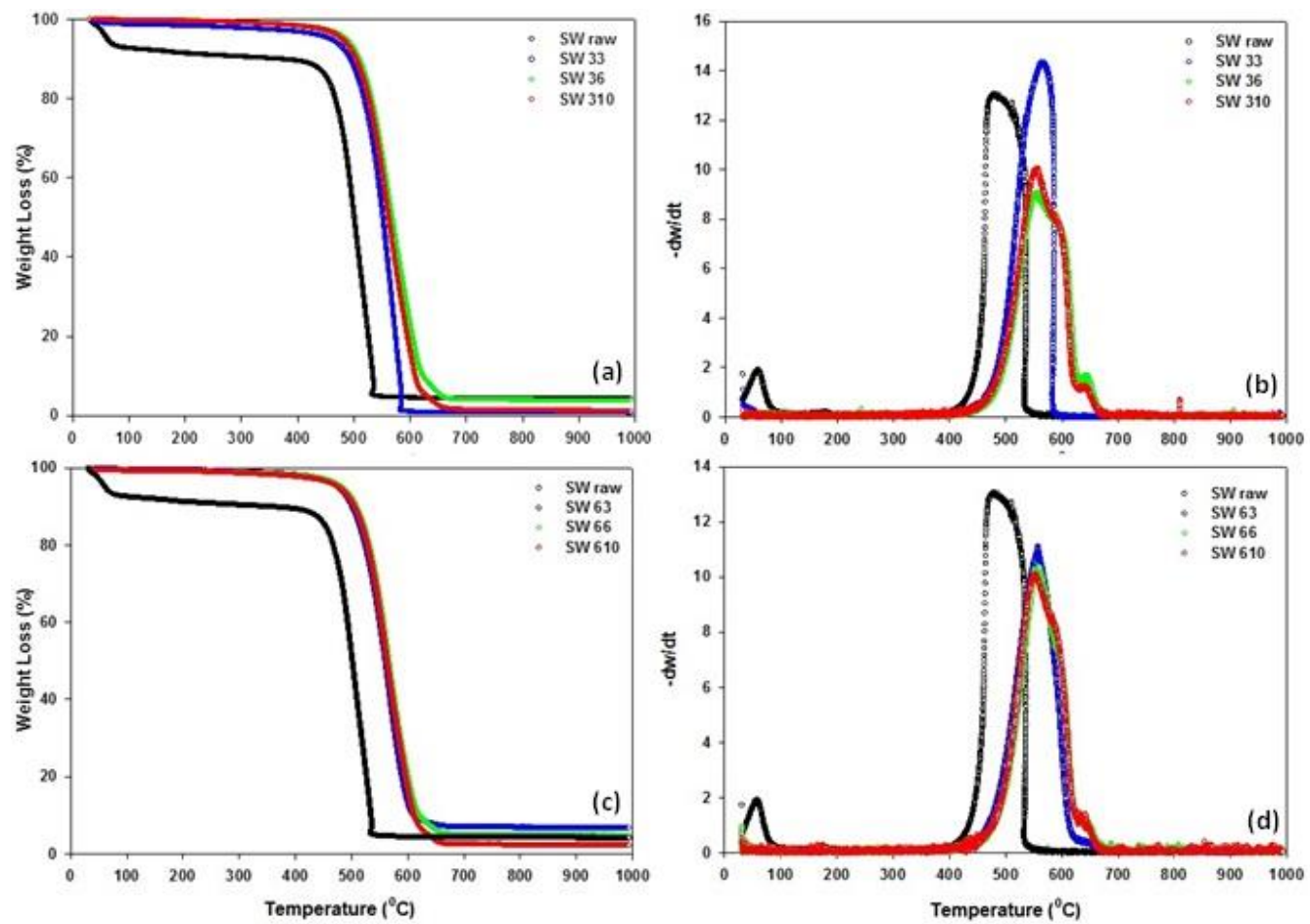


Figure 4.14: Thermogravimetric (a) Weight loss curves and (b) First derivative plots of SW raw and 3N acid treated samples and (c) Weight loss curves and (d) First derivative plots of SW raw and 6N acid treated samples

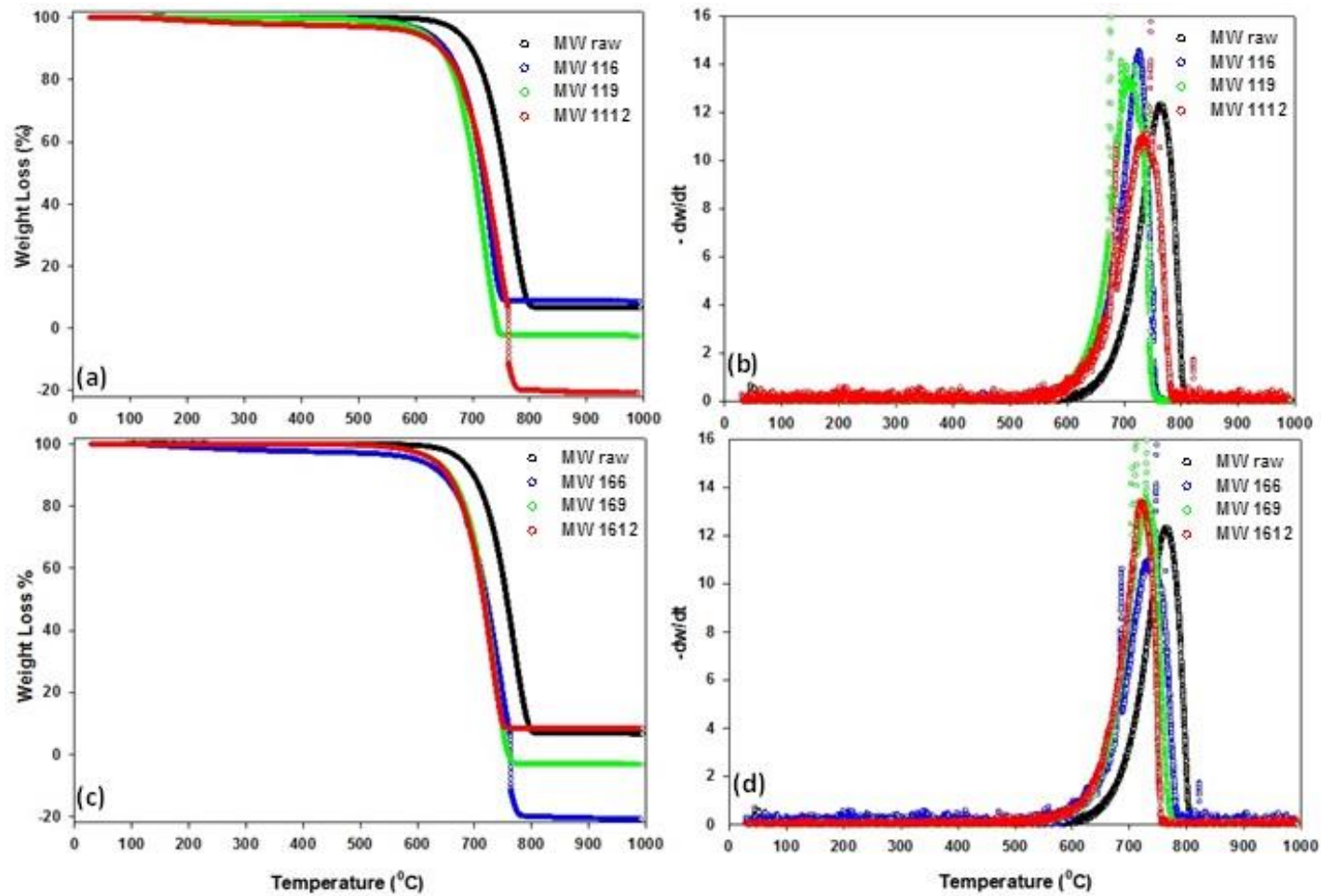


Figure 4.15: Thermogravimetric (a) Weight loss curves and (b) First derivative plots of MW raw and 11N acid treated samples and (c) Weight loss curves and (d) First derivative plots of MW raw and 16N acid treated samples

4.1.6 Surface Area and Pore Size Analysis

Physical activation process conditions and physical properties of the SWNTs, MWNTs, and GAC are provided in Table 4.4. Surface area and pore volume were determined from the N₂ adsorption isotherms using the BET method at 77 K. Pore size distributions were plotted for both the raw and purified samples and analyzed to characterize the porosity of the samples.

The surface area and porosity (Table 4.4) of the MWNTs and SWNTs after heat treatment were very similar to the surface area of the CNTs with no pretreatment. Considering these results, we concluded that there was no effect on the CNTs due to this heat treatment alone; windows to the interior space were not opened. So, for the heat and acid treatment we choose 400^oC as our heat treatment temperature for both SWNTS and MWNTs, as it is the temperature which could oxidize amorphous carbon in the sample (Colomer et al., 1998 and 1999; An et al., 2004; Hu et al., 2003).

According to Table 4.4, the SWNTs pristine sample had a surface area of 1136 m²/g; 5 out the 6 purified samples had surface areas between 897 – 1076 m²/g, which were lower than the pristine sample. Only the SW 33 had a higher surface area (1347 m²/g) than the pristine sample; TGA testing showed the SW 33 sample to have the lowest amount of impurities. The complete removal of impurities indicates the higher percent of carbon nanotubes available for adsorption, shown by the higher purity levels of SW 33 sample in the TGA testing is justified with the surface area analysis experiment. According to the right-hand columns in Table 4.3, the micropore volumes for the SWNT samples are greater than the mesopore volumes, showing the microporous nature of the SWNT samples (Appendix B6).

According to Table 4.4, there is no substantial change in the surface area or the porosity of the MWNTs with purification. According to the right-hand columns in Table 4.4, the mesopore volumes for the MWNT samples are greater than the micropore volumes. The MWNTs adsorption isotherms are Type II, showing them to be meso-porous adsorbents and the V-t plots (Appendix B7) agree with the adsorption isotherms.

In the micro-pore size distribution (Figure 4.16a), we can observe a peak for the raw sample of SWNTs and GAC at 10 Å and 6 Å, respectively. In the meso-pore size distribution (Figure 4.16b), only the MWNTs have a peak at 25 Å, while the other two samples do not have any peak as they are micro-porous adsorbents.

Comparing Figure 4.17 and 4.18, we can observe SW 33 sample shows higher adsorption in microporous region, while the rest of the samples exhibit the same trend as the raw samples. There has been no major change in the samples with acid treatment and that once again has been shown by the surface area pore size analysis experiments. The insets of Figures 4.19b and 4.20b show that there is a slight change in the peaks of the purified MWNTs compared to the pristine sample, but the change is relatively small and likely not substantial enough to impact the sample's overall physical and chemical properties.

Table 4.5 provided at the end of this section summarizes the characterization results for the treated SWNTs and MWNTs.

Table 4.4: Process conditions and physical properties of the carbon nanotube samples and GAC

Sample Name	Heat Treatment Temperature/ Conc. of HNO ₃	Time Treated	N ₂ - BET Surface Area	Average Pore Size	Total Pore Volume at P/P ₀ = 0.99	Mesopore Volume (20 - 500 Å)	Micropore Volume (< 20 Å)
	^o C/N	(hours)	(m ² /g)	(Å)	(cc/g)	BJH method (cc/g)	DA method (cc/g)
GAC	None		818	170	0.46	0.062	0.446
SW raw	None		1136	197	1.08	0.663	0.871
HEAT TREATMENT							
SW	300	1	1183	41	1.11	0.627	0.932
SW	700	1	1182	41	1.05	0.554	0.884
HEAT AND ACID TREATMENT							
SW 33	3	3	1347	280	1.17	0.640	0.979
SW 36	3	6	897	155	0.94	0.615	0.709
SW 310	3	10	956	192	0.96	0.604	0.731
SW 63	6	3	1076	200	1.01	0.605	0.804
SW 66	6	6	1008	226	0.99	0.614	0.761
SW 610	6	10	1014	178	0.99	0.611	0.766
MW raw	None		12	187	0.023	0.019	0.012
HEAT TREATMENT							
MW	300	1	11	47	0.017	0.012	0.011
MW	400	1	12	46	0.017	0.013	0.011
MW	500	1	13	45	0.018	0.013	0.013
MW	600	1	12	46	0.017	0.012	0.011
MW	700	1	16	45	0.022	0.016	0.015
MW	800	1	13	46	0.021	0.016	0.014
HEAT AND ACID TREATMENT							
MW 116	11	6	12	219	0.024	0.021	0.012
MW 119	11	9	11	250	0.022	0.018	0.011
MW 1112	11	12	12	178	0.022	0.018	0.012
MW 166	16	6	12	238	0.024	0.020	0.012
MW 169	16	9	13	170	0.024	0.020	0.013
MW 1612	16	12	10	209	0.021	0.018	0.009

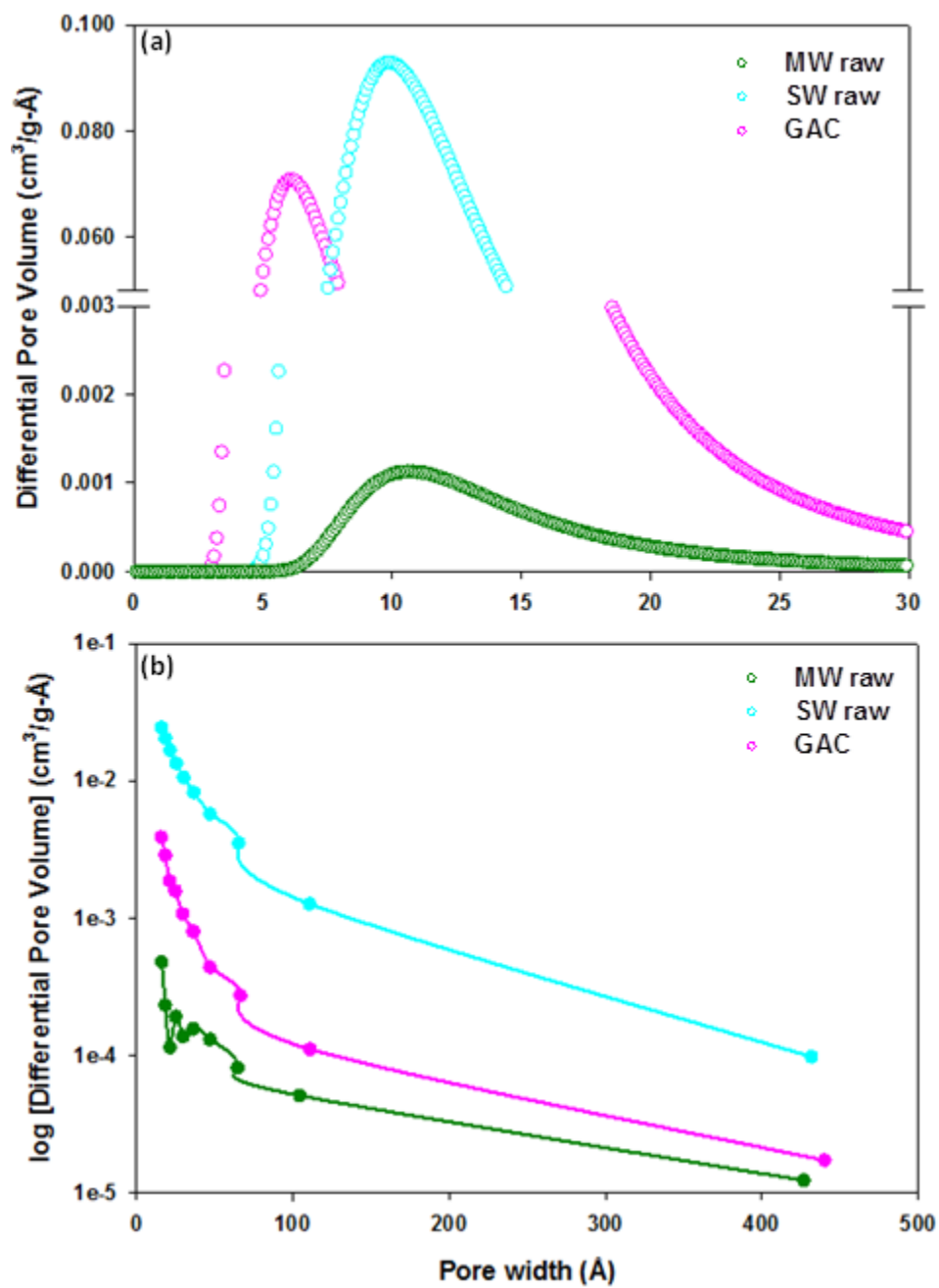


Figure 4.16: Pore size distribution for SW raw, MW raw and GAC samples using (a) the DA method (micropore Region) and (b) the BJH Method (mesopore Region)

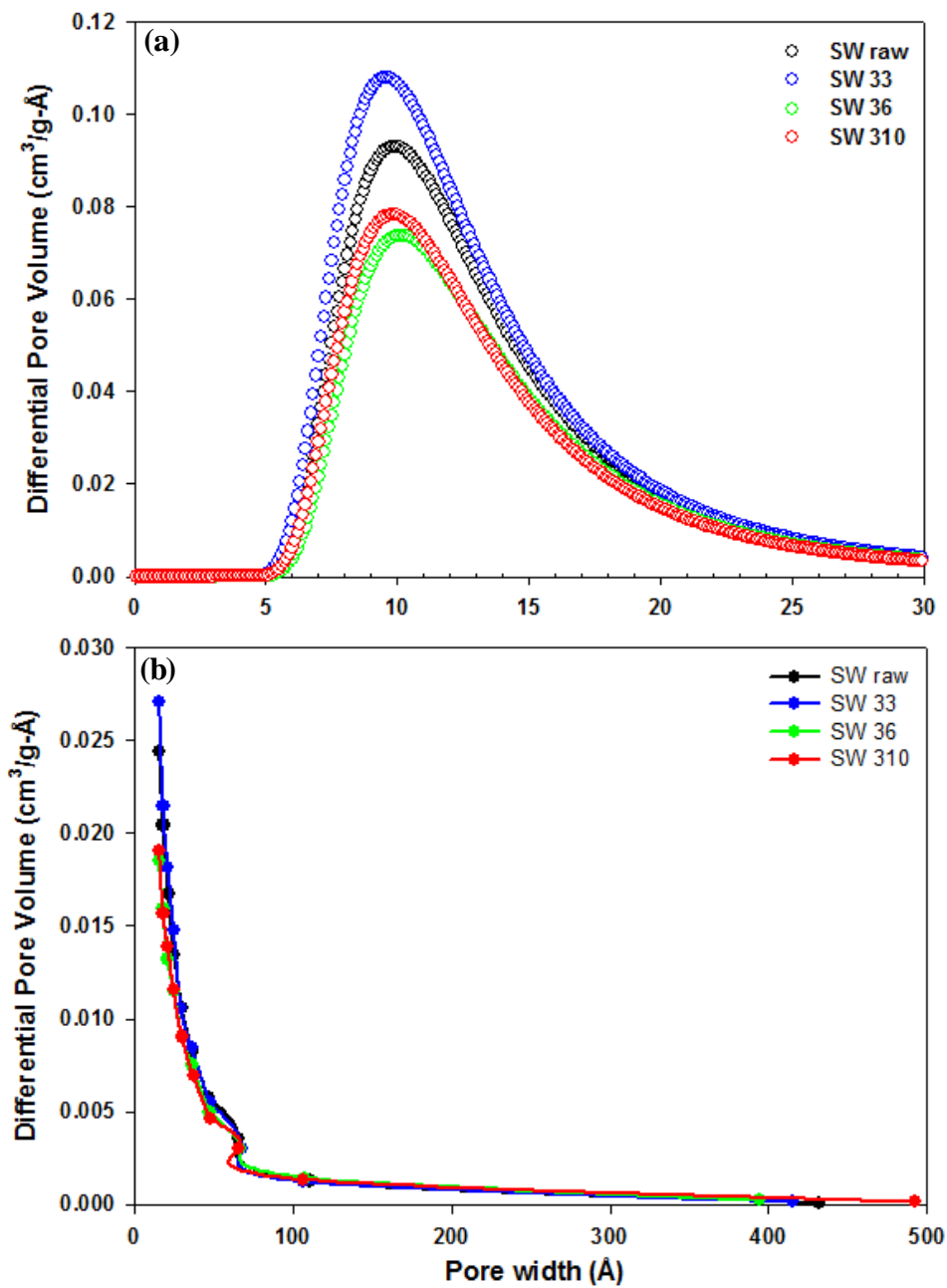


Figure 4.17: Pore size distribution for SWNTs treated with 3N nitric acid using (a) the DA method (micropore Region) and (b) the BJH Method (mesopore Region)

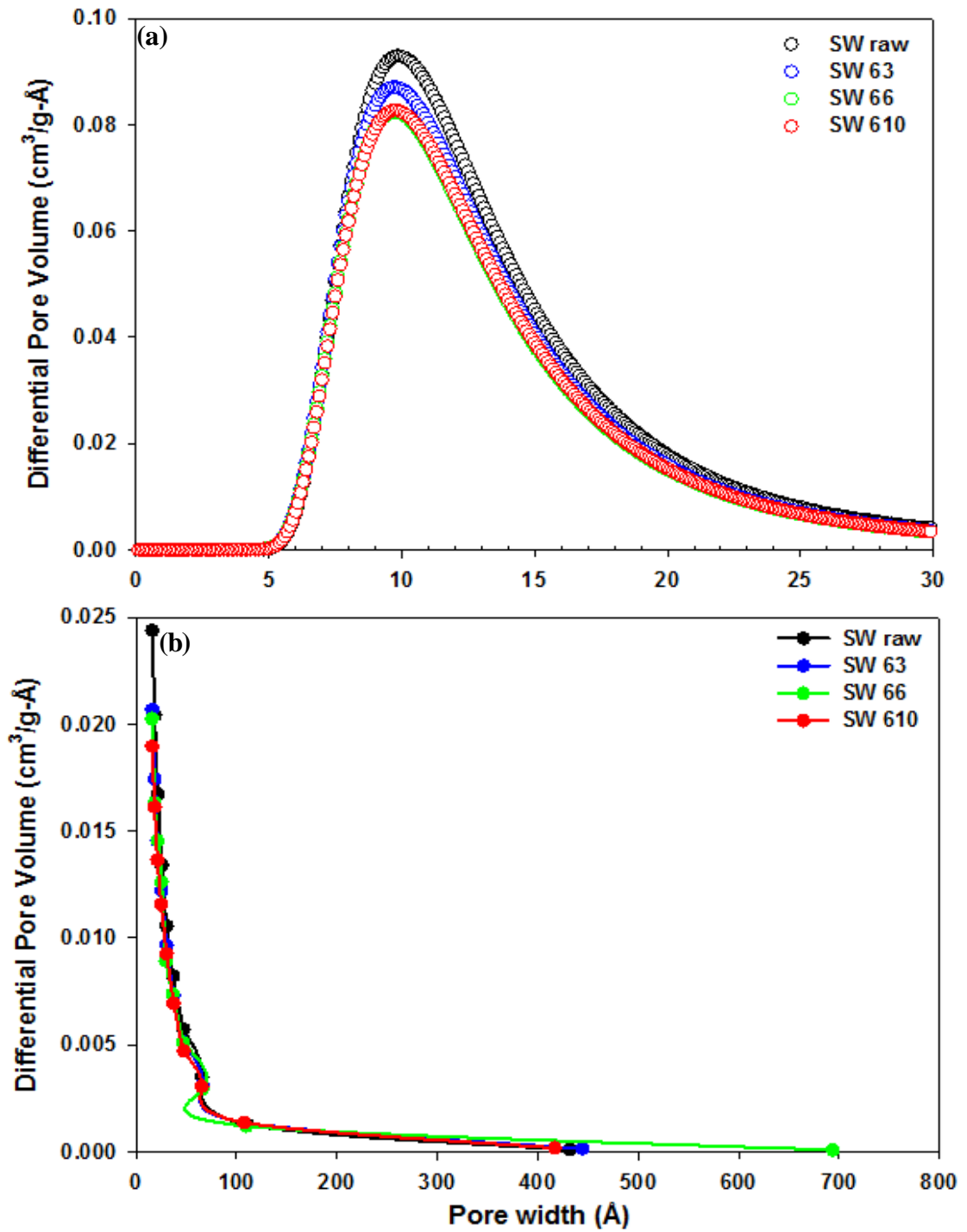


Figure 4.18: Pore size distribution for SWNTs treated with 6N nitric acid using (a) the DA method (micropore Region) and (b) the BJH Method (mesopore Region)

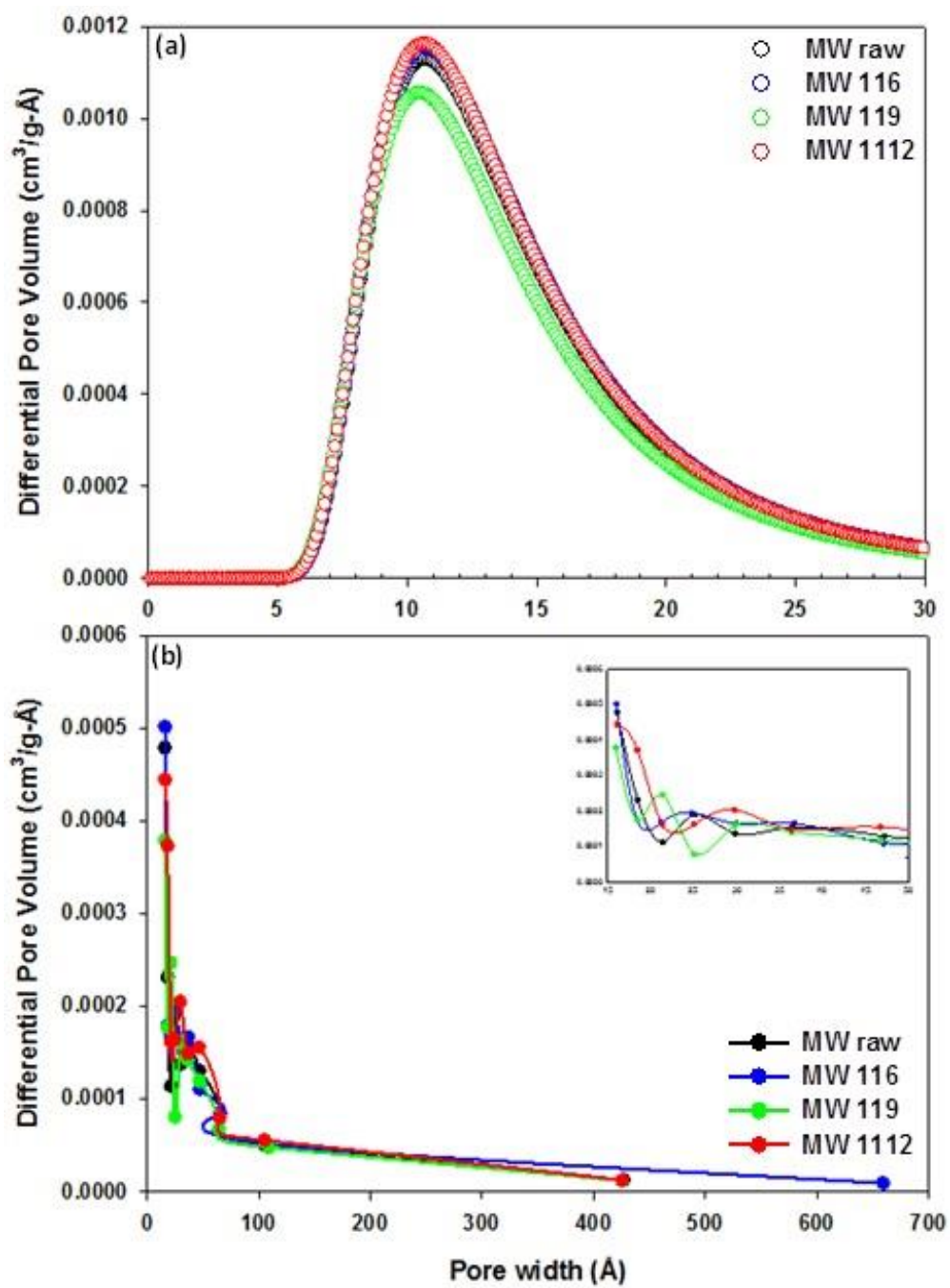


Figure 4.19: Pore size distribution for MWNTs treated with 11N nitric acid using (a) the DA method (micropore Region) and (b) the BJH Method (mesopore Region)

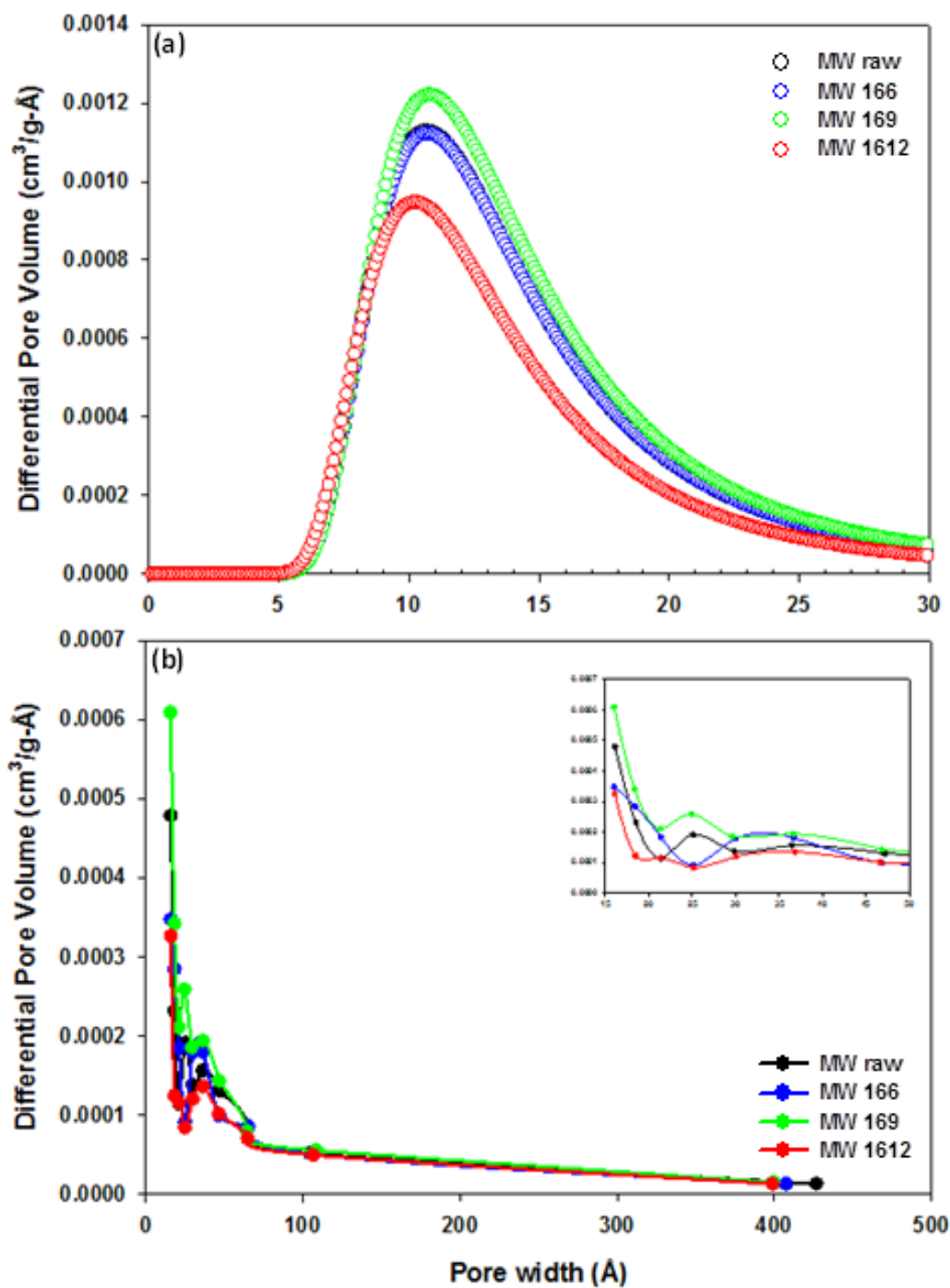


Figure 4.20: Pore size distribution for MWNTs treated with 16N nitric acid using (a) the DA method (micropore Region) and (b) the BJH Method (mesopore Region)

Table 4.5: Summary of characterization results for SWNTs and MWNTs

Characterization Techniques	SWNT Results	MWNT Results
Inductively Coupled Plasma – Mass Spectrometry (ICPMS)	Various metal impurities like Fe, Mg, Na, Ni and some amount of silica were present in the raw SWNT sample.	Various metal impurities like Al, Na, Zn, Fe and some amount of silica were present in the raw MWNT sample
Transmission Electron Microscopy (TEM)	Treated SW samples showed the formation of ridges on the walls. The SWNTs treated with 6N HNO ₃ showed the formation of crystalline graphene structure.	The TEM results showed that the HNO ₃ treatment led to the formation of shorter and thinner tubes than the raw MWNT sample.
Raman Spectroscopy	The amorphous carbon was observed to decrease with treatment time for the SWNTs treated with 3N HNO ₃ while it increased for the ones treated with 6N HNO ₃ , up to a point. The decrease of I _G /I _D ratio for SW 33 showed the formation of defects on the samples.	The D-bands in MWNTs were broader and of less intensity than compared to the SWNTs. No prominent difference was observed between the raw and the treated samples using the Raman Spectroscopy.
X-ray Photoelectron Spectroscopy (XPS)	The C-O bond was observed on both the SW 33 and SW 36, but not on SW 310. SW 66 and SW 610 showed the presence of a carbonyl group, while the SW 63 had no surface functional groups.	No surface functional groups were shown in the treated MWNT samples, except for the MW 169, which showed the presence of carbonyl groups.
Thermogravimetric Analysis (TGA)	Treated SWNT samples showed higher stability than the raw sample, indicating the removal of impurities and amorphous carbon in the treated samples.	Treated MWNTs showed much lower stability than the raw sample; however the difference among the treated samples was not large.
Surface Area and Pore Size Analysis	The SW 33 (383.2 m ² /g) sample showed an increase in surface area compared to the raw sample (240.3 m ² /g), while rest of the samples showed a decrease in surface area. The V-t plots showed that the SWNTs are micro-porous in nature. SW 33 sample showed higher adsorption in the micro-porous region than the remaining treated samples and the SW raw sample.	The treated MWNT samples showed no change in their surface area as compared to the raw sample. The V-t plots showed that the MWNTs are meso-porous in nature.

4.2 Adsorption Testing

Adsorption experiments were conducted on carbon nanotubes and granular activated carbon samples using toluene. Adsorption capacity and removal efficiency were obtained from breakthrough curves of the adsorption process for the SWNTs and MWNTs and compared with GAC. Kinetic parameters were also developed by analysis of the time series plots and the kinetic curves of the adsorption process.

4.2.1 Breakthrough and Time Series Curves

Breakthrough curves of the adsorption of the three pristine samples are shown in Figure 4.21. The outlet concentration of toluene is close to zero until t/t_{50} of 0.62 and 0.24, for SWNTs and GAC, respectively. Unlike the other two carbon forms, the MWNTs started to have breakthrough within 15 minutes of the adsorption run; this is well justified by its low surface area and low pore volume results obtained from the surface area analysis experiments. Figure 4.22 is the time curve for the adsorption process of the three pristine samples. Both the SWNTs pristine sample and the GAC had their breakthrough start at 165 minutes, as shown in Figure 4.22; however, the breakthrough curve was sharp for SWNT and gradual for GAC. This resulted in raw GAC having the highest adsorption capacity of 384.6 mg toluene/g GAC, compared to 240.3 mg toluene/g SWNTs and 8.9 mg toluene/g MWNTs (Table 4.6).

If we compare the amount of toluene adsorbed at $C/C_0 = 0.1$, the SW 33 has adsorbed 240 mg of toluene per gram while the GAC sample has adsorbed only 150 mg of toluene per gram of GAC. This is an important point to note because in industries this is an example indication level for the carbon beds to be changed for cleaning. So using the SW33 sample would be advantageous, as it adsorbs more pollutant for the same exit concentration level.

Figures 4.23 and 4.24 depict the breakthrough curves and the time series of the adsorption of purified SWNTs and the raw SWNTs. From Figure 4.24 we can state that the breakthrough started at 165, 120, 90 and 75 minutes and complete saturation was achieved at 225, 375, 255, and 300 minutes for SW raw, SW 33, SW 36, and SW 63, respectively. The time

series and breakthrough curves show a higher adsorption capacity (383.2 mg/g) for the SW 33 than the other purified samples and the raw sample that have been tested. The SW 33 has shown an adsorption capacity similar to that of a GAC.

The time series plots show that it took around 20 hours for GAC to reach its saturation with an adsorption capacity of 384.6 mg/g, while it took only 3.5 hours to reach the saturation adsorption capacity of the SW raw, which was 240.3 mg/g. The SW treated samples showed an improvement in their adsorption capacity. The SW 33, SW 36, and SW 63 took 6, 3.75, and 4.75 hours to reach saturation adsorption capacity. So we can say that the pre-treatment done on the single-wall nanotubes has likely opened pores in the samples, increasing the adsorption capacity compared to the raw sample. The SW 33 has almost the same adsorption capacity as the GAC sample and also comparable removal efficiency to the GAC, showing promise for use as an adsorbent in real world applications in the place of GAC. GAC has taken almost double the time the SW 33 sample has taken to reach its saturation because 0.33 g of GAC sample was used for testing, while only 0.1198 g of SW 33 samples was used. Even though the carbon nanotubes have a higher initial cost, they may last more regeneration cycles. This is an area for future study.

MWNTs after purification have shown no change in their structure and properties, and this was confirmed by the adsorption testing (Figure 4.25 and Figure 4.26). MW 169 and MW 1612 were used for the adsorption testing along with the raw sample. The breakthrough of the adsorption of the MWNTs started in 15 minutes, exhibiting its low adsorption capacity and unopened pores.

Developing the adsorption isotherms could provide a better understanding of the adsorption capacities of the samples and also their levels of adsorption at various relative pressures. Adsorption isotherms were not able to be developed because the needed equipment was not in working order.

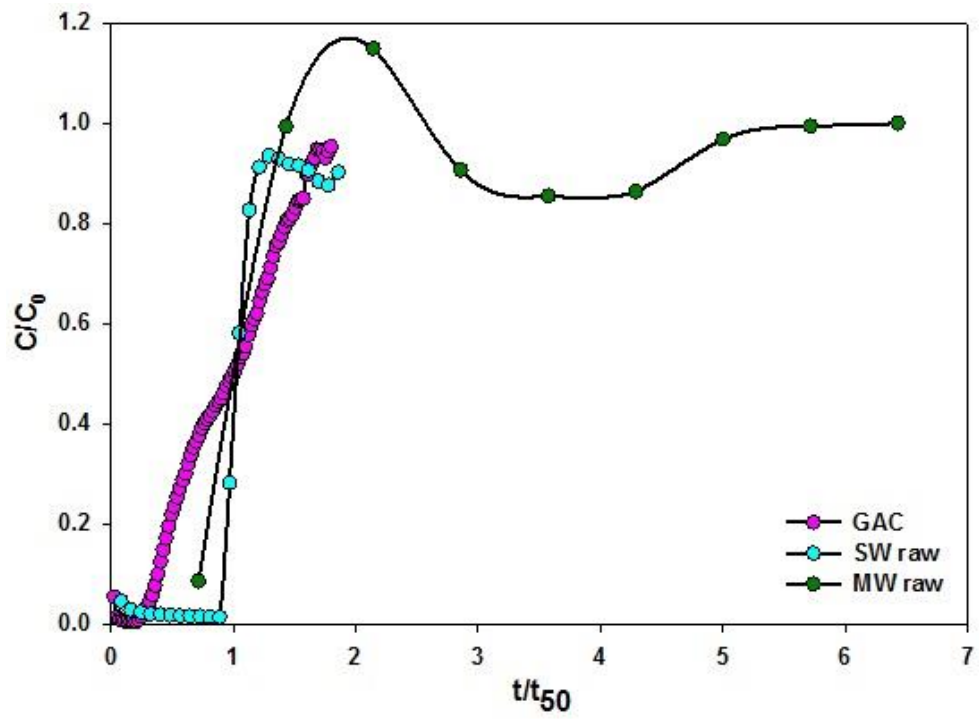


Figure 4.21: Breakthrough curves for adsorption of toluene on to SW raw, MW raw and GAC

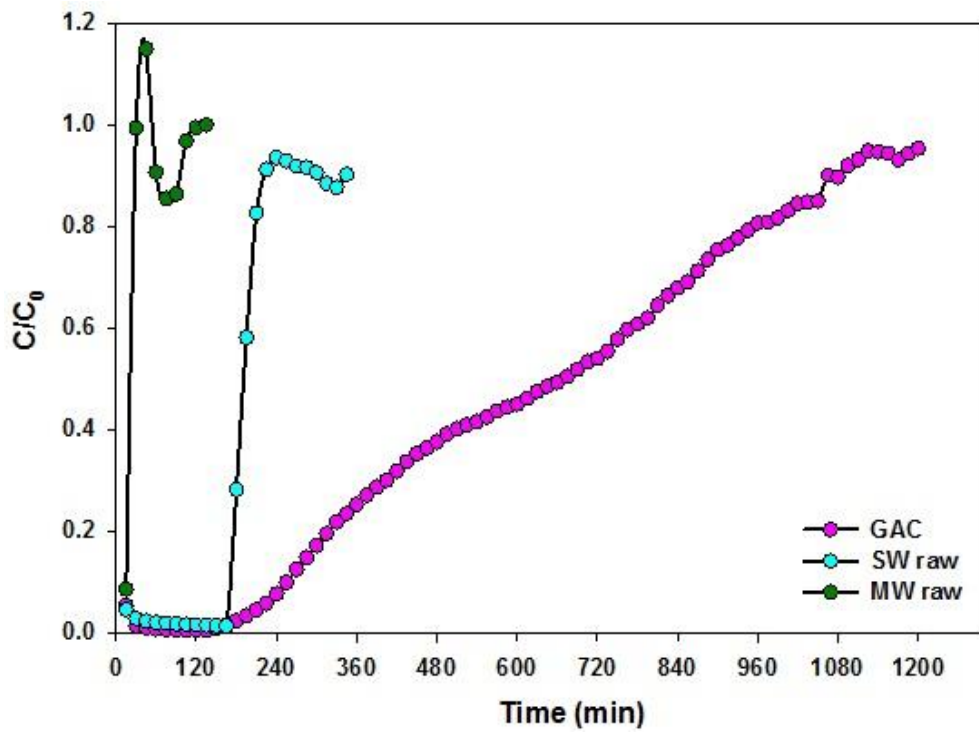


Figure 4.22: Time series for the adsorption of toluene onto SW raw, MW raw and GAC

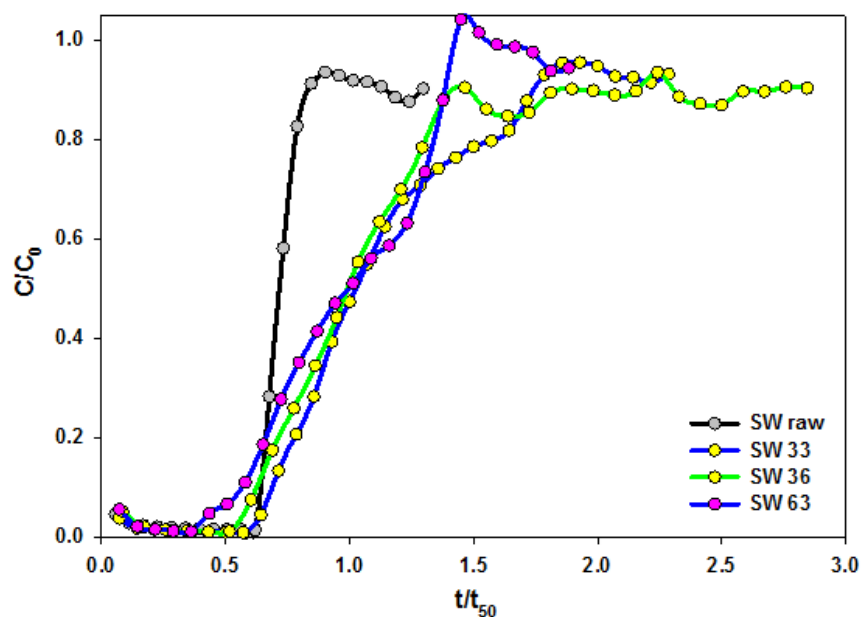


Figure 4.23: Breakthrough curves for adsorption of toluene onto SW raw, SW 33, SW 36 and SW 63

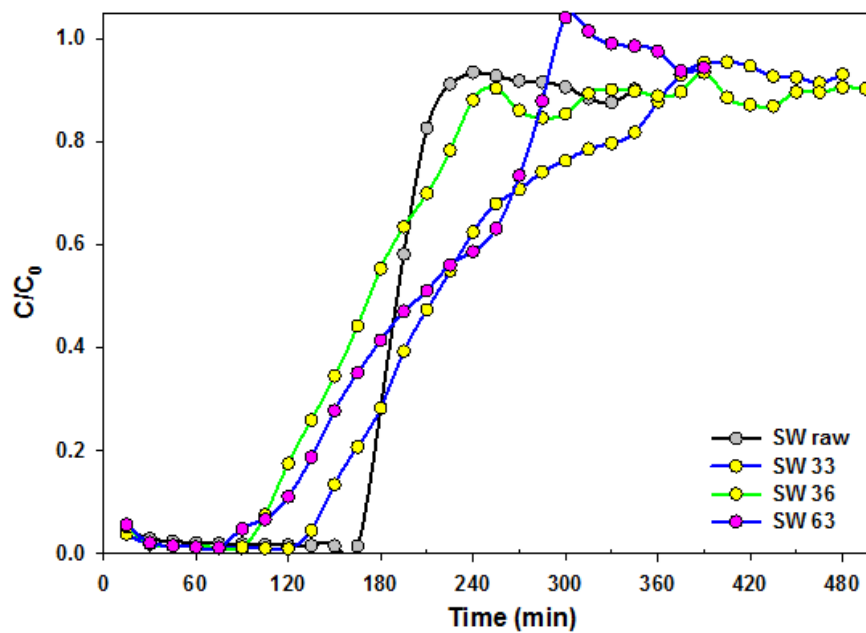


Figure 4.24: Time series for the adsorption of toluene onto SW raw, SW 33, SW 36, and SW 63

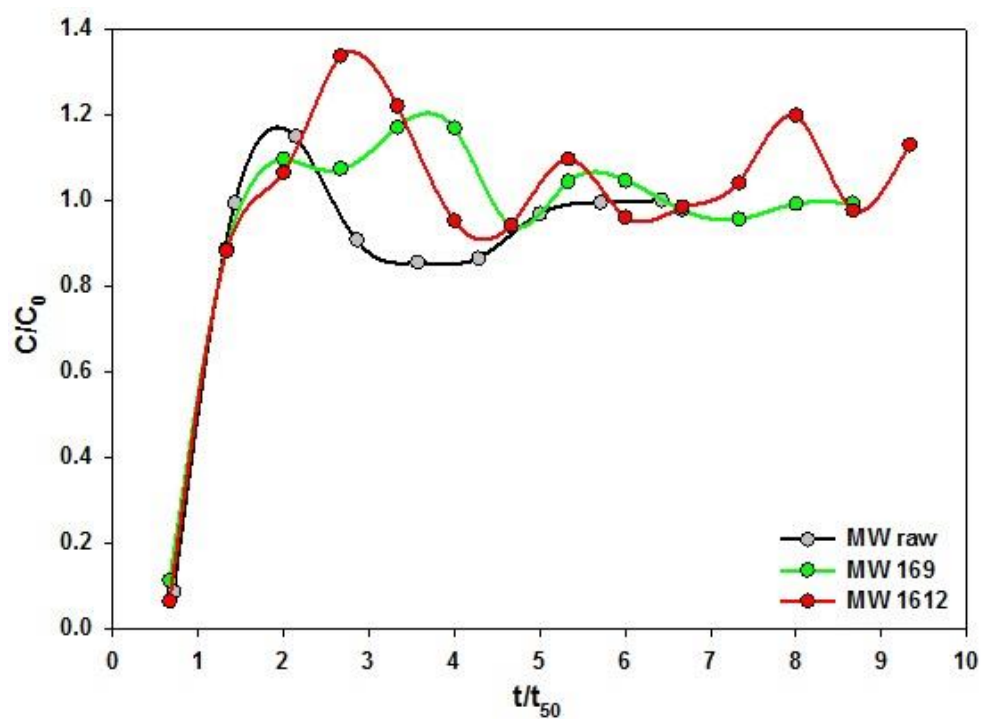


Figure 4.25: Breakthrough curves for adsorption of toluene on to MW raw, MW 169 and MW 1612

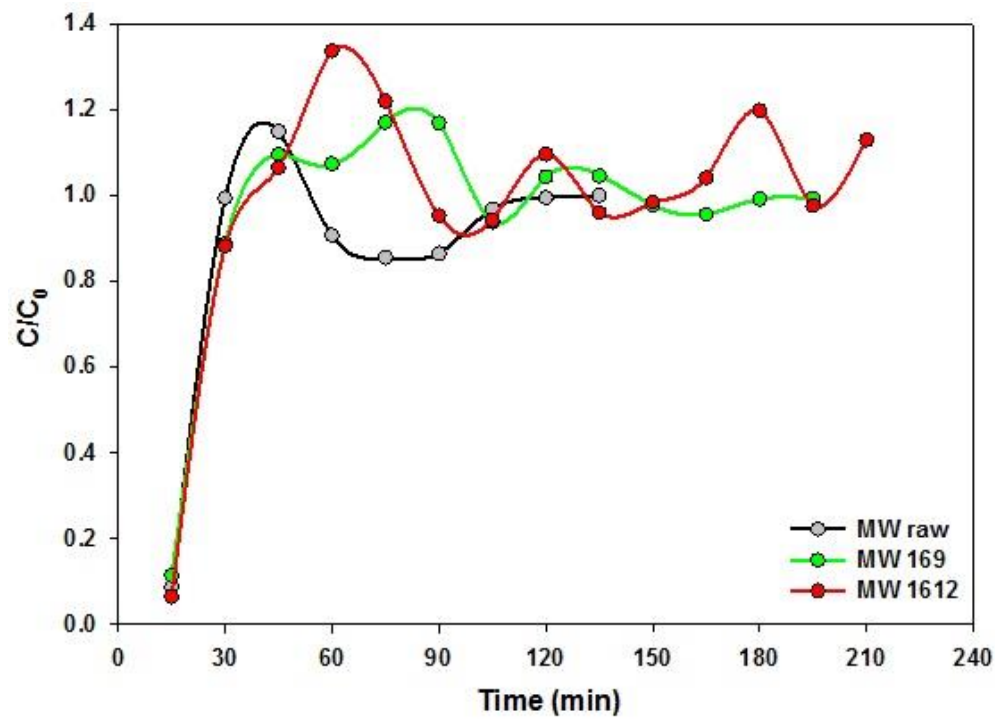


Figure 4.26: Time series for the adsorption of toluene onto MW raw, MW 169 and MW 1612

Table 4.6: Maximum removal efficiency and adsorption capacity of the samples

Sample Name	Amount of Sample (g)	Maximum Removal Efficiency (%)	Adsorption Capacity (mg/g)
GAC	0.330	98.6	384.6
SW raw	0.1138	98.0	240.3
SW 33	0.1198	98.5	383.2
SW 36	0.1223	98.1	261.0
SW 63	0.1303	97.7	277.8
MW raw	0.1893	90.9	8.9
MW 169	0.2571	91.9	10.7
MW 1612	0.2574	91.7	11.0

4.2.2 Explanation of Adsorption Results in Light of Nanotube Physical/Chemical Properties

The SW 33 showed a higher adsorption capacity compared to its raw sample and the rest of the treated samples. This increase in its adsorption capacity can be attributed to its increase in its surface area and its total and micropore volume after treatment. The TGA test results showed that only 0.6 wt% of the SW 33 sample was remaining after the testing, indicating a high purity of the sample and the availability of more carbon nanotubes for adsorption.

Unlike the SWNTs, the MWNTs did not show any promising changes in the treated samples compared to the raw sample when characterized with the various characterization techniques, and this is well supported by the adsorption testing results. The various samples used for sorption testing did not show any substantial difference in their adsorption capacity values.

Thus, the characterization testing done on the raw and the treated samples helps in better understanding the sorption of toluene onto the adsorbent.

4.2.3 Estimation of Kinetic Parameters

Sorption kinetics modeled with the pseudo-first order model are plotted with the experimental data for toluene on to GAC, SW raw, SW 33, SW 36 and SW 63 in Figures 4.27, 4.28a-d. Pseudo-first order model parameters k_1 and equilibrium adsorption capacity (q_e , modeled) are provided in Table 4.7. The conformity between experimental data and the model was expressed by the total relative error (Table 4.7). The fitted PFOM showed a good fit with the experimental data with low total relative error for all the model fits. GAC data showed the best fit with a low total relative error of 2.6% and the SW raw with the highest of 10.2%. The estimated equilibrium adsorption capacities were comparable to the experimental values and this is well explained by the low sum of squared values. The modeled and the experimental adsorption capacities had the highest adsorption capacity values for the GAC ($q_{e,modelled} = 497.7$ mg/g and $q_{e,experimental} = 384.6$ mg/g) and SW raw ($q_{e,modelled} = 299.6$ mg/g and $q_{e,experimental} = 240.3$ mg/g) sample respectively. All the adsorption capacity values estimated by the model were higher than the experimental values showing the trend of overestimation by the model being consistent. The SW raw and the treated samples had higher rate constants values compared to the GAC, showing the higher rate of reaction in the carbon nanotubes. The PFOM at equilibrium is known to become the Langmuir equation and it is known that Langmuir equation follows the one-site occupancy adsorption (Rudzinski and Plazinski, 2007). So we can say just like the Langmuir equation, the adsorption onto the SW samples follows the mechanism of one-site occupancy adsorption. As the adsorption follows the PFOM, we can also say that the controlling step of adsorption is the intra-particle diffusion, as the surface diffusion is a fast step. Models were not fitted for the MWNTs kinetic data as there were inadequate data points for the MW samples. The adsorption testing for the MW samples showed that the breakthrough for these samples started in less than 15 minutes after the adsorption had started.

Table 4.7: Adsorption capacities experimental and modeled and pseudo-first order model constants for adsorption of toluene onto GAC and SWNTs

Sample Name	q_e , experimental (mg/g)	q_e , modeled (mg/g)	k_1 , Equilibrium rate constant (min^{-1})	Sum of Squared Errors (SSE)	Total Relative Error (%)
GAC	384.6	497.7	0.0014	1752	2.6
SW raw	240.3	299.6	0.0070	3709	10.2
SW 33	383.2	443.2	0.0054	4958	6.7
SW 36	261.0	315.9	0.0071	2031	5.5
SW 63	277.8	308.4	0.0059	2431	7.7

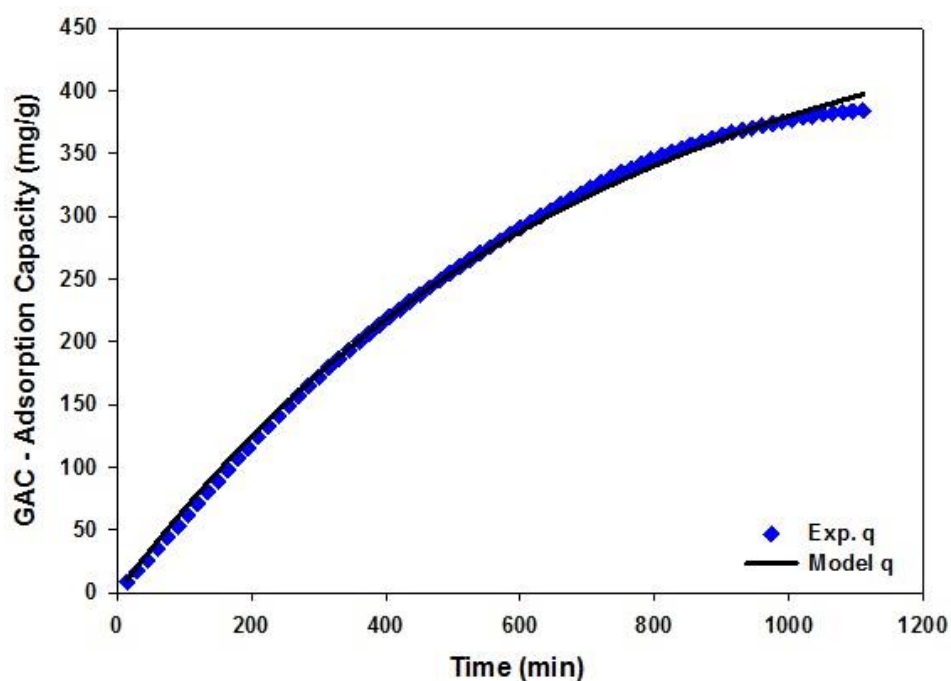


Figure 4.27: Adsorption capacities that were measured and fitted with the pseudo-first order model for GAC

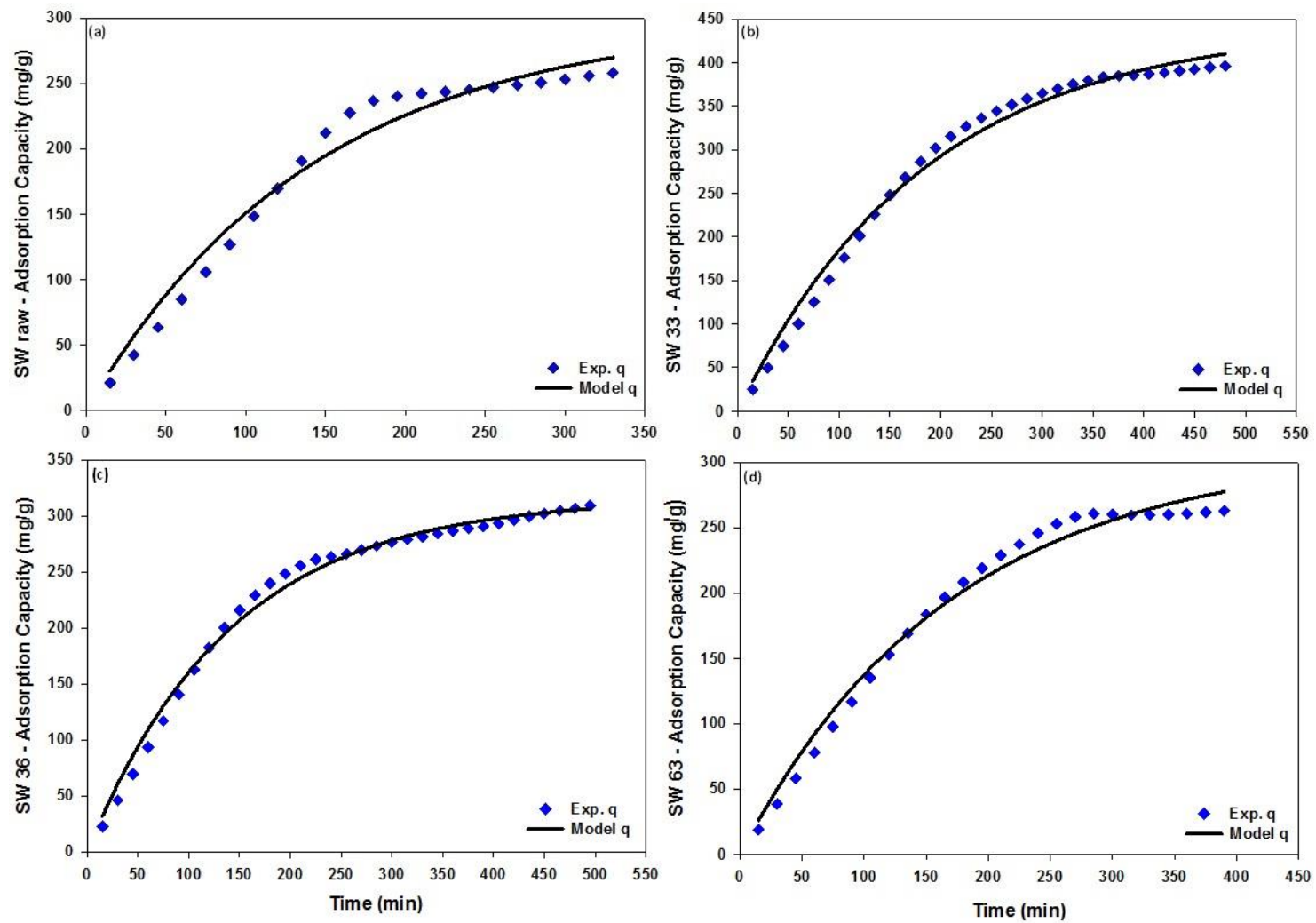


Figure 4.28: Adsorption capacities that were measured and fitted with the pseudo-first order model for (a) SW raw (b) SW 33, (c) SW 36 and (d) SW 63

CHAPTER 5

CONCLUSIONS AND RECOMMENDATIONS

This study focused on characterization of raw and purified single-wall carbon nanotubes and multi-wall carbon nanotubes. Granular activated carbon (GAC) was used as the base sample to compare the physical and chemical properties and adsorption capacity of the carbon nanotubes. Various characterization techniques were used for this comparative study. Adsorption testing was also done and kinetic parameters were obtained for single-wall nanotubes and granular activated carbon.

5.1 Summary and Conclusions

The following results and conclusions are solely based on the findings of this study:

1. Heat treatment alone, without accompanying nitric acid treatment, did not substantially modify the physical/chemical properties of the SWNTs or MWNTs.
2. The Transmission Electron Microscopy results showed that the steam and nitric acid treatment induced ridges on the walls and decreased the amorphous carbon in the purified SWNTs compared to the raw sample. The treated MWNTs showed a crystalline graphene structure and thinner and smaller tubes (lower quality) compared to the raw sample.
3. In the Raman spectroscopy, the decrease in the I_G/I_D value shows the defects in the sample and also the formation of smaller graphitic structure. As the acid treatment got harsher for the SWNTs, the amount of amorphous carbon generated exceeded the amount of amorphous carbon removed.
4. The increased generation of amorphous carbon for the harsher treatments in case of the treated SWNTs was confirmed by the X-ray photoelectron spectroscopy results. Nitric acid treatment showed generation of a combination of alcohol/ether functional groups on two of the SWNT samples and carbonyl groups on one of the MWNT samples.

5. The treated SWNTs showed higher stability than the pristine sample, while the SW 33 had the highest weight loss after the TGA testing, showing the highest percent of carbon nanotubes in the sample. The treated MWNTs showed decreased stability compared to the pristine sample.
6. The SW33 sample had an increase in surface area from 1136 m²/g (SW raw) to 1347 m²/g after the heat and acid treatment, while rest of the SWNTs showed a decrease in the surface area. There was minimal change in the surface area for the MWNTs.
7. The t-plots show that the MWNTs and GAC sample are meso-porous adsorbents, while the SWNTs are micro-porous in nature.
8. In the SWNTs, SW 33 showed a higher adsorption capacity (383 mg/g) than the pristine sample (261 mg/g) and also had a comparable adsorption capacity to that GAC (385 mg/g). This could have been due to its higher purity and/or high surface area.
9. At $C/C_0 = 0.1$, a gram of SW 33 sample adsorbed 240 mg of toluene, whereas a gram of GAC adsorbed only 150 mg of toluene ($C/C_0 = 0.1$ is an important estimate as it is used as a mark for the cleaning the carbon beds at industrial level).
10. The pseudo-first order model showed a good fit, with the total relative error (TRE) ranging between 2.65%-10.2% for the GAC, SW raw, SW 33, SW 36 and SW 63 samples.
11. The rate of adsorption of toluene on to SWNTs was higher than that on the GAC, shown by the rate constant values. GAC had a rate constant value of 0.0014 min⁻¹, while the SW raw and treated samples had a rate constant value greater than 0.0054 min⁻¹.

5.2 Global Conclusions

The single-wall carbon nanotubes treated for 3 hours with 3N nitric acid look the most promising adsorbent in this study, as they showed higher adsorption capacity of toluene at $C/C_0 = 0.1$, which is an indication levels for changing the carbon beds in industries. It has also shown comparable adsorption capacity to that of GAC, which is common and most widely used adsorbent for capture of organic vapors. Its BET surface area was greater than GAC.

The thermal and chemical treatments used for the multi-wall carbon nanotubes were not effective in altering their physical/chemical properties, including surface area, and thus not effective substantially increasing their adsorption capacity for toluene. This was likely due to high wall thickness of the MWNTs, which made them withstand the harsh treatment of the high concentration nitric acid. Perhaps an increase in treatment time could oxidize these MWNTs and lead to increase in surface area, which could enhance the adsorption capacity of the sample.

5.3 Recommendations for Future Studies

1. Using more than one kind of pristine sample could help us better understand the nature of the sample and the possible changes that occur during treatment.
2. Removal of the impurities during the treatment could not be identified properly as the level of the impurities was below the sensitivity level of the instruments, so using a sample with a higher level of impurities could help us understand the level of purity achieved by each of the treatment combinations.
3. Acid treatment with different acids would develop different functional groups on the surface of the adsorbent, which will provide us with better understanding of the preferential sorption of the adsorbate depending on the surface functional groups.
4. Current research used only one solvent (toluene) for testing the adsorption capacity. Using different solvents with different physical properties can provide good understanding of the adsorbent-adsorbate interaction.
5. Using computer software like “Threshold Image” for the TEM imaging could help us draw quantitative conclusions.
6. Conducting experiments for developing adsorption isotherms and determining a best kinetic model for the sorption kinetics as a future research could help better understand the rate mechanism of the carbon nanotubes and potential rate controlling step of the sorption.

7. Regeneration tests should be conducted for the single-wall nanotubes treated with 3N nitric acid for 3 hours, to determine how many cycles the nanotubes last. Regeneration tests should be conducted for GAC for comparison.

APPENDIX A
SAMPLE EXPERIMENTAL RESULTS

A.1. Example data from the Raman scattering spectra experiment for SW raw

Raman shift	Intensity	Raman shift	Intensity	Raman shift	Intensity	Raman shift	Intensity	Raman shift	Intensity
800	102.856	810.076	105.934	820.151	105.978	830.227	106.229	840.302	107.922
800.42	103.335	810.495	105.384	820.571	106.565	830.647	105.465	840.722	107.112
800.84	103.038	810.915	106.726	820.991	105.94	831.066	107.065	841.142	106.209
801.259	102.616	811.335	107.573	821.411	105.321	831.486	108.581	841.562	105.471
801.679	102.904	811.755	105.585	821.83	106.006	831.906	108.888	841.982	107.822
802.099	103.169	812.175	103.729	822.25	106.786	832.326	109.261	842.401	110.355
802.519	103.085	812.594	103.154	822.67	106.392	832.746	108.979	842.821	110.254
802.939	103.458	813.014	103.034	823.09	105.983	833.165	108.316	843.241	109.615
803.359	104.265	813.434	104.913	823.51	107.022	833.585	107.919	843.661	108.474
803.778	105.438	813.854	107.11	823.929	108.548	834.005	107.834	844.081	106.905
804.198	105.101	814.274	106.929	824.349	108.317	834.425	107.767	844.5	106.637
804.618	104.644	814.694	105.237	824.769	106.851	834.845	107.394	844.92	108.096
805.038	104.551	815.113	104.868	825.189	105.816	835.264	107.345	845.34	109.156
805.458	104.431	815.533	106.331	825.609	105.179	835.684	107.826	845.76	109.228
805.877	104.141	815.953	107.422	826.029	104.963	836.104	107.849	846.18	109.257
806.297	103.387	816.373	107.242	826.448	106.226	836.524	106.56	846.599	108.328
806.717	102.762	816.793	107.135	826.868	107.502	836.944	105.343	847.019	107.4
807.137	103.769	817.212	106.226	827.288	107.99	837.364	106.194	847.439	108.256
807.557	105.146	817.632	105.397	827.708	108.627	837.783	107.17	847.859	109.198
807.977	107.596	818.052	106.287	828.128	108.484	838.203	106.465	848.279	108.96
808.396	110.124	818.472	107.476	828.547	108.242	838.623	105.297	848.699	108.816
808.816	109.634	818.892	106.927	828.967	108.155	839.043	105.72	849.118	109.015
809.236	108.841	819.312	105.486	829.387	107.926	839.463	107.601	849.538	108.845
809.656	107.697	819.731	105.089	829.807	107.42	839.882	108.705	849.958	108.578

Note: Data for Raman spectra is from 800 Å – 1800 Å (data provided here is only for 800 Å – 850 Å).

A.2. Data from the X-ray Photoelectron Spectroscopy experiment for SW raw

Binding Energy (eV)	Intensity (cps)	Binding Energy (eV)	Intensity (cps)	Binding Energy (eV)	Intensity (cps)	Binding Energy (eV)	Intensity (cps)	Binding Energy (eV)	Intensity (cps)	Binding Energy (eV)	Intensity (cps)	Binding Energy (eV)	Intensity (cps)
292	133.167	289.6	123.5	287.2	244.5	284.8	1023.333	282.4	156	280	26	277.6	21.6667
291.9	120	289.5	129.667	287.1	237.833	284.7	1161.167	282.3	125.167	279.9	24.8333	277.5	20.8333
291.8	121	289.4	129.5	287	227.167	284.6	1307.833	282.2	99	279.8	24.5	277.4	17.6667
291.7	133.333	289.3	140.5	286.9	215.667	284.5	1524.5	282.1	83.3333	279.7	24.5	277.3	23.3333
291.6	128.5	289.2	143.667	286.8	210.833	284.4	1787.667	282	79.6667	279.6	25	277.2	20.3333
291.5	123	289.1	143.667	286.7	228.333	284.3	2068.833	281.9	63.8333	279.5	20.5	277.1	21.1667
291.4	127.833	289	155.667	286.6	235.5	284.2	2375.167	281.8	62.6667	279.4	26.6667	277	20.3333
291.3	123.833	288.9	153.167	286.5	242.333	284.1	2617.167	281.7	52.5	279.3	24.5	276.9	21.6667
291.2	126.5	288.8	157.833	286.4	247.5	284	2668	281.6	51.5	279.2	20.8333	276.8	22.3333
291.1	131	288.7	166.167	286.3	255.333	283.9	2547.5	281.5	48.8333	279.1	23.3333	276.7	18.5
291	134.167	288.6	176.167	286.2	273.333	283.8	2384	281.4	41.5	279	23.1667	276.6	20.5
290.9	126.667	288.5	197.833	286.1	299.333	283.7	2103.167	281.3	36	278.9	21.5	276.5	17.8333
290.8	124.833	288.4	203	286	331.333	283.6	1797	281.2	28.8333	278.8	22.5	276.4	21.5
290.7	129	288.3	215.833	285.9	343.5	283.5	1562.167	281.1	32	278.7	21.5	276.3	22.1667
290.6	135.667	288.2	226.167	285.8	382.833	283.4	1355.667	281	30.5	278.6	18	276.2	22.3333
290.5	139.167	288.1	242	285.7	410.833	283.3	1175.833	280.9	30.6667	278.5	19.6667	276.1	18.8333
290.4	128	288	262	285.6	464.833	283.2	981.6667	280.8	26.6667	278.4	19.5	276	21.3333
290.3	129.333	287.9	271.667	285.5	505.667	283.1	816.6667	280.7	26.8333	278.3	20.3333		
290.2	145.167	287.8	284	285.4	572.167	283	667.3333	280.6	28.8333	278.2	19		
290.1	130.667	287.7	296.667	285.3	628.833	282.9	541.6667	280.5	24.3333	278.1	19.3333		
290	132.167	287.6	290.5	285.2	703.333	282.8	417.8333	280.4	27.5	278	20.6667		
289.9	125.833	287.5	307.667	285.1	742.5	282.7	327.5	280.3	23.6667	277.9	20.8333		
289.8	129.667	287.4	279.5	285	855.167	282.6	254.6667	280.2	25.8333	277.8	22		
289.7	132.167	287.3	263	284.9	909.5	282.5	204.8333	280.1	24.6667	277.7	19.8333		

A.3. Example data from the thermogravimetric analysis experiment for SW raw

Time (min)	Temp. (°C)	Weight (mg)	Weight (%)	Negative dw/dt	Time (min)	Temp. (°C)	Weight (mg)	Weight (%)	Negative dw/dt
6.11E-04	31.26914	9.006015	9.00628		1.88E-01	31.15548	9.005765	9.00603	-0.001800
4.17E-03	31.26604	9.00603	9.00630	-0.004219	1.96E-01	31.15352	9.005734	9.00600	0.003720
1.25E-02	31.2616	9.006059	9.00632	-0.003480	2.04E-01	31.14436	9.00575	9.00602	-0.001920
2.08E-02	31.2542	9.006086	9.00635	-0.003240	2.13E-01	31.14562	9.00578	9.00605	-0.003600
2.92E-02	31.2498	9.006102	9.00637	-0.001920	2.21E-01	31.14006	9.005766	9.00603	0.001680
3.75E-02	31.24406	9.006102	9.00637	0.000000	2.29E-01	31.13923	9.005828	9.00609	-0.007440
4.58E-02	31.24036	9.006093	9.00636	0.001080	2.38E-01	31.1395	9.005903	9.00617	-0.009000
5.42E-02	31.23613	9.006099	9.00636	-0.000720	2.46E-01	31.1418	9.00595	9.00622	-0.005640
6.25E-02	31.23324	9.006106	9.00637	-0.000840	2.54E-01	31.14217	9.006012	9.00628	-0.007440
7.08E-02	31.22426	9.006109	9.00637	-0.000360	2.63E-01	31.1363	9.00608	9.00635	-0.008160
7.92E-02	31.21404	9.006106	9.00637	0.000360	2.71E-01	31.1274	9.006141	9.00641	-0.007320
8.75E-02	31.20616	9.00609	9.00636	0.001920	2.79E-01	31.12715	9.006259	9.00652	-0.014160
9.58E-02	31.19927	9.006051	9.00632	0.004680	2.88E-01	31.12798	9.006339	9.00660	-0.009600
1.04E-01	31.19426	9.005997	9.00626	0.006480	2.96E-01	31.12894	9.006426	9.00669	-0.010440
1.13E-01	31.19608	9.005988	9.00625	0.001080	3.04E-01	31.12938	9.006524	9.00679	-0.011760
1.21E-01	31.18697	9.005941	9.00621	0.005640	3.13E-01	31.12772	9.006586	9.00685	-0.007440
1.29E-01	31.1824	9.005899	9.00616	0.005040	3.21E-01	31.13344	9.006664	9.00693	-0.009360
1.38E-01	31.18402	9.005899	9.00616	0.000000	3.29E-01	31.13259	9.006741	9.00701	-0.009240
1.46E-01	31.17791	9.005856	9.00612	0.005160	3.38E-01	31.13579	9.006811	9.00708	-0.008400
1.54E-01	31.17314	9.005806	9.00607	0.006000	3.46E-01	31.13812	9.006874	9.00714	-0.007560
1.63E-01	31.16654	9.005785	9.00605	0.002520	3.54E-01	31.13859	9.006938	9.00720	-0.007680
1.71E-01	31.16619	9.005757	9.00602	0.003360	3.63E-01	31.13668	9.006982	9.00725	-0.005280
1.79E-01	31.16199	9.00575	9.00602	0.000840	3.71E-01	31.1421	9.007038	9.00730	-0.006720

Note: Data for TGA experiment is from 30°C – 1000°C (data provided here is only for part of 31°C)

A.4. Example data for micro-pore size distribution (DA method) for the SW raw sample

Pore Width (Å)	Differential Pore Vol. (cc/g-Å)	Pore Width (Å)	Differential Pore Vol. (cc/g-Å)	Pore Width (Å)	Differential Pore Vol. (cc/g-Å)	Pore Width (Å)	Differential Pore Vol. (cc/g-Å)	Pore Width (Å)	Differential Pore Vol. (cc/g-Å)
0.1	6.06E-28	2.5	1.55E-33	4.9	1.05E-04	7.3	0.0434	9.7	0.0928
0.2	3.79E-29	2.6	1.41E-30	5	1.84E-04	7.4	0.047	9.8	0.0929
0.3	7.49E-30	2.7	2.98E-27	5.1	3.08E-04	7.5	0.0504	9.9	0.093
0.4	2.37E-30	2.8	2.17E-24	5.2	4.93E-04	7.6	0.0539	10	0.0929
0.5	9.70E-31	2.9	6.46E-22	5.3	7.58E-04	7.7	0.0572	10.1	0.0927
0.6	4.68E-31	3	9.13E-20	5.4	1.13E-03	7.8	0.0605	10.2	0.0924
0.7	2.53E-31	3.1	6.87E-18	5.5	1.62E-03	7.9	0.0636	10.3	0.0921
0.8	1.48E-31	3.2	3.03E-16	5.6	2.26E-03	8	0.0666	10.4	0.0916
0.9	9.24E-32	3.3	8.48E-15	5.7	3.08E-03	8.1	0.0695	10.5	0.091
1	6.06E-32	3.4	1.61E-13	5.8	4.09E-03	8.2	0.0722	10.6	0.0904
1.1	4.14E-32	3.5	2.17E-12	5.9	5.31E-03	8.3	0.0748	10.7	0.0897
1.2	2.92E-32	3.6	2.20E-11	6	6.75E-03	8.4	0.0771	10.8	0.089
1.3	2.12E-32	3.7	1.73E-10	6.1	8.43E-03	8.5	0.0794	10.9	0.0882
1.4	1.58E-32	3.8	1.09E-09	6.2	0.0103	8.6	0.0814	11	0.0874
1.5	1.20E-32	3.9	5.68E-09	6.3	0.0125	8.7	0.0833	11.1	0.0865
1.6	9.25E-33	4	2.50E-08	6.4	0.0149	8.8	0.0849	11.2	0.0855
1.7	7.26E-33	4.1	9.50E-08	6.5	0.0175	8.9	0.0865	11.3	0.0845
1.8	5.78E-33	4.2	3.17E-07	6.6	0.0202	9	0.0878	11.4	0.0835
1.9	4.65E-33	4.3	9.39E-07	6.7	0.0232	9.1	0.089	11.5	0.0825
2	3.79E-33	4.4	2.52E-06	6.8	0.0264	9.2	0.09	11.6	0.0814
2.1	3.12E-33	4.5	6.15E-06	6.9	0.0296	9.3	0.0908	11.7	0.0803
2.2	2.59E-33	4.6	1.38E-05	7	0.033	9.4	0.0915	11.8	0.0792
2.3	2.17E-33	4.7	2.90E-05	7.1	0.0364	9.5	0.0921	11.9	0.0781
2.4	1.83E-33	4.8	5.68E-05	7.2	0.0399	9.6	0.0925	12	0.077

Note: Data for Micro-pore Size Distribution for SW raw is from 0.1 Å – 30 Å (data provided here is only for 0.1 Å–12 Å)

A.5. Data for mesopore size distribution (BJH method) for the SW raw sample

Pore Width (Å)	Differential Pore Volume (cc/g-Å)
16.0578	0.0244
18.4062	0.0204
21.5992	0.0167
25.5294	0.0134
30.2919	0.0106
36.715	8.22E-03
47.0196	5.74E-03
65.4249	3.52E-03
110.7005	1.27E-03
431.5107	9.75E-05

A.6. Data from the t curves for micropore analysis by de Boer's method

V-t method summary		
Thickness method: DeBoer		
Sample Name	Intercept	Type of Sample
SW raw	191.926	micro-porous
GAC	222.263	micro-porous
SW 33	266.680	micro-porous
SW 36	145.592	micro-porous
SW 310	166.801	micro-porous
SW 63	198.463	micro-porous
SW 66	178.624	micro-porous
SW 610	174.145	micro-porous
MW raw	0.707	meso-porous
MW 506	0.160	meso-porous
MW 509	0.429	meso-porous
MW 5012	0.628	meso-porous
MW 706	0.015	meso-porous
MW 709	0.383	meso-porous
MW 7012	0.278	meso-porous

Note: The t-curves are plots of the volume of gas adsorbed against statistical thickness of an adsorbed film, as shown in a sample plots (B6 and B7). A t-plot for a microporous sample is a good fit and hence would have an intercept, while a sample with no micropores will have a line close to the origin (with no intercept).

A.7. Data for the adsorption experiments for toluene onto SW raw

Cycle	Time (min)	C _{in} (ppmv)	C _{out} (ppmv)	C _{in} - C _{out} (ppmv)	C _{in} - C _{out} (mg/m ³)	Flow rate (m ³ /min)	Time for each reading (min)	Mass of Tol. adsorbed (mg)	
BP 1	15	217.80	195.34						
BP 2	30	217.80	237.29						
BP 3	45	217.80	213.53						
BP 4	60	217.80	213.67						
BP 5	75	217.80	228.96						
RUN 1	90	217.80	9.88	207.920	781.95	0.0002	15	2.346	
RUN 2	105	217.80	6.05	211.750	796.35	0.0002	15	2.389	
RUN 3	120	217.80	4.98	212.820	800.38	0.0002	15	2.401	
RUN 4	135	217.80	4.30	213.500	802.93	0.0002	15	2.409	
RUN 5	150	217.80	4.04	213.760	803.91	0.0002	15	2.412	
RUN 6	165	217.80	3.76	214.040	804.97	0.0002	15	2.415	
RUN 7	180	217.80	3.47	214.330	806.06	0.0002	15	2.418	
RUN 8	195	217.80	3.29	214.510	806.73	0.0002	15	2.420	
RUN 9	210	217.80	3.14	214.660	807.30	0.0002	15	2.422	
RUN 10	225	217.80	3.02	214.780	807.75	0.0002	15	2.423	
RUN 11	240	217.80	2.90	214.900	808.20	0.0002	15	2.425	
RUN 12	255	217.80	61.42	156.380	588.12	0.0002	15	1.764	
RUN 13	270	217.80	126.51	91.290	343.32	0.0002	15	1.030	
RUN 14	285	217.80	179.92	37.880	142.46	0.0002	15	0.427	
RUN 15	300	217.80	198.65	Total mass of toluene adsorbed (mg)					29.701
RUN 16	315	217.80	203.64						
RUN 17	330	217.80	202.22						
RUN 18	345	217.80	200.01						
RUN 19	360	217.80	199.44						
RUN 20	375	217.80	197.31						
RUN 21	390	217.80	192.65						

A.8. Sample data set of the SW raw used for plotting the breakthrough and kinetic curves

Time (min)	t ₅₀ (min)	t/t ₅₀	C _{out} (ppmv)	C ₀ (ppmv)	C _{out} /C ₀
15	186	0.080645	9.88	217.8	0.045363
30	186	0.16129	6.05	217.8	0.027778
45	186	0.241935	4.98	217.8	0.022865
60	186	0.322581	4.30	217.8	0.019743
75	186	0.403226	4.04	217.8	0.018549
90	186	0.483871	3.76	217.8	0.017264
105	186	0.564516	3.47	217.8	0.015932
120	186	0.645161	3.29	217.8	0.015106
135	186	0.725806	3.14	217.8	0.014417
150	186	0.806452	3.02	217.8	0.013866
165	186	0.887097	2.90	217.8	0.013315
180	186	0.967742	61.42	217.8	0.282002
195	186	1.048387	126.51	217.8	0.580854
210	186	1.129032	179.92	217.8	0.826079
225	186	1.209677	198.65	217.8	0.912075
240	186	1.290323	203.64	217.8	0.934986
255	186	1.370968	202.22	217.8	0.928466
270	186	1.451613	200.01	217.8	0.91832
285	186	1.532258	199.44	217.8	0.915702
300	186	1.612903	197.31	217.8	0.905923
315	186	1.693548	192.65	217.8	0.884527
330	186	1.774194	190.81	217.8	0.876079
345	186	1.854839	196.46	217.8	0.90202

APPENDIX B
SAMPLE OUTPUTS AND PLOTS

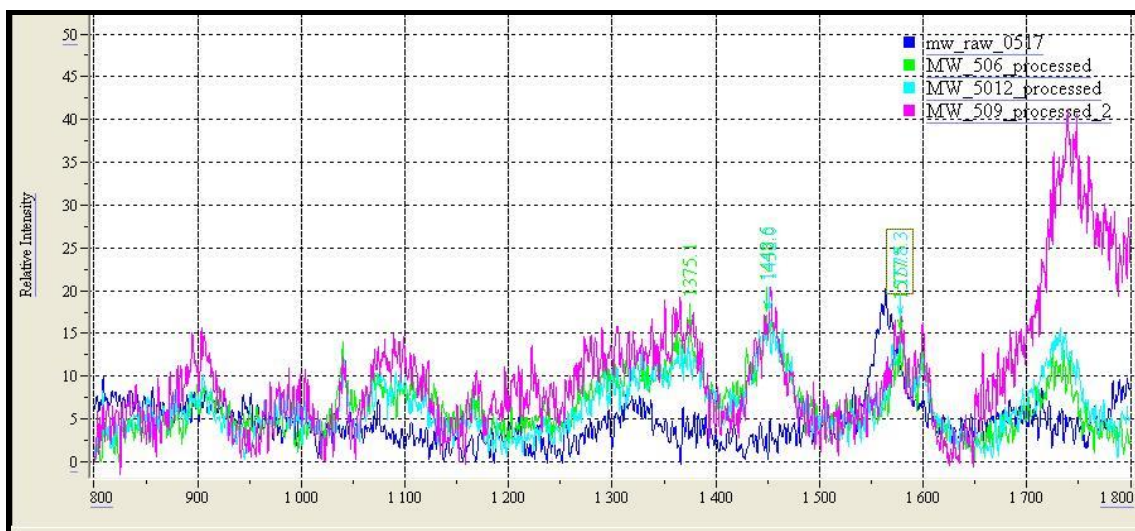


Figure B.1. Sample chromatogram from the Raman spectroscopy for MWNTs

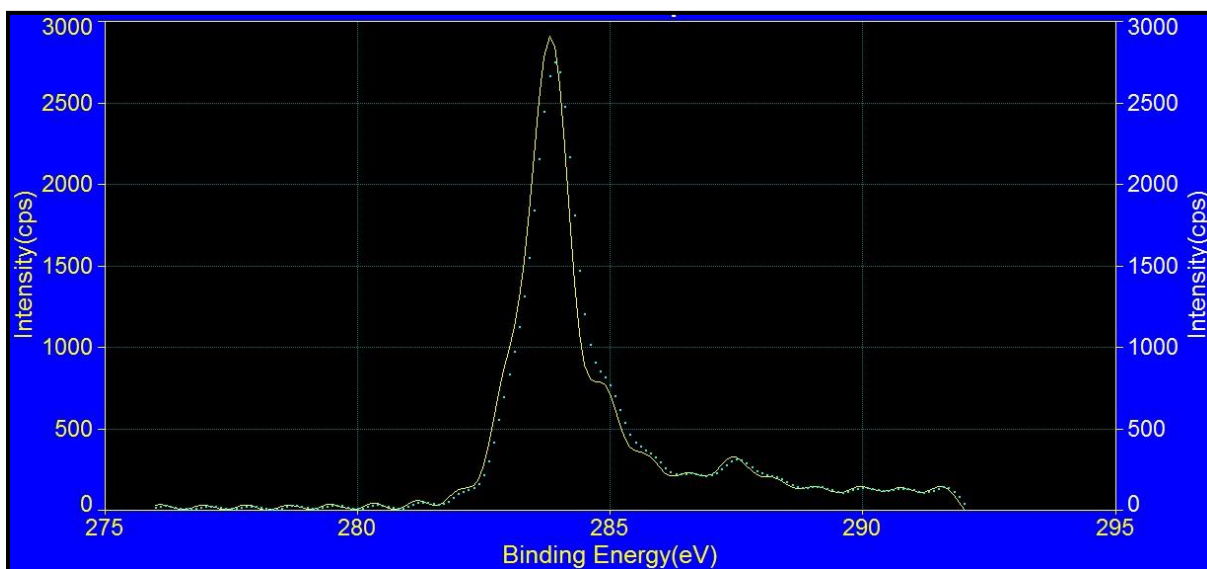


Figure B.2. Sample chromatogram from the XPS experiment for SW raw sample

Sample: SW_raw_air_T2_0531
Size: 0.1910 mg
Method: Ramp

DSC-TGA

File: C:\SW_raw\SW_raw_air_T2_0531.001
Operator: Roja
Run Date: 31-May-2012 20:03
Instrument: SDT Q600 V20.9 Build 20

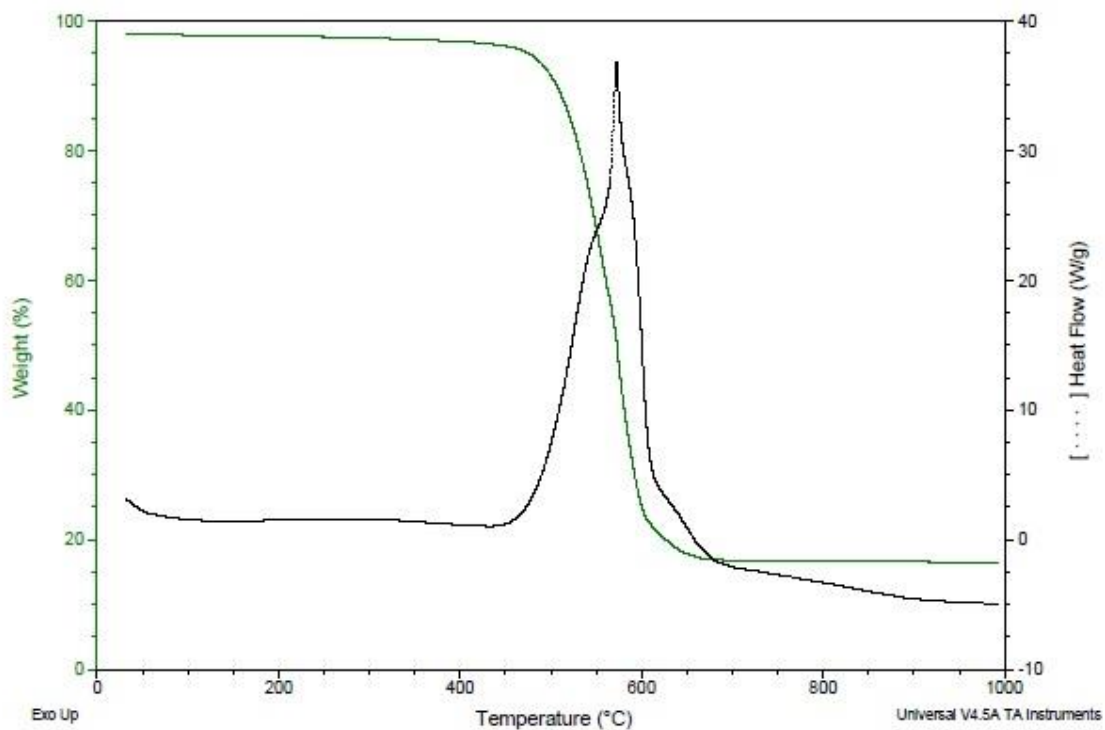


Figure B.3. Sample output from the thermogravimetric analysis experiment

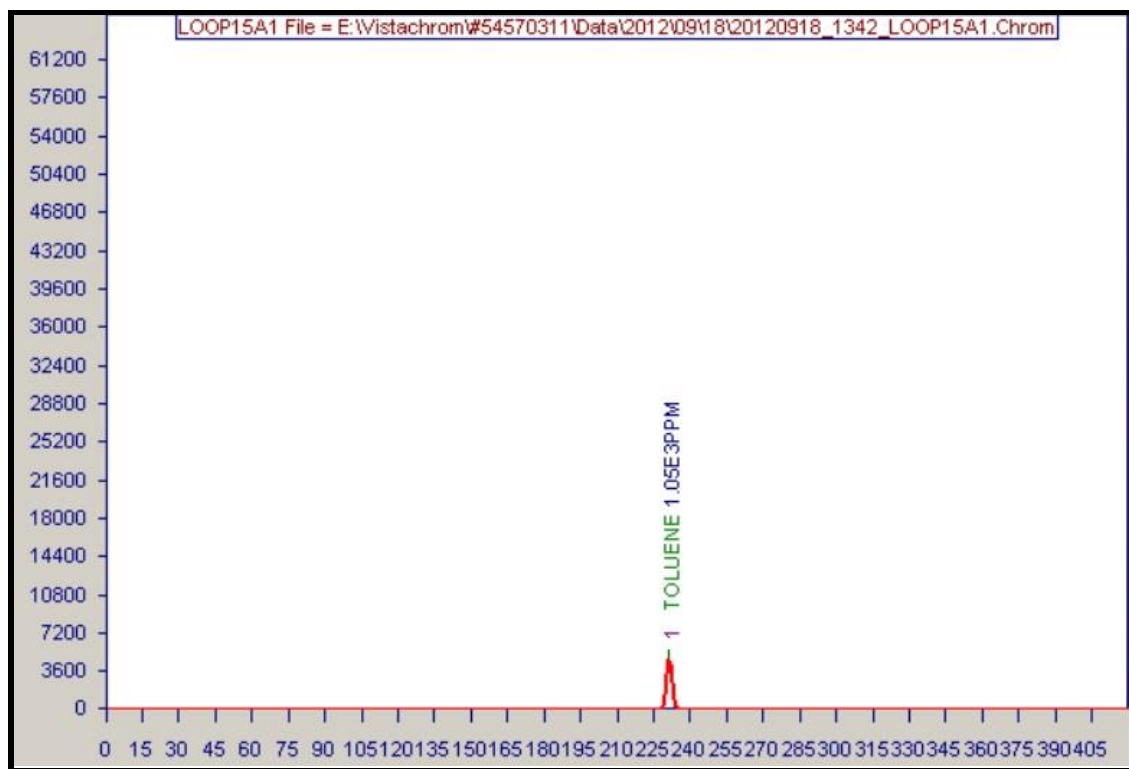


Figure B.4. Sample chromatogram from the GC-FID experiment

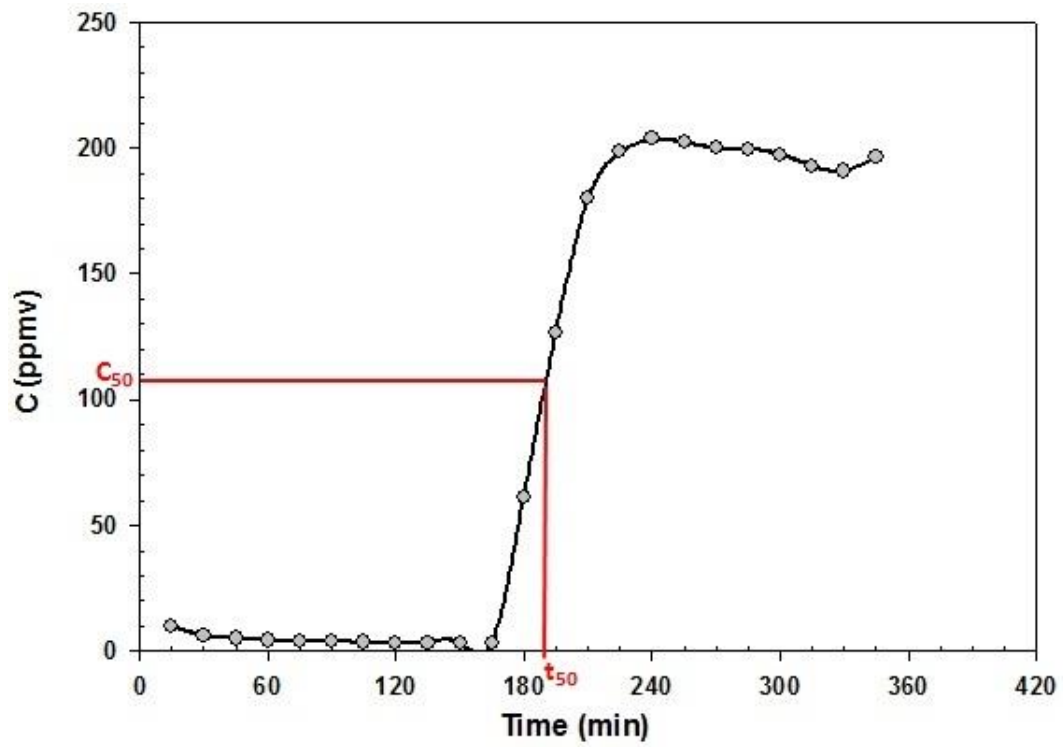


Figure B.5. Plot of the concentration versus time for the adsorption of toluene onto SW raw sample, depicting the calculation of t_{50} from the plot

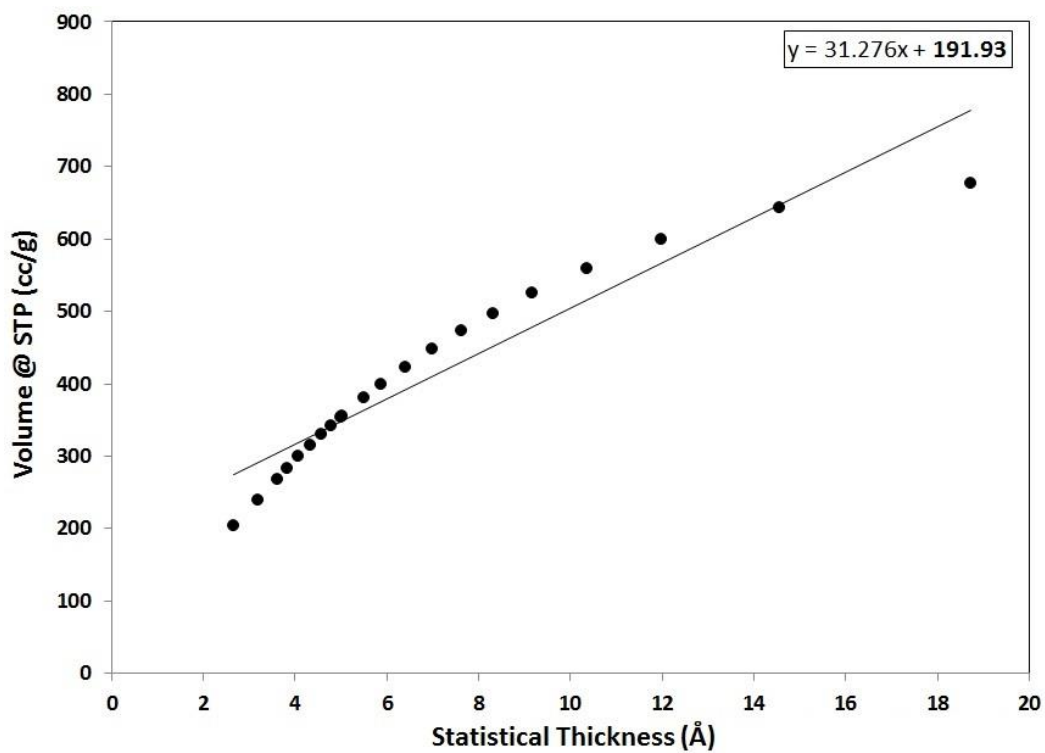


Figure B.6. V-t plots for SW raw sample using de Boer's method

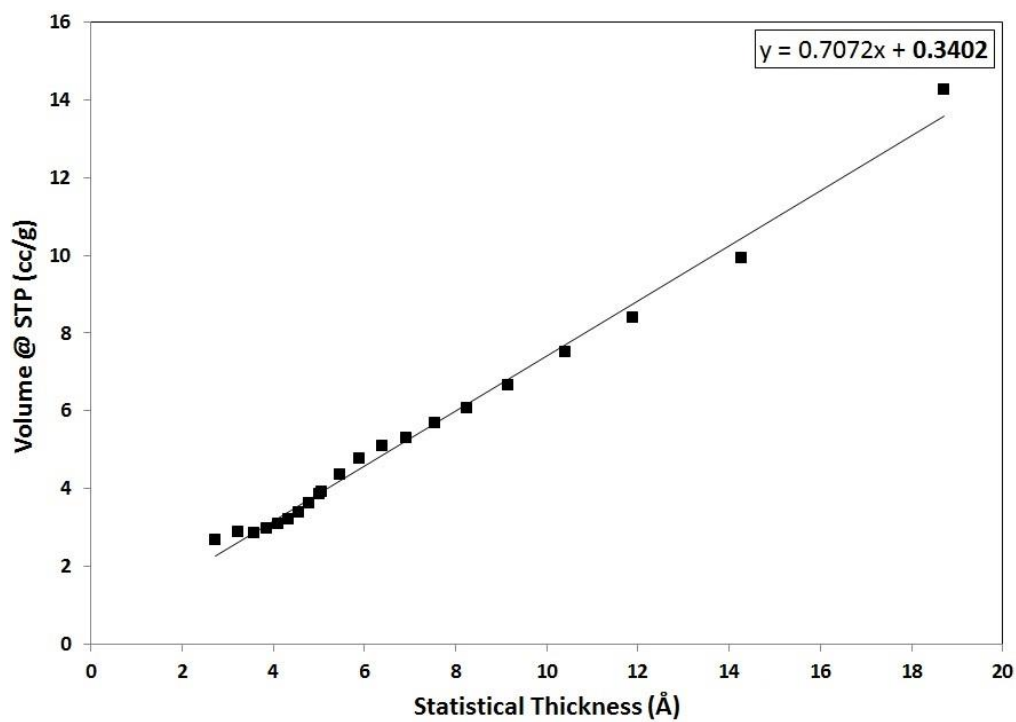


Figure B.7. V-t plots for MW raw sample using de Boer's method

REFERENCES

- Agnihotri, S.; Rood, M.J.; and Rostam-Abadi, M. (2005). "Adsorption equilibrium of organic vapors on single-walled carbon nanotubes." *Carbon*, 43, 2379-2388.
- Agnihotri, S.; Rostam-Abadi, M.; Rood, M.J.; and Clarkson, R.B. (2005). "Adsorption of Water Vapor and Organic vapors on Single-Wall Carbon Nanotubes." *Journal of the Air & Waste Management Association*, 55(6), 708-746.
- Ajayan, P. M. (2000). *Carbon Nanotubes*, Academic Press. from Nalwa, H. S. (2002). *Nanostructured Materials and Nanotechnology*, Academic Press.
- Ajayan, P.M.; and Iijima, S. (1993). "Capillarity-induced filling of carbon nanotubes." *Nature*, 361, 333-334.
- Ana, K.H.; Jeona, K.K.; Moona, J-M.; Eumb, S.J.; Yang, C.W.; Park, G-S.; Parka, C.Y.; and Lee, Y.H. (2001). "Transformation of singlewalled carbon nanotubes to multiwalled carbon nanotubes and onion-like structures by nitric acid treatment." *Synthetic Metals*, 140, 1-8.
- Aqel, A.; Abou El-Nour, K.M.M.; Ammar, R.A.A.; and Al-Warthan, A. (2012). "Carbon nanotubes, science and technology part (I) structure, synthesis and characterization." *Arabian Journal of Chemistry*, 5, 1-23.
- Babaa, M.R.; Dupont-Pavlovsky, N.; McRae, E; and Masenelli-Varlot, K. (2004). "Physical adsorption of carbon tetrachloride on as-produced and on mechanically opened single walled carbon nanotubes." *Carbon*, 42, 1549-1554.
- Bansal, R.C.; and Donnet, J.B. (1988). *Active Carbon*, New York, Marcel Dekker, Inc.
- Bansal, R.C.; and Goyal, M. (2005). *Activated Carbon Adsorption*, Florida, CRC Press.
- Barrett, E.P.; Joyner, L.G.; and Halenda, P.H. (1951). "The Determination of Pore Volume and Area Distributions in Porous Substances. I. Computations from Nitrogen Isotherms." *Journal of American Chemical Society*, 73, 373-380.
- Bekyarova, E.; Kaneko, K.; Yudasaka, M.; Kasuya, D.; Iijima, S.; Huidobro, A.; and Rodriguez-Reinoso, F. (2003). "Controlled Opening of Single-Wall Carbon Nanohorns by Heat Treatment in Carbon Dioxide." *Journal of Physical Chemistry B*, 107(19), 4479-4484.
- Bethune, D.S.; Klang, C.H.; deVries, M.S.; Gorman, G.; Savoy, R.; Vazquez, J.; and Beyers, R. (1993). "Cobalt-catalysed growth of carbon nanotubes with single-atomic-layer walls." *Nature*, 363.
- Biswas, P.; and Wu, C-Y. (2005). "Nanoparticles and the Environment." *Journal of the Air & Waste Management Association*, 55(6), 708-746.

- Bittner, E.W.; Smith, M.R.; and Bockrath, B.C. (2003). "Characterization of the surfaces of single-walled carbon nanotubes using alcohols and hydrocarbons: a pulse adsorption technique." *Carbon*, 41, 1231-1239.
- Bom, D.; Andrews, R.; Jacques, D.; Anthony, J.; Chen, B.; Meier, M.S.; and Selegue, J.P. (2002). "Thermogravimetric Analysis of the Oxidation of Multiwalled Carbon Nanotubes: Evidence for the Role of Defect Sites in Carbon Nanotube Chemistry." *Nano Letters*, 2(6), 615-619.
- Bougrine, A.; Pavlovsky, D.; Naji, A.; Ghanbaja, J.; Mareche, J.F.; and Billaud, D. (2001). "Influence of high temperature treatments on single-walled carbon nanotubes structure, morphology and surface properties." *Carbon*, 39, 685-695.
- Byl, O.; Kondratyuk, P.; and Yates, Jr., J.T. (2003). "Adsorption and Dimerization of NO Inside Single-Walled Carbon Nanotubes – An Infrared Spectroscopic Study." *Journal of Physical Chemistry B*, 107(18), 4277-4279.
- Chen, H.; Chen, C.S.; Chen, Q.; Cheng, F.Q.; Zhang, G.; and Chen, Z.Z. (2002). "Non-destructive purification of multi-walled carbon nanotubes produced by catalyzed CVD." *Materials Letters*, 57, 734– 738.
- Chen, J.; Chen, W.; and Zhu, D.Q. (2008). "Adsorption of nonionic aromatic compounds to single-walled carbon nanotubes: Effects of aqueous solution chemistry." *Environmental Science & Technology*, 42, 7225-7230.
- Chen, W.; Duan, L.; Wang, L.; and Zhu, D.Q. (2008). "Adsorption of hydroxyl- and amino-substituted aromatics to carbon nanotubes." *Environmental Science & Technology*, 42, 6862-6868.
- Chen, W.; Duan, L.; and Zhu, D. (2007). "Adsorption of Polar and Nonpolar Organic Chemicals to Carbon Nanotubes." *Environ. Sci. Technol.*, 41, 8295-8300.
- Chen, Z.; Pierre, D.; He, H.; Tan, S.; Pham-Huy, C.; Hong, H.; and Huang, J. (2011). "Adsorption behavior of epirubicin hydrochloride on carboxylated carbon nanotubes." *International Journal of Pharmaceutics*, 405, 153-161.
- Chen, D.Z.; Zhang, J.X.; and Chen, J.M. (2010). "Adsorption of methyl *tert*-butyl ether using granular activated carbon: Equilibrium and kinetic analysis." *Int. J. Environ. Sci. Tech.*, 7(2), 235-242.
- Chin, C-J. M.; Shih, M-W; and Tsai, H-J. (2010). "Adsorption of nonpolar benzene derivatives on single-walled carbon nanotubes." *Applied Surface Science*, 256, 6035-6039.
- Cho, H.H.; Smith, B.A.; Wnuk, J.D.; Fairbrother, D.H.; and Ball, W.P. (2008). "Influence of surface oxides on the adsorption of naphthalene onto multiwalled carbon nanotubes." *Environmental Science & Technology*, 42, 2899-2905.
- Colomer, J-F.; Pavlovsky, P.; Willems, I.; Journet, C.; Bernier, P.; Tendeloo, G.V.; Fonseca, A.; and Nagy, J.B. (1998). "Purification of catalytically produced multi-wall nanotubes." *J. Chem. Soc.*, 94, 3753-3758.

Colomer, J-F.; Piedigrosso, P.; Fonseca, A.; and Nagy, J.B. (1999). "Different purification methods of carbon nanotubes produced by catalytic synthesis." *Synthetic Metals*, 103, 2482-2483.

Cooper, C. David and F.C. Alley. (2002). *Air Pollution Control: A Design Approach*. 3rd Edition, Waveland Press, Inc., Illinois.

Datsyuk, V.; Kalyva, M.; Papagelis, K.; Parthenios, J.; Tasis, D.; Siokou, A.; Kallitis, I.; and Galiotis, C. (2008). "Chemical oxidation of multiwalled carbon nanotubes." *Carbon*, 46, 833-840.

David, R. L. (2003). CRC Handbook of chemistry and physics, Boca Raton, Fl; *CRC Press*, P C154-321.

Diaz, E.; Ordonez, S.; Vega, A. (2007). "Adsorption of volatile organic compounds onto carbon nanotubes, carbon nanofibers, and high-surface-area graphites." *Journal of Colloid Interface Science*. 305, 7-16.

Dillon, A.C.; Gennett, T.; Jones, K.M.; Alleman, J.L.; Parilla, P.A.; and Heben, M.J. (1999). "A Simple and Complete Purification of Single-Walled Carbon Nanotube Materials." *Advanced Materials*, 11(16).

Dockery, Douglas W.; Pope, C. Arden; Xu, Xiping; Spengler, John D.; James H. Ware, Martha E. Fay, Benjamin G. Ferris; and Speizer Frank E. (1993). "An Association between Air Pollution and Mortality in Six U.S. Cities." *The New England Journal of Medicine*, 329(24), 1753-1759.

Dresselhaus, M.S.; Dresselhaus, G.; Saito, R.; and Jorio, A. (2004). "Raman spectroscopy of carbon nanotubes." *Physics Reports*, 409(9), 47-99.

Droppa Jr, R.; Hammer, P.; Carvalho, A.C.M.; dos Santos, M.C.; and Alvarez, F. (2002). "Incorporation of nitrogen in carbon nanotubes." *Journal of Non-Crystalline Solid*, 874-879.

Ebbesen, T.W. and Ajayan, P.M. (1992). "Large-scale synthesis of carbon nanotubes." *Nature*, 358, 220-221.

Environmental Protection Agency (EPA) (2007). "8-Hour Ground-level Ozone Designations." <http://www.epa.gov/ozonedesignations/> 2007, accessed June 2007.

Environmental Protection Agency. (2007). *Nanotechnology White Paper*. EPA-100/B07/001.

Environmental Protection Agency. "Toxics Release Inventory." 2011 Public Data Release. http://iaspub.epa.gov/triexplorer/tri_release.chemical, accessed January 2013.

Environmental Protection Agency. "Technology Transfer Network Air Toxics Website." <http://www.epa.gov/ttn/atw/allabout.html>, accessed January 2013.

Fang, H-T.; Liu, C-G.; Liu, C.; Li, F.; Liu, M.; and Cheng, H-M. (2004). "Purification of Single-Wall Carbon Nanotubes by Electrochemical Oxidation." *Chem. Mater.*, 16, 5744-5750.

Gotovac, S.; Yang, C-M.; Hattori, Y.; Takahashi, K.; Kanoh, H.; and Kaneko, K. (2001). "Adsorption of polyaromatic hydrocarbons on single wall carbon nanotubes of different functionalities and diameters." *Journal of Colloid and Interface Science*, 314, 18-24.

- Gregg, S. J.; and Sing, K. S. W. (1995). *Adsorption, Surface Area and Porosity*, Academic Press.
- Guo, T.; Nikolaev, P.; Thess, A.; Colbert, D.T.; and Smalley, R.E. (1995). "Catalytic growth of single-walled nanotubes by laser vaporization." *Chemical Physics Letters*, 243, 49-54.
- Haddon, Robert C. (2002). "Carbon Nanotubes." *Accounts of Chemical Research*, 35(12).
- Hafner, J.H.; Bronikowski, M.J.; Bobak, R.A.; Nikolaev, P.; Rinzler, A.G.; Colbert, D.T.; Smith, K.A.; and Smalley, R.E. (1998). "Catalytic growth of single-wall carbon nanotubes from metal particles." *Chemical Physics Letters*, 296, 195-202.
- Heinsohn, R.J.; and Kabel, R.L. (1999). *Sources and Control of Air Pollution*, Prentice-Hall, Inc.
- Hernadi, K.; Fonseca, A.; Nagy, J.B.; Bernaerts, D.; Riga, J.; and Lucas, A. (1996). "Catalytic synthesis and purification of carbon nanotubes." *Synthetic Metals*, 77, 31-34.
- Hernadi, K.; Siska, A.; Thien-Nga, L.; Forro, L.; and I. Kiricsi. (2001). "Reactivity of different kinds of carbon during oxidative purification of catalytically prepared carbon nanotubes." *Solid State Ionics*, 141, 203-209.
- Ho, Y.S.; and McKay, G. (1998). "A Comparison of Chemisorption Kinetic Models Applied to Pollutant Removal On various Sorbents." *Institution of Chemical Engineers*, 76 B.
- Hou, P.X.; Bai, S.; Yang, Q.H.; Liu, C.; and Cheng, H.M. (2002). "Multi-step purification of carbon nanotubes." *Carbon*, 40, 81-85.
- Hu, H.; Zhao, B.; Itkis, M.E.; and Haddon, R.C. (2003). "Nitric Acid Purification of Single-Walled Carbon Nanotubes." *J. Phys. Chem.*, 107, 13838-13842.
- Hussain, S.; Jha, P.; Chouksey, A.; Raman, R.; Islam, S.S.; Islam, T.; Choudhary, P.K.; Raman, R.; and Harsh. (2011). "Spectroscopic Investigation of Modified Single Wall Carbon Nanotube (SWNT)." *Journal of Modern Physics*, 2, 538-543.
- Iijima, S. (1991). "Helical microtubules of graphitic carbon." *Nature*, 354.
- Iijima, S. (1993). "Growth of carbon nanotubes." *Materials Science and Engineering*, 172-180.
- ICP-MS Inductively-Coupled Plasma-Mass Spectrometry, Agilent Solutions. (2005).
- Ji, L.; Chen, W.; Duan, L.; and Zhu, D. (2009). "Mechanisms for strong adsorption of tetracycline to carbon nanotubes: A comparative study using activated carbon and graphite as adsorbents." *Environmental Science & Technology*, 43, 2322-2327.
- Jorio, A.; Dresselhaus, M.S.; and Dresselhaus, G. (2008). *Topics in Applied Physics III Carbon Nanotubes: Advanced Topics in the Synthesis, Structure, Properties and Applications*, New York, Springer.
- Khezami, L.; Chetouani, B.; Taouk, B.; and Capart, R. (2005). "Production and characterization of activated carbon from wood components in powder." *Power Technology*, 157, 48-56.

- Kiang, C-H; Choi, J-S; Tran, T.T.; and Alfred, D.B. (1999). "Molecular Nanowires of 1 nm Diameter from Capillary Filling of Single-Walled Carbon Nanotubes." *Journal of Physical Chemistry B*, 103, 7449-7451.
- Kiang, C-H; Endo, M.; Ajayan, P.M.; Dresselhaus, G.; and Dresselhaus, M.S. (1998). "Size Effects in Carbon Nanotubes." *Physical Review Letters*, 81(9), 1869-1872.
- Kim; Y.; Lee, D.; Oha, Y.; Choi, J.; and Baik, S. (2006). "The effects of acid treatment methods on the diameter dependent length separation of single walled carbon nanotubes." *Synthetic Metals*, 156, 999-1003.
- Lagergren, S. (1898). "About the theory so-called adsorption of soluble substances." *Kungliga Svenska Vetenskapsakademiens*, 24(4), 1-39.
- Lehmann, C.M.B.; Rostam-Abadi, M.; Rood, M.J.; and Sun, J. (1998). "Reprocessing and Reuse of Waste Tire Rubber to Solve Air-Quality Related Problems." *Energy and Fuels*, 12(6), 1095-1099.
- Lin, K-Y.; Chang, J-K.; Chen, C-Y.; and Tsai, W-T. (2009). "Effects of heat treatment on materials characteristics and hydrogen storage capability of multi-wall carbon nanotubes." *Diamond and Related Materials*, 18, 553-556.
- Lin, D.H.; and Xing, B.S. (2008). "Adsorption of phenolic compounds by carbon nanotubes: Role of aromaticity and substitution of hydroxyl groups." *Environmental Science & Technology*, 42, 7254-7259.
- Long, R.Q.; and Yang, R.T. (2001). "Carbon Nanotubes as Superior Sorbent for Nitrogen Oxides." *Industrial Engineering Chemistry Research*, 40(20), 4288-4291.
- Long, R.Q.; and Yang, R.T. (2001). "Carbon Nanotubes as Superior Sorbent for Dioxin Removal." *Journal of the American Chemical Society*, 123(9), 2058-2059.
- Lu, C.S.; Chung, Y.L.; Chang, K.F. (2005). "Adsorption of trihalomethanes from water with carbon nanotubes." *Water Research*, 39, 1183-1189.
- Lu, C.; Chung, Y-L.; and Chang, K-F. (2006). "Adsorption thermodynamic and kinetic studies of trihalomethanes on multiwalled carbon nanotubes." *Journal of Hazardous Materials B*, 138, 304-310.
- Lu, C.; Su, F.; and Hu, S. (2008). "Surface modification of carbon nanotubes for enhancing BTEX adsorption from aqueous solutions." *Applied Surface Science*, 254, 7035-7041.
- Luo, L.; Ramirez, D.; Rood, M. J.; Grevillot, G.; Hay, K. J. and Thurston, D. L. (2006). "Adsorption and electrothermal desorption of organic vapors using activated carbon adsorbents with novel morphologies." *Carbon*, 44(13), 2715-2723.
- Lv, H.; Cheng, N.; Mu, S.; and Pan, M. (2011). "Heat-treated multi-walled carbon nanotubes as durable supports for PEM fuel cell catalysts." *Electrochimica Acta*, 58, 736-742.
- Marsh, H. and Rodriguez-Reinoso, F. (2006). *Activated Carbon*, Elsevier Ltd.

- Martinez, M.T.; Callejas, M.A.; Benito, A. M.; Cochet, M.; Seeger, T.; Anson, A.; Schreiber, J.; Gordon, C.; Marhic, C.; Chauve, O.; and Maser, W.M. (2003). "Modifications of single-wall carbon nanotubes upon oxidative purification treatments." *Nanotechnology*, 14, 691-695.
- Masciangioli, T. and Zhang, W. (2003). "Environmental Technologies at the Nanoscale." *Environmental Science & Technology*, 37(5), 102A-108A.
- McConnell, R.; Berhane, K.; Gilliland, F.; London, Stephanie J.; Vora, Nita; Avol, Edward; Gauderman, W. James; Margolis, Helene G.; Lurmann, Fred; Thomas, Duncan C.; and Peters, John M. (1999). "Air Pollution and Bronchitic Symptoms in Southern California Children with Asthma." *Environmental Health Perspectives*, 107(9), 757.
- Mongillo, J.F. (2007). *Nanotechnology 101*, Greenwood Press.
- Moon, J-M.; An, K.H.; Lee, Y.H.; Park, Y.S.; Bae, D.J.; and Park, G-S. (2001). "High-Yield Purification Process of Singlewalled Carbon Nanotubes." *J. Phys. Chem.*, 105, 5677-5681.
- Nagasawa, S.; Yudasaka, M.; Hirahara, K.; Ichihashi, T.; and Iijima, S. (2000). "Effect of oxidation on single-wall carbon nanotubes." *Chemical Physics Letters*, 328, 374-380.
- National Science and Technology Council Committee on Technology, Subcommittee on Nanoscale Science, Engineering, and Technology. (2003). "Nanotechnology and the Environment: Report of the National Nanotechnology Initiative Workshop." Arlington, VA, May 8-9, 2003.
- National Science and Technology Council. (2004). *National Nanotechnology Initiative Strategic Plan*. Nanoscale Science, Engineering, and Technology Subcommittee, Committee on Technology.
- O'Meara, Molly. (1999). "The Coming Urban Environmental Revolution." *Environmental Manager*, October 1999, 43-46.
- Pan, B.; Lin, D.H.; Mashayekhi, H.; and Xing, B.S. (2008). "Adsorption and hysteresis of bisphenol A and 17 α -ethinyl estradiol on carbon nanomaterials." *Environmental Science & Technology*, 42, 5480-5485.
- Pan, B. and Xing, B. (2008). "Adsorption Mechanisms of Organic Chemicals on Carbon Nanotubes." *Environmental Science & Technology*, 42(24), 9005-9013.
- Peng, X.J.; Li, Y.H.; Luan, Z.K.; Di, Z.C.; Wang, H.Y.; Tian, B.H.; and Jia, Z.P. (2003). "Adsorption of 1,2-dichlorobenzene from water to carbon nanotubes." *Chemical Physics Letters*, 376, 154-158.
- Popov, V.N. (2004). "Carbon nanotubes: properties and application." *Materials Science and Engineering*, 43, 61-102.
- Pumera, M.; Smid, B.; and Veltruska, K. (2009). "Influence of Nitric Acid Treatment of Carbon Nanotubes on Their Physico-Chemical Properties." *J. of Nanoscience and Nanotechnology*, 9, 2671-2676.
- Qiu, H.; Lv, L.; Zhang, Q-j.; Zhang, W-m.; and Zhang, Q-x. (2009). "Critical review in adsorption kinetic models." *Journal of Zhejiang University SCIENCE A*, 10(5), 716-724.

- Qiu, H.; Lv, L.; Pan, B.-c.; Zhang, Q.-j.; Zhang, W.-m.; and Zhang, Q.-x. (2009). "Critical review in adsorption kinetic models." *J. of Zhejiang University Science*, 10(5), 716-724.
- Quantachrome Instruments. NOVA Operational Manual (2006).
- Ramirez, D.; Sullivan, P.D.; Rood, M.J. and Hay, K.J. (2004). "Equilibrium Adsorption of Phenol, Toluene, and Coal-Derived Activated Carbons for Organic Vapors." *Journal of Environmental Engineering*, 130(3), 231-241.
- Ramirez, D.; Sakaray, A.; Gangupomu, R.H.; Perez, J. "Manufacture and Characterization of Carbonaceous Engineered Adsorbents from Waste Mesquite Plants for Air Pollution Control." In *A&WMA's 101st Annual Conference & Exhibition*. 2008. Portland, OR.
- Reid, R.C.; Prausnitz, J.M.; and Poling, B.E. (1984). "The Properties of Gases and Liquids." *McGraw-Hill Inc.*, US.
- Ren, X.; Chen, C.; Nagatsu, M.; and Wang, X. (2011). "Carbon nanotubes as adsorbents in environmental pollution management: A review." *Chemical Engineering Journal*, 170, 395-410.
- Rinzler, A.G.; Liu, J.; Dia, H.; Nikolaev, P.; Nikolaev, P.; Huffman, C.B.; Rodriguez-Macias, F.J.; Boul, P.J.; Liu, A.H.; Heymann, D.; Colbert, D.T.; Lee, R.S.; Fischer, J.E.; Rao, A.M.; Eklund, P.C.; and Smalley, R.E. (1998). "Large-scale purification of single-wall carbon nanotubes: process, product, and characterization." *Applied Physics*, 67, 29-37.
- Ritz, B.; Yu, F.; Fruin, S.; Chapa, G.; Shaw, G.M.; and Harris, J.A. (2002). "Ambient air pollution and risk of birth defects on Southern California." *American Journal of Epidemiology*, 155(1), 17-25.
- Rosca, I.D.; Watari, F.; Uo, M.; and Akasaka, T. (2005). "Oxidation of multiwalled carbon nanotubes by nitric acid." *Carbon*, 43, 3124-3131.
- Rudzinski, W.; and Plazinski, W. (2007). "Theoretical description of the kinetics of solute adsorption at heterogeneous solid/solution interfaces on the possibility of distinguishing between the diffusional and the surface reaction kinetics models." *Applied Surface Science*, 253, 5827-5840.
- Salam, M.A. (2012). "Effect of oxidation treatment of multi-walled carbon nanotubes on the adsorption of pentachlorophenol from aqueous solution: Kinetics study." *Arabian Journal of Chemistry*, 291-296.
- Saito, R.; Dresselhaus, G.; and Dresselhaus, M.S. (2003). *Physical Properties of Carbon Nanotubes*, Imperial College Press.
- Shi, Z.; Lian, Y.; Liao, F.; Zhou, X.; Gu, Z.; Zhang, Y.; Iijima, S. (1999). "Purification of single-wall carbon nanotubes." *Solid State Communications*, 112, 35-37.
- Su, F.; and Lu, C. (2007). "Adsorption kinetics, thermodynamics and desorption of natural dissolved organic matter by multiwalled carbon nanotubes." *Journal of Environmental Science and Health Part A*, 42, 1543-1552.

Su, F.; Lu, C.; and Hu, S. (2010). "Adsorption of benzene, toluene, ethylbenzene and p-xylene by NaOCl-oxidized carbon nanotubes." *Colloids and Surfaces*, 353, 83-91.

Sullivan, P.D.; Rood, M.J.; Dombrowski, K.D.; and Hay, K.J. (2004). "Capture of Organic Vapors Using Adsorption and Electrothermal Regeneration." *Journal of Environmental Engineering*, 130(3), 258-267.

Trivedi, H.C.; Patel, V.M.; and Patel, R.D. (1973). "Adsorption of cellulose triacetate on calcium silicate." *European Polymer Journal*, 9, 525-531.

Tsang, S.C.; Harris, P.J.F.; and Green, M.L.H. (1993). "Thinning and opening of carbon nanotubes by oxidation using carbon dioxide." *Nature*, 362.

Vaccarini, L.; Goze, C.; Aznar, R.; Micholet, V.; Journet, C.; and Bernier, P. (1999). "Purification Procedure of Carbon Nanotubes." *Synthetic Metals*, 103, 2492-2493.

Wang, Y.; Wu, J.; and Wei, F. (2003). "A treatment method to give separated multi-walled carbon nanotubes with high purity, high crystallization and a large aspect ratio." *Carbon*, 41, 2939-2948.

Wang, H.J.; Zhou, A.L.; Peng, F.; Yu, H.; and Chen, L.F. (2007). "Adsorption characteristic of acidified carbon nanotubes for heavy metal Pb(II) in aqueous solution." *Materials Science and Engineering*, 466, 201-206.

Wark, K.; Warner, C.F.; and Davis, W. T. (1998). *Air Pollution: Its Origin and Control*, Addison Wesley Longman, Inc.

Webb, P. A. and Orr, C. (1997). *Analytical Methods in Fine Particle Technology*. Norcross, GA, Micromeritics.

Website of Calgon Carbon Corporation: <http://www.environmental-expert.com/products/bpl-4x6-granular-activated-carbon-60486/view-comments#down>, accessed March 2013.

Website of Cornell Center for Materials Research: http://www.ccmr.cornell.edu/igert/modular/docs/Appl_of_Raman_Spectroscopy.pdf, accessed March 2013.

Website of MER Corporation: <http://www.mercorp.com/products.htm>, accessed March 2013.

Website of Nanostructured & Amorphous Materials, Inc.: <http://www.nanoamor.com/inc/sdetail/9539>, accessed March 2013.

Website of Perkin Elmer: http://www.perkinelmer.com/CMSResources/Images/44-74556GDE_TGABeginnersGuide.pdf, accessed March 2013.

Website of West Virginia University: <http://www2.cemr.wvu.edu/~wu/mae649/xps.pdf>, accessed March 2013.

Woods, L.M.; Badescu, S.C.; and Reinecke, T.L. (2007). "Adsorption of simple benzene derivatives on carbon nanotubes." *Physical Review B*, 75.

World Resources Institute. (2000). "The Weight of Nations: Material Outflows from Industrial Economies."

Xia, W.; Wang, Y.; Bergstraßer, R.; Kundu, S.; and Muhler, M. (2007). "Surface characterization of oxygen-functionalized multi-walled carbon nanotubes by high-resolution X-ray photoelectron spectroscopy and temperature-programmed desorption." *Applied Surface Science*, 254, 247–250.

Yu, F.D.; Luo, L.A.; and Grevillot, G. (2002). "Adsorption Isotherms of VOCs onto an Activated Carbon Monolith: Experimental Measurement and Correlation with Different Models." *J. Chem. Eng. Data*, 47, 467-473.

Yudasaka, M.; Ichihashi, T.; Kasuya, H.; Kataura, H.; and Iijima, S. (2003). "Structure changes of single-wall carbon nanohorns caused by heat treatment." *Carbon*, 41, 1273-1280.

Zhang, S.; Shao, T.; Bekaroglu, S.S.K.; and Karanfil, T. (2009). "The Impacts of Aggregation and Surface Chemistry of Carbon Nanotubes on the Adsorption of Synthetic Organic Compounds." *Environmental Science & Technology*, 43, 5719-5725.

Zhou, G.; Duan, W.H.; and Gu, B.L. (2001). "First-principles study on morphology and mechanical properties of single-walled carbon nanotube." *Chemical Physics Letters*, 333, 344-349.

BIOGRAPHICAL INFORMATION

Roja Haritha Gangupomu was born in Visakhapatnam, Andhra Pradesh, India. She obtained her bachelor's degree in Chemical Engineering from Maharaja Vijayaram Gajapathi Raj College of Engineering (MVGRCE), India. She was the valedictorian of her class of 2004. She received the Manasas Educational Institution award for academic excellence for 2003-2004 and also placed 8th of the University which had 234 colleges under its affiliation. She joined the Department of Civil and Environmental Engineering at the University of Texas at Arlington and received her master's degree in 2006.

She started her doctoral program in the Department of Environmental Engineering at Texas A&M University-Kingsville (TAMUK) in Fall 2007 and then transferred to the University of Texas at Arlington (UTA) in Spring 2009. During her graduate studies at TAMUK and UTA, Roja received first place for a Ph.D. student paper competition at Fifth Annual Texas A&M University System Pathways Student Research Symposium. She has authored 3 peer reviewed journal articles, 8 conference presentations/posters/proceedings, gave 2 oral presentations at national conferences, and contributed to writing one research proposal. In addition, Roja was awarded Air and Waste Management Association's (AWMA) student scholarship for the year 2008-2009. During her candidacy at UTA, she received the Civil Engineering Department's Outstanding Graduate Student Award for 2013. Also, Roja served as president of AWMA student chapter at UTA.

Her research interests include, air pollution control, air pollution modeling, sustainable energy and climate change.